

SEISMIC ROOF ISOLATION OF HALKAPINAR GYMNASIUM

A THESIS SUBMITTED TO  
THE GRADUATE SCHOOL OF NATURAL AND APPLIED SCIENCES  
OF  
MIDDLE EAST TECHNICAL UNIVERSITY

BY

CİHAN KURTULUŞ DURAN

IN PARTIAL FULFILLMENT OF THE REQUIREMENTS  
FOR  
THE DEGREE OF MASTER OF SCIENCE  
IN  
CIVIL ENGINEERING

NOVEMBER 2007

Approval of the thesis:

**SEISMIC ROOF ISOLATION OF HALKAPINAR GYMNASIUM**

submitted by **CİHAN KURTULUŞ DURAN** in partial fulfillment of the requirements for the degree of **Master of Science in Civil Engineering Department, Middle East Technical University** by,

Prof. Dr. Canan ÖZGEN  
Dean, Graduate School of **Natural and Applied Sciences**

\_\_\_\_\_

Prof. Dr. Güney ÖZCEBE  
Head of Department, **Civil Engineering**

\_\_\_\_\_

Prof. Dr. Çetin YILMAZ  
Supervisor, **Civil Engineering Dept., METU**

\_\_\_\_\_

**Examining Committee Members:**

Assoc. Prof. Dr. Cem TOPKAYA  
Civil Engineering Dept., METU

\_\_\_\_\_

Prof. Dr. Çetin YILMAZ  
Civil Engineering Dept., METU

\_\_\_\_\_

Assoc. Prof. Dr. Uğur POLAT  
Civil Engineering Dept., METU

\_\_\_\_\_

Asst. Prof. Dr. Alp CANER  
Civil Engineering Dept., METU

\_\_\_\_\_

Dr. Nuri Çelebi  
YÜKSEL PROJE A.Ş.

\_\_\_\_\_

**Date: 23.11.2007**

**I hereby declare that all information in this document has been obtained and presented in accordance with academic rules and ethical conduct. I also declare that, as required by these rules and conduct, I have fully cited and referenced all material and results that are not original to this work.**

Name, Last name:

Signature :

# **ABSTRACT**

## **SEISMIC ROOF ISOLATION OF HALKAPINAR GYMNASIUM**

Duran, Cihan Kurtuluş  
M. Sc., Department of Civil Engineering  
Supervisor: Prof. Dr. Çetin Yılmaz

November 2007, 157 pages

In this study seismic roof isolation solutions were investigated with a case study of Halkapınar Gymnasium, Izmir.

In the first part, seismic isolation was explained and philosophy behind it was given. Then, geometric and structural properties of Halkapınar Gymnasium were introduced. Furthermore, studies in the literature were presented with basic formulations and explanatory figures. At the end of this section, object and scope of this study was presented.

In the second part, existing seismic roof isolators, elastomeric bearing and viscous damper, were investigated with different support isolation combinations and tried to find the most effective combination. Elastomeric bearings had been used together with viscous dampers in the design.

In the third part, two more types of seismic isolators, lead rubber bearing and friction pendulum isolators, were also analyzed by using the same model and all results were compared with each other and that of non – isolated roof system. Furthermore, in this chapter bilinear effect of the non-linear isolators were also

studied. System behavior was investigated for these types of isolators by comparing column moments, shear forces, roof support displacements and system modal behavior under seven different time-history analysis cases.

Finally, all results are compared with each other considering structure responses and effectiveness of the seismic isolators. It has been tried to find the most efficient seismic isolation solution for the Halkapınar Gymnasium.

In this thesis, theory of seismic isolation, different seismic isolator types on a steel truss roof, effective and economical solutions for seismic roof isolation were presented.

Keywords: Seismic isolation, Roof, Isolator Types, Effectiveness.

# ÖZ

## HALKAPINAR SPOR SALONUNUN SİSMİK ÇATI İZALASYONU

Duran, Cihan Kurtuluş  
Yüksek Lisans, İnşaat Mühendisliği Bölümü  
Tez Yöneticisi: Prof.Dr. Çetin Yılmaz

Kasım 2007, 157 sayfa

Bu çalışmada sismik çatı izolasyon çözümleri İzmir Halkapınar Spor Salonu örnek çalışma alınarak incelenmiştir.

İlk bölümde sismik izolasyon açıklanmış ve sahip olduğu felsefe verilmiştir. Ardından Halkapınar Spor Salonu'nun geometrik ve yapısal özellikleri tanıtılmıştır. Buna ek olarak, literatürde yer alan çalışmalar, temel formül ve grafikler ile sunulmuştur. Bu ilk bölümün sonunda ise, bu tez çalışmasının amacı ve kapsamı sunulmuştur.

İkinci bölümde mevcut sismik çatı izalatörleri (elastomerik mesnet ve viskoz sönümleyici) farklı mesnet izolasyon koşulları için incelenmiş ve en uygun mesnet koşulu tespit edilmeye çalışılmıştır. Mevcut tasarımda elastomerik mesnetler viskoz sönümleyicilerle beraber kullanılmış.

Üçüncü bölümde, iki tip sismik izalatör daha, (kurşun kauçuk mesnet ve sürtünmeli sarkaç izalatörleri) aynı model kullanılarak analiz edilmiş ve sonuçları kendi içlerinde ve izolasyon olmamış çatı sistemiyle karşılaştırılmıştır. Buna ek olarak, doğrusal davranış sergilemeyen mesnetlerin çift doğrusal etkileri de çalışılmıştır. İkinci ve üçüncü bölümlerde, bu izalatörlerin sistem davranışlarına

olan etkileri yedi farklı zaman-tanım alanı analiz koşulları doğrultusunda kolon momentleri, kolon kesme kuvvetleri, çatı mesnet noktası deplasmanları ve sistem mod davranışları karşılaştırılarak incelenmiştir.

Son olarak, tüm sonuçlar yapının davranışlarına göre sismik izalatörlerin etkileri düşünülerek karşılaştırılmıştır. Halkapınar Sporsalonu için en etkili sismik izolasyon çözümü bulunmaya çalışılmıştır.

Bu tezde, sismik izolasyon teorisi, çelik kafes çatı üzerinde farklı sismik izalatör tipleri ve sismik çatı izolasyonu için etkili ve ekonomik sonuçlar sunulmaktadır.

Anahtar Kelimeler : Sismik izolasyon, Çatı, İzalatör Tipleri, Yeterlilik.

**TO MY BABE...**

## **ACKNOWLEDGEMENTS**

The author wishes to express his sincere thanks and appreciations to Prof. Dr. Çetin Yılmaz for the help, expert guidance, suggestions, criticism and sensibility throughout this thesis study.

My Special thanks go to Assoc. Prof. Dr. Kemal Önder Çetin for providing earthquake data sources.

I would like to offer my special thanks to H. Tulu Tunçay, group manager of Yüksel Proje's railway system division, for his encouragement, patience and sensibility throughout my graduate programme.

I also would like to thank Dr. Nuri Çelebi and Fikret Tulumtaş, group manager of Yüksel Proje's superstructure division, for their valuable support and help.

I owe thanks to my Sakarya friends for their friendship during my undergraduate and graduate life.

I want to present this thesis study to Güldem with whom I will marry after my active service in the military.

Finally, I want to thank to my family, my mother, my father, my brother and his wife and my nephew Onurkan and my niece Ecem for their confidence in me, for their support and love.

# TABLE OF CONTENTS

ABSTRACT .....	iv
ÖZ .....	vi
ACKNOWLEDGEMENTS.....	ix
TABLE OF CONTENTS.....	x
LIST OF TABLES .....	xv
LIST OF FIGURES .....	xvi
LIST OF SYMBOLS.....	xxii
CHAPTER – 1.....	xxii
CHAPTER – 2.....	xxiii
CHAPTER – 3.....	xxiv
<b>CHAPTER - 1 .....</b>	<b>1</b>
INTRODUCTION.....	1
1.1 LITERATURE SURVEY .....	5
1.1.1 General .....	5
1.1.2 Seismic Isolations of Steel Roofs.....	7
1.1.2.1 Elastomeric Bearings.....	10
1.1.2.2 Viscous Dampers.....	13
1.1.2.3 Lead Rubber Bearings.....	16
1.1.2.4 Friction Pendulum System Isolators .....	18
1.1.3 Bilinear Modeling .....	22
1.2 OBJECT AND SCOPE .....	24
<b>CHAPTER 2 .....</b>	<b>26</b>
EFFECTS OF ROOF SUPPORT CONDITIONS ON SYSTEM BEHAVIOR	26
2.1 SYSTEM DESCRIPTION .....	26
2.2 EXISTING ROOF ISOLATIONS .....	30

2.2.1 Elastomeric Bearings.....	31
2.2.1.1 Qualities and Specifications of Materials.....	31
2.2.1.1.1 Steel.....	31
2.2.1.1.2 Elastomeric.....	32
2.2.1.2 Check of Bearings.....	32
2.2.1.2.1 Check of Shear Strains.....	32
2.2.1.2.2 Check of Reinforcing Plates Thickness.....	33
2.2.1.2.3 Rotational Limitation Conditional.....	33
2.2.1.2.4 Buckling Stability.....	33
2.2.1.3 Design Loads.....	34
2.2.1.4 Calculation of Elastomeric Bearings.....	35
2.2.2 Modeling of the Link Elements.....	37
2.2.2.1 Step by Step Non-Linear Dynamic Analysis.....	39
2.3 DIFFERENT EXISTING ISOLATOR COMBINATIONS.....	46
2.3.1 Elastomeric Bearing and Viscous Damper (Two Sided).....	46
2.3.2 Elastomeric Bearing and Viscous Damper (One Sided).....	47
2.3.3 Elastomeric Bearings (Two Sided).....	47
2.3.4 Elastomeric Bearings (One Sided).....	48
2.3.5 Viscous Dampers (Two Sided).....	49
2.3.6 Viscous Dampers (One Sided).....	49
2.3.7 Non-isolated.....	50
2.3.8 Results of Different Isolation Cases.....	50
2.3.8.1 Comparisons of Modal Periods.....	50
2.3.8.2 Comparisons of Roof Support Displacements.....	54
2.3.8.3 Comparisons of Column Responses (Shear Forces & Moments)	
.....	56
<b>CHAPTER 3.....</b>	<b>61</b>
DIFFERENT ISOLATOR TYPES and THEIR EFFECTS ON THE SYSTEM	
BEHAVIOUR.....	61
3.1 LEAD RUBBER BEARING.....	61
3.1.1 Minimum Required Diameter of Lead Core.....	62
3.1.1.1 The Wind Force On the Roof of the Gymnasium.....	62

3.1.2 Lead Core Diameter and Rubber Stiffness.....	65
3.1.2.1 Design Displacement.....	65
3.1.2.2 Required Effective Stiffness of the Isolators.....	66
3.1.2.3 Initial Required Characteristic Strength (Seismic Resistance) of the Lead Core and Final Diameter of the Lead Core .....	66
3.1.2.4 Initial Post-Elastic Stiffness of the Bearing and Final Characteristic Strength (Seismic Resistance) Q, of the Lead Core.....	67
3.1.2.5 Final Post-Elastic Stiffness of the Bearing.....	68
3.1.2.6 Contribution of the Rubber, to the Post-Elastic Stiffness .....	69
3.1.3 Isolator Diameter and Rubber Thickness .....	69
3.1.4 Thickness of Rubber Layers.....	71
3.1.5 Isolator Stability Check.....	74
3.1.5.1 Factor of Safety against Buckling Instability.....	74
3.1.5.2 Isolator Condition in Deformed State .....	75
3.1.6 SAP2000 Input Values for Lead Rubber Bearing.....	76
3.2 ISOLATOR COMBINATIONS OF LRB .....	77
3.2.1 Lead Rubber Isolator (Two Sided).....	77
3.2.2 Lead Rubber Isolator (One Sided) .....	77
3.2.3 Results of Isolator Combinations .....	77
3.2.3.1 Comparisons of Modal Periods .....	78
3.2.3.2 Comparisons of Roof Support Displacements .....	79
3.2.3.3 Comparisons of Column Responses (Shear Forces & Moments) .....	81
3.3 FRICTION PENDULUM ISOLATOR .....	84
3.3.1 Minimum Required Friction Coefficient.....	84
3.3.1.1 The Wind Force On the Roof of the Gymnasium .....	85
3.3.2 Minimum and Maximum Friction Coefficient.....	86
3.3.2.1 Initial Lower and Upper Bound Friction Coefficients .....	87
3.3.2.2 System Property Modification Factors.....	87
3.3.2.3 System Property Adjustment Factor .....	88
3.3.2.4 Minimum and Maximum Probable Friction Coefficient.....	89
3.3.3 Radius of Concave Surface .....	90

3.3.4 Preliminary Seismic Design Displacement .....	92
3.3.5 SAP2000 Input Values for Friction Isolator .....	93
3.4 ISOLATOR COMBINATIONS OF FPS.....	95
3.4.1 Friction Pendulum System (Two Sided).....	95
3.4.2 Friction Pendulum System (One Sided).....	95
3.4.3 Results of Isolator Combinations .....	96
3.4.3.1 Comparisons of Modal Periods .....	96
3.4.3.2 Comparisons of Roof Support Displacements .....	97
3.4.3.3 Comparisons of Column Responses (Shear Forces & Moments)	
.....	99
3.5 BILINEAR MODELLING .....	103
3.5.1 Analyze Type – 1 (Elastic Stiffness Changing, Post – Elastic	
Stiffness Constant) .....	106
3.5.2 Analyze Type – 2 (Elastic Stiffness Constant, Post – Elastic Stiffness	
Changing).....	107
3.5.3 Comparisons of Modal Periods.....	107
3.5.4 Comparisons of Roof Support Displacements .....	108
3.5.5 Comparisons of Column Responses (Shear Forces & Moments)..	110
<b>CHAPTER 4 .....</b>	<b>114</b>
CONCLUSIONS AND RECOMMENDATIONS.....	114
4.1 SUMMARY .....	114
4.2 CONCLUSIONS.....	116
4.2.1 Elastomeric Bearing with Viscous Dampers.....	116
4.2.2 Other Isolator Types and Bilinear Behavior .....	117
4.3 RECOMMENDATIONS .....	118
<b>REFERENCES.....</b>	<b>119</b>
<b>APPENDIX .....</b>	<b>123</b>
A.1 SYSTEM PROPERTY MODIFICATION FACTORS FOR SLIDING	
ISOLATORS.....	123
A.2 DESIGN SPECTRUMS .....	125
A.3 NORMALIZED RESPONSE SPECTRUMS .....	128

A.4 MAXIMUM AXIAL FORCES ON ISOLATORS.....	130
A.5 MODE SHAPES OF ISOLATION CASES FOR FIRST FOURTH MODES.....	131
A.6 DEFORMED ENVELOPE SHAPES OF TWO SIDED EB+VD ISOLATION CASE FOR TIME-HISTORY ANALYSES .....	151

## LIST OF TABLES

Table 2.1 Seven Response Spectrums Used in Time – History Analyses .....	39
Table 2.2 14 Time-History Combinations used in the Model (For Each Direction X and Y).....	43
Table 2.3 Amplification Factors of 7 Time-History Data.....	45
Table 3.1 System Property Adjustment Factors [18] (From AASHTO 1999) .....	89
Table A.1.1 Maximum Values for Temperature $\lambda$ – factors for Sliding Isolators .....	123
Table A.1.2 Maximum Values for Aging $\lambda$ – factors for Sliding Isolators.....	123
Table A.1.3 Maximum Values for Travel and Wear $\lambda$ – factors for Sliding Isolators .....	124
Table A.1.4 Maximum Values for Contamination $\lambda$ – factors for Sliding Isolators .....	124
Table A.4.1 Maximum Axial Forces on the Isolators for Each Analysis Case...	130

## LIST OF FIGURES

Figure 1.1 Response Spectrums (Period and Damping Shift).....	2
Figure 1.2 Steel Truss Beams Key Plan (Dimensions are in mm).....	4
Figure 1.3 Steel Truss Beams Cross Section (Dimensions are in mm).....	4
Figure 1.4 Behaviors of Doweled & Bolted Rubber Bearings At Large Shear Strains [9] ( <i>From Journal of Engineering Mechanics</i> ) .....	11
Figure 1.5 Monotonic Shear Loading Test for $P = 0$ and $P = 78.5$ kN [9] ( <i>From Journal of Engineering Mechanics</i> ).....	12
Figure 1.6 Force-Velocity Relationships of Viscous Dampers [13] ( <i>From National Science Council</i> ).....	15
Figure 1.7 Hysteresis Loops of Dampers with (a) Pure Viscous and (b) Viscoelastic Behavior [13] ( <i>From National Science Council</i> ) .....	16
Figure 1.8 Friction Pendulum Isolator [18] ( <i>From MCEER, Federal Highway Administration</i> ) .....	19
Figure 1.9 Multiple Friction Pendulum System (MFPS) [28] ( <i>From ASME, Pressure Vessels and Piping Conference</i> ) .....	20
Figure 1.10 Force – Displacement Responses: (a) idealized bilinear model; (b) lead – rubber isolator; (c) hysteretic bearing; and (d) friction pendulum system [34]. ( <i>From Structural Control and Health Monitoring</i> ) .....	23
Figure 2.1 Main Parts of Halkapınar Gymnasium .....	27
Figure 2.2 Columns Application plan .....	28
Figure 2.3 Installations of Steel Truss Beams.....	29
Figure 2.4 Halkapınar Gymnasium Finite Element (FE) Model.....	30
Figure 2.5 Link Elements .....	37
Figure 2.6 Time-History of 290YA.....	40
Figure 2.7 Time-History of 333XA.....	40
Figure 2.8 Time-History of 591YA.....	41
Figure 2.9 Time-History of 879XA.....	41
Figure 2.10 Time-History of 879YA.....	41

Figure 2.11 Time-History of HSP000 .....	42
Figure 2.12 Time-History of STC090 .....	42
Figure 2.13 EB + VD (Two Sided) .....	46
Figure 2.14 EB + VD (One Sided).....	47
Figure 2.15 EB (Two Sided) .....	48
Figure 2.16 EB (One Sided).....	48
Figure 2.17 VD (Two Sided).....	49
Figure 2.18 VD (One Sided) .....	50
Figure 2.19 Modal Period Behaviors of EB+VD (Two & One Sided) & Non- Isolated Support Conditions for First 10 Modes. ....	51
Figure 2.20 Modal Period Behaviors of EB (Two & One Sided) & Non-Isolated Support Conditions for First 10 Modes.....	52
Figure 2.21 Modal Period Behaviors of VD (Two & One Sided) & Non-Isolated Support Conditions for First 10 Modes.....	53
Figure 2.22 Global Directions.....	54
Figure 2.23 Maximum Roof Support Displacement (U1 (mm))For Different Isolator Conditions. ....	55
Figure 2.24 Maximum Roof Support Displacement (U2 (mm)) For Different Isolator Conditions. ....	56
Figure 2.25 Column Local Directions.....	57
Figure 2.26 Maximum Column Bottom Shear Forces V2 (ton) For Different Isolator Conditions. ....	58
Figure 2.27 Maximum Column Bottom Shear Forces V3 (ton) For Different Isolator Conditions. ....	58
Figure 2.28 Maximum Column Bottom Moments M2 (ton.m) For Different Isolator Conditions. ....	59
Figure 2.29 Maximum Column Bottom Moments M3 (ton.m) For Different Isolator Conditions. ....	60
Figure 3.1 Length and angle of steel profile of eave.....	62
Figure 3.2 Overlap Areas $A_r$ , [18] (From AASHTO 1999).....	71
Figure 3.3 Modal Period Behaviors of EB+VD (Two & One Sided), LRB (Two & One Sided) & Non-Isolated Support Conditions for First 10 Modes.....	78

Figure 3.4 Maximum Roof Support Displacements ( $U_1$ (mm))For Different Isolator Conditions. ....	80
Figure 3.5 Maximum Roof Support Displacements ( $U_2$ (mm))For Different Isolator Conditions. ....	80
Figure 3.6 Maximum Column Bottom Shear Forces $V_2$ (ton) For Different Isolator Conditions. ....	82
Figure 3.7 Maximum Column Bottom Shear Forces $V_3$ (ton) For Different Isolator Conditions. ....	82
Figure 3.8 Maximum Column Bottom Moments $M_2$ (ton.m) For Different Isolator Conditions. ....	83
Figure 3.9 Maximum Column Bottom Moments $M_3$ (ton.m) For Different Isolator Conditions. ....	84
Figure 3.10 Modal Period Behaviors of EB+VD (Two & One Sided), FPS (Two & One Sided) & Non-Isolated Support Conditions for First 10 Modes.....	97
Figure 3.11 Maximum Roof Support Displacements ( $U_1$ (mm))For Different Isolator Conditions. ....	98
Figure 3.12 Maximum Roof Support Displacements ( $U_2$ (mm))For Different Isolator Conditions. ....	99
Figure 3.13 Maximum Column Bottom Shear Forces $V_2$ (ton) For Different Isolator Conditions. ....	100
Figure 3.14 Maximum Column Bottom Shear Forces $V_3$ (ton) For Different Isolator Conditions. ....	101
Figure 3.15 Maximum Column Bottom Moments $M_2$ (ton.m) For Different Isolator Conditions. ....	102
Figure 3.16 Maximum Column Bottom Moments $M_3$ (ton.m) For Different Isolator Conditions. ....	102
Figure 3.17 Characteristics of Bilinear Isolation Bearings ( <i>From AASHTO Guide Specifications for Seismic Isolation Design, Figure C4.</i> ).....	103
Figure 3.18 Type-1 Analysis                      Figure 3.19 Type-2 Analysis.....	105
Figure 3.20 Modal Period Behaviors of Analyze Type-1 & Type-2 (Two & One Sided) and Actual Case (Two & One Sided) Support Conditions.....	108

Figure 3.21 Maximum Roof Support Displacements (U1 (mm))For Different Isolator Conditions. ....	109
Figure 3.22 Maximum Roof Support Displacements (U2 (mm)) For Different Isolator Conditions. ....	109
Figure 3.23 Maximum Column Bottom Shear Forces V2 (ton) For Different Isolator Conditions. ....	111
Figure 3.24 Maximum Column Bottom Shear Forces V3 (ton) For Different Isolator Conditions. ....	111
Figure 3.25 Maximum Column Bottom Moments M2 (ton.m) For Different Isolator Conditions. ....	112
Figure 3.26 Maximum Column Bottom Moments M3 (ton.m) For Different Isolator Conditions. ....	113
Figure A.2.1 Spectrum Comparisons of 290Y & 333X.....	125
Figure A.2.2 Spectrum Comparisons of 591Y, 879X & 879Y .....	125
Figure A.2.3 Spectrum Comparisons of HSP000 & STC090 .....	126
Figure A.2.4 Design Spectrums - 1 .....	126
Figure A.2.5 Design Spectrums - 2 .....	127
Figure A.3.1 Normalized Acceleration Response Spectrums .....	128
Figure A.3.2 Not Normalized Acceleration Response Spectrums .....	129
Figure A.3.3 Displacement Response Spectrums .....	129
Figure A.5.1 Two Sided EB+VD Isolation Shape of First Mode (0.94sec). ....	131
Figure A.5.2 Two Sided EB + VD Isolation Shape of Second Mode (0.87sec.)..	131
Figure A.5.3 Two Sided EB + VD Isolation Shape of Third Mode (0.84sec.)..	132
Figure A.5.4 Two Sided EB + VD Isolation Shape of Fourth Mode (0.59). ....	132
Figure A.5.5 One Sided EB + VD Isolation Mode Shape of First Mode (0.89sec). .....	133
Figure A.5.6 One Sided EB+VD Isolation Shape of Second Mode (0.82sec.)..	133
Figure A.5.7 One Sided EB+VD Isolation Mode Shape of Third Mode (0.79sec). .....	134
Figure A.5.8 One Sided EB + VD Isolation Shape of Fourth Mode (0.60sec.)..	134
Figure A.5.9 Two Sided EB Isolation Mode Shape of First Mode (1.62sec.) ...	135

Figure A.5.10 Two Sided EB Isolation Mode Shape of Second Mode (1.62sec.).	135
Figure A.5.11 Two Sided EB Isolation Mode Shape of Third Mode (1.38sec.).	136
Figure A.5.12 Two Sided EB Isolation Mode Shape of Fourth Mode (0.74sec.).	136
Figure A.5.13 One Sided EB Isolation Mode Shape of First Mode (1.28sec.)...	137
Figure A.5.14 One Sided EB Isolation Mode Shape of Second Mode (0.98sec.).	137
Figure A.5.15 One Sided EB Isolation Mode Shape of Third Mode (0.84sec.).	138
Figure A.5.16 One Sided EB Isolation Mode Shape of Fourth Mode (0.62sec.).	138
Figure A.5.17 Two Sided VD Isolation Mode Shape of First Mode (0.85sec.).	139
Figure A.5.18 Two Sided VD Isolation Mode Shape of Second Mode (0.77sec.).	139
Figure A.5.19 Two Sided VD Isolation Mode Shape of Third Mode (0.75sec.).	140
Figure A.5.20 Two Sided VD Isolation Mode Shape of Fourth Mode (0.58sec.).	140
Figure A.5.21 One Sided VD Isolation Mode Shape of First Mode (0.85sec.).	141
Figure A.5.22 One Sided VD Isolation Mode Shape of Second Mode (0.77sec.).	141
Figure A.5.23 One Sided VD Isolation Mode Shape of Third Mode (0.75sec.).	142
Figure A.5.24 One Sided VD Isolation Mode Shape of Fourth Mode (0.59sec.).	142
Figure A.5.25 Two Sided LRB Isolation Shape of First Mode (1.53sec.).....	143
Figure A.5.26 Two Sided LRB Isolation Shape of Second Mode (1.51sec.). ....	143
Figure A.5.27 Two Sided LRB Isolation Shape of Third Mode (1.34sec.). ....	144
Figure A.5.28 Two Sided LRB Isolation Shape of Fourth Mode (0.80sec.). ....	144
Figure A.5.29 One Sided LRB Isolation Shape of First Mode (1.25sec.). ....	145
Figure A.5.30 One Sided LRB Isolation Shape of Second Mode (0.99sec.).....	145
Figure A.5.31 One Sided LRB Isolation Shape of Third Mode (0.86sec.).....	146
Figure A.5.32 One Sided LRB Isolation Shape of Fourth Mode (0.64sec.). ....	146
Figure A.5.33 Two Sided FPS Isolation Shape of First Mode (0.90sec.).....	147

Figure A.5.34 Two Sided FPS Isolation Shape of Second Mode (0.83sec.).	147
Figure A.5.35 Two Sided FPS Isolation Shape of Third Mode (0.76sec.).	148
Figure A.5.36 Two Sided FPS Isolation Shape of Fourth Mode (0.55sec.).	148
Figure A.5.37 One Sided FPS Isolation Shape of First Mode (0.87sec.).	149
Figure A.5.38 One Sided FPS Isolation Shape of Second Mode (0.80sec.).	149
Figure A.5.39 One Sided FPS Isolation Shape of Third Mode (0.78sec.).	150
Figure A.5.40 One Sided FPS Isolation Shape of Fourth Mode (0.59sec.).	150
Figure A.6.1 290YA_X Analyze Case Deformed Shape	151
Figure A.6.2 290YA_Y Analyze Case Deformed Shape	151
Figure A.6.3 333XA_X Analyze Case Deformed Shape	152
Figure A.6.4 333XA_Y Analyze Case Deformed Shape	152
Figure A.6.5 591YA_X Analyze Case Deformed Shape	153
Figure A.6.6 591YA_Y Analyze Case Deformed Shape	153
Figure A.6.7 879XA_X Analyze Case Deformed Shape	154
Figure A.6.8 879XA_Y Analyze Case Deformed Shape	154
Figure A.6.9 879YA_X Analyze Case Deformed Shape	155
Figure A.6.10 879YA_Y Analyze Case Deformed Shape	155
Figure A.6.11 HSP000_X Analyze Case Deformed Shape	156
Figure A.6.12 HSP000_Y Analyze Case Deformed Shape	156
Figure A.6.13 STC090_X Analyze Case Deformed Shape	157
Figure A.6.14 STC090_Y Analyze Case Deformed Shape	157

# LIST OF SYMBOLS

## CHAPTER – 1

S	Shape Factor
$K_h$	Horizontal Stiffness
G	Shear Modulus of Rubber
A	Cross Sectional Area of Bearing
$P_s$	Shear Stiffness of Bearing
h	Total Height of Bearing
$t_r$	Total Height of Rubber
I	Moment of Inertia of Bearing
$E_c$	Effective Compression Modulus
$P_E$	Euler Load
$P_{crit}$	Buckling Load
$F_D$	Damper Force
C	Damping Constant
$\dot{u}$	Relative Velocity
$K_{eff}$	Effective Stiffness
$K_2$	Post – Elastic Stiffness
Q	Characteristic Strength
D	Design Displacement
$D_y$	Yield Displacement
w	Natural Frequency
$\beta_{eff}$	Effective Damping
$K_1$	Elastic Stiffness
F	Restoring Force
R	Radius of Curvature

## CHAPTER – 2

$\epsilon_{t,d}$	Maximum Shear Strain
$\epsilon_{c,d}$	Design Strain Due to Compressive Loads
$\epsilon_{q,d}$	Design Strain Due to Horizontal Movements
$\epsilon_{\alpha,d}$	Design Strain Due to Angular Rotation
$K_L$	Type Loading Factor
A	Plan Area of Elastomer
$A_r$	Reduced Area of Elastomer
G	Shear Modulus
S	Shape Factor
$h_e$	Effective Height of Elastomer
$h_g$	Net Height of Rubber
$V_p$	Vertical Permanent Load
$V_l$	Vertical Live Load
V	Vertical Design Load
$V_{min}$	Minimum Vertical Design Load
$H_a$	Horizontal Load Parallel to the Shortest Side (Longitudinal)
$H_b$	Horizontal Load Parallel to the Longest Side (Transversal)
$H_{vm}$	Horizontal Load Acting with $V_{min}$
$V_x$	Longitudinal Movement
$V_y$	Transversal Movement
$\alpha_x$	Rotation across the Shortest Side
$\alpha_y$	Rotation across the Longest Side
t	Minimum Thickness of The Reinforcing Steel Plates
$K_h$	Factor for Induced Tensile Stresses in Reinforcing Steel Plates
$\gamma_m$	Partial Safety Factor
$K_p$	Correction Factor
$v_{z,d}$	Total Vertical Deflection
$K_{r,d}$	Rotation Factor
$K_x$	Horizontal Stiffness in X direction
$K_y$	Horizontal Stiffness in Y direction

F	Axial Force Acting in Fluid Damper
C	Damping Constant
V	Velocity
$\alpha$	Damping Exponent

### CHAPTER – 3

q	Horizontal Wind Force acting on the Roof
C	Shape Coefficient
wL	Wind Load
W	Total Weight of the Steel Truss Roof on One Side Supports
F <sub>T</sub>	Factored Wind Load
Q	Characteristic Strength
F <sub>y</sub>	Yield Strength
d <sub>Lmin</sub>	Minimum Required Diameter of Lead Core
$\Psi$	Factor for Service Loads
n	Factor for Service Loads
f <sub>yL</sub>	Effective Shear Yield Stress of Lead
T <sub>e</sub>	Effective Period
$\beta_e$	Effective Damping
D <sub>D</sub>	Design Displacement
C <sub>V<sub>D</sub></sub>	Constant - Velocity Regions of DBE Spectrum
T <sub>D</sub>	Target Isolated Period
B <sub>D</sub>	Damping Coefficient
$\beta$	Damping Ratio
K <sub>e</sub>	Effective Stiffness
g	Gravitational Acceleration
n <sub>b</sub>	Number of Bearings
T <sub>e</sub>	Effective Period
Q <sub>i</sub>	Initial Required Strength
D <sub>y</sub>	Yield Displacement
d <sub>L</sub>	Diameter of Lead Core
K <sub>d,i</sub>	Initial Post-Elastic Stiffness of the Bearing

$K_u$	Elastic Stiffness
$K_d$	Post-Elastic Stiffness of the Bearing
$K_r$	Contribution of the Rubber
$f$	Factor $f$ for the Effect of Lead on Post-Elastic Stiffness
$A_b$	Bonded Plan Area of the Bearing
$P$	Total Axial Load
$f_c$	Allowable Compressive Stress
$d_b$	Bonded Diameter of a Lead Rubber Bearing
$d_L$	Central Lead Core Diameter
$c$	Thickness of the Rubber Cover
$d$	Total Rubber Diameter
$T_r$	Total Rubber Thickness
$G$	Shear Modulus of Rubber
$K_r$	Rubber Stiffness
$A_r$	Overlap Area
$S$	Shape Factor
$P$	Vertical Load
$k'$	Material Constant for Rubber
$K$	Bulk Modulus of Rubber
$\gamma_c$	Maximum Shear Strain due to Compression
$t_i$	Maximum Layer Thickness
$FS$	Factor of Safety
$P_{cr}$	Critical Load
$E_c$	Modulus of Elasticity of Rubber in Compression
$I$	Moment of Inertia
$K_1$	Elastic Stiffness
$K_2$	Post-Elastic Stiffness
$\mu_{min,req}$	Minimum Required Friction Coefficient
$\mu_L$	Lower Bound Friction Coefficients
$\mu_U$	Upper Bound Friction Coefficients
$\lambda_{min}$	Minimum Value of the System Property Modification Factor
$\lambda_{max}$	Maximum Value of the System Property Modification Factor

$\lambda_{\max,t}$	System Property Modification Factor for the Effect of Temperature
$\lambda_{\max,a}$	System Property Modification Factor for the Effect of Aging
$\lambda_{\max,v}$	System Property Modification Factor for the Effect of Velocity
$\lambda_{\max,tr}$	System Property Modification Factor for the Effect of Travel and Wear
$\lambda_{\max,c}$	System Property Modification Factor for the Effect of Contamination
$\lambda_{\max,scrag}$	System Property Modification Factor for the Effect of Scragging
$f_a$	Adjustment Factor
$\mu_{\min}$	Minimum Probable Friction Coefficient
$\mu_{\max}$	Maximum Probable Friction Coefficient
R	Radius of the Concave Surface
$\Delta_m$	Maximum Bearing Displacement

# **CHAPTER - 1**

## **INTRODUCTION**

Earthquake is a kind of energy and this energy travels from the source, depth of the ground and reaches to its final location, structural member connections. If this energy is not absorbed before reaching to its target points, it will be hard issue for the structure to resist this energy and structure will tend to absorb this energy by its own methods, possibly by losing some of its own members to provide required flexibility to get rid of this excess energy. Earthquake is the main threat for most of the structures. Structural responses against earthquake may be at high levels of accelerations, which mean that structures try to make high displacements demands. The rigidity of the structures does not allow these required displacements and this cause producing of high stress levels and finally, failure of the structures. If we allow the structures to be more flexible, than the floor accelerations would be less by the way of showing higher modes and damping values.

This required flexibility is achieved up to some level by forming plastic hinges in reinforced concrete structures to supply higher modal periods to the structure and thus, reducing the floor accelerations. Traditional structural design is aimed at to prevent major failures and loss of life. Immediate occupation, the maintenance of operation is not considered in this design approach. Traditional design is based on damage to the structure by yielding and plastic formation to dissipate earthquake's energy. Collapse of the structures is prevented by ductile design of the yielding members. Therefore, there are always possibility of significant damage to the structure and contents.

Plastic hinge formation does not always help to get desired displacement capacities under severe earthquakes, because of the fixed bearings at the base of the structures to transfer the system load to the ground and to prevent interstory drifts. Flexible bearings isolating the structures from the ground provide both minimizing interstory drifts and floor accelerations as well. Seismic isolation minimizes interstory drifts by providing displacement ability to the base of the structure and minimizes floor acceleration by increasing flexibility and increasing the natural period of the structure. ( $>1.5$  sec., usually 2.0 – 3.0 sec.) [1].

Many non – isolated buildings have fundamental periods of 0,2 – 0,5 sec. [2]. This period interval generally falls within the typical range of high spectral acceleration. This means that the maximum energy content of the response spectrum is concentrated for the structure. Thus, the non – isolated buildings show resonance that cause high levels of floor accelerations and interstory drifts. However, the fundamental periods of isolated buildings are shifted to a level that correspond to lower spectral accelerations, in addition to that, damping of the system is increased by isolators , so that, resonance effects are prevented and floor accelerations and interstory drifts are decreased considerably. (Figure 1.1)

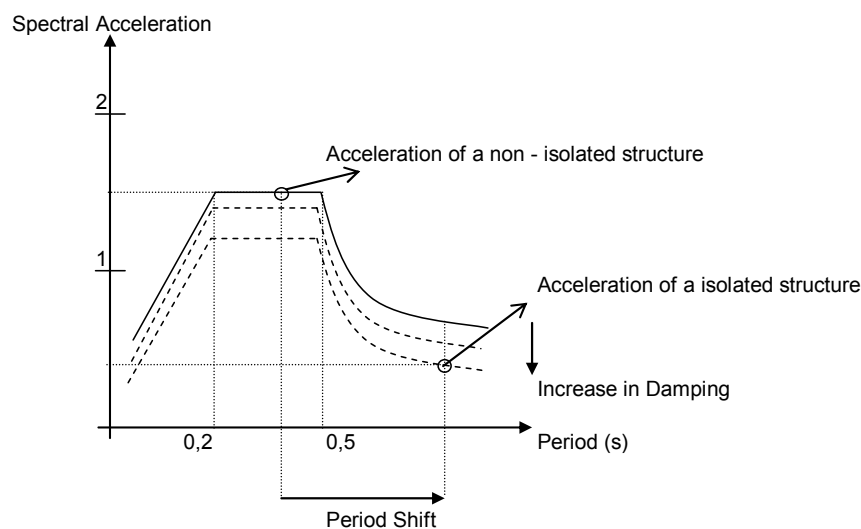


**Figure 1.1** Response Spectrums (Period and Damping Shift)

Seismic isolation thus is a seismic design approach aimed at protecting structures against damage from earthquakes by limiting the earthquake forces by not providing resistance to them. Seismic isolation is used for many kind of structures such that, important structures required to remain relatively undamaged in severe earthquakes (hospitals, nuclear power plants, museums, city halls etc.), rehabilitation of existing buildings (strengthening of structures in high seismic zones), public buildings (hospitals, schools, gymnasiums etc.). Gymnasiums are public places where more than 5,000 people come together and high cost of investments are made. Therefore, special attention must be given to their design stages. As being the most important structural element, their roofs compose the actual mass being most vulnerable to seismic forces.

Izmir Halkapınar Gymnasium was constructed for the Universiade 2005 and gained to the public for many competitive tournaments in coming years. Due to the need of large spacing in the hall, there is not any pier in the middle of the roof of the structure. While Gymnasium was located on an area having 109m x 189m in plan, roof of the main court of the gymnasium have 80m x 110m dimensions in plan and therefore, the piers on both sides are the only bearings for the roof of the structure. As being 20 piers on each side of the roof, there are total 40 piers having 6.11m distance interval on both sides of the structure. Only 10 piers on one side of the roof compose supports of the steel truss beams due to the 6.11m distance interval between top of two steel tubes of the steel truss beams (Figure 1.2 and Figure 1.3).

Halkapınar Gymnasium was designed by Yuksel Project International Corporate Company. Seismic isolators were used by the designers due to the high levels of column responses occurred during earthquake simulations. Analysis results of different seismic isolator types are aimed in this thesis by using and developing the model created by Yuksel Project.

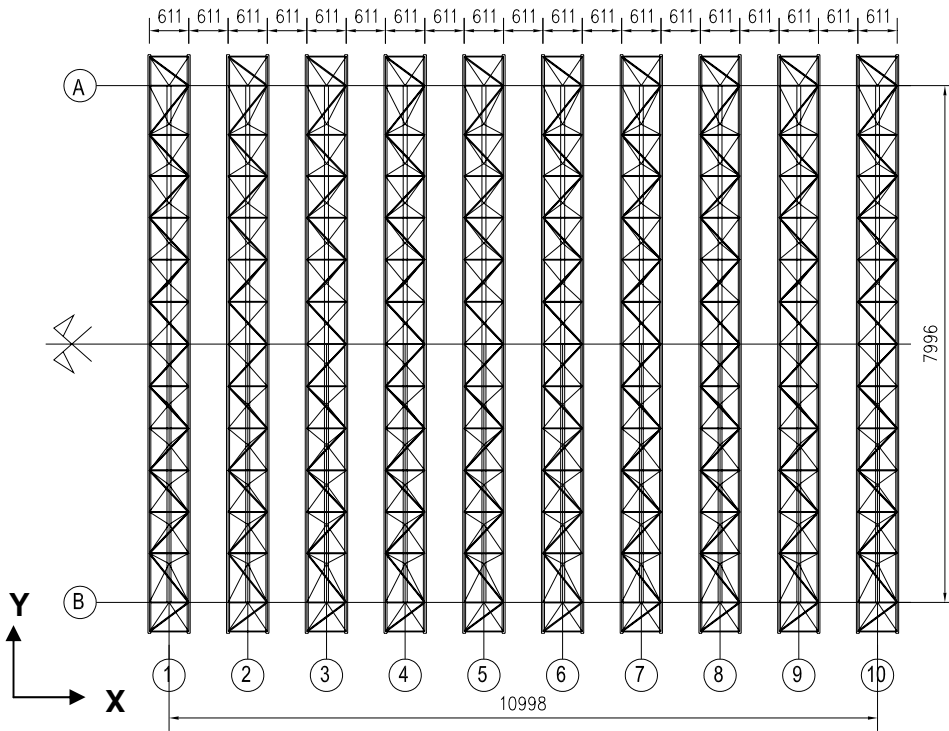


**Figure 1.2** Steel Truss Beams Key Plan (Dimensions are in mm)

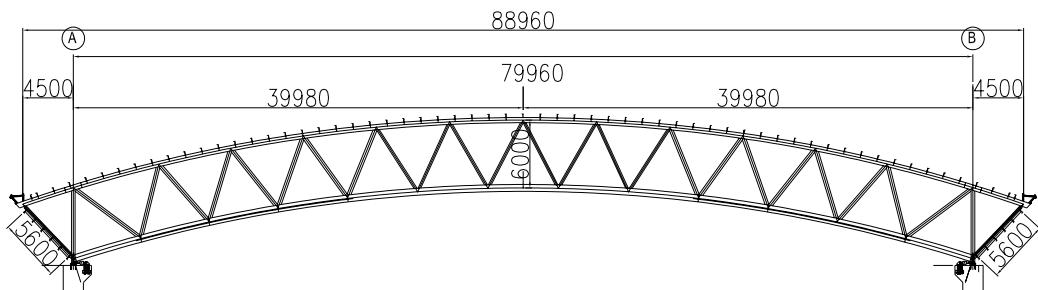


**Figure 1.3** Steel Truss Beams Cross Section (Dimensions are in mm)

Elastomeric bearings with viscous dampers were chosen by the designers as the seismic isolators for the roof of the gymnasium in order to decrease support displacements and earthquake forces. The isolation pattern was set up on both sides of the support of the gymnasium's roof. Viscous dampers are installed for

both horizontal directions as X and Y plan directions respectively. 10 piers on one side of the roof are provided as supports for roof of the structure. Therefore, there are total 20 elastomeric bearings and 40 viscous dampers on top of structure piers. Structural system details are explained in section 2.1 (System Details) by illustrations.

## **1.1 LITERATURE SURVEY**

### **1.1.1 General**

The idea that a structure can be protected from the damaging effects of earthquakes by uncoupling the structure from the ground is not a new technique considered by human beings. There was no link between the column root and the base in timber – frame buildings in valleys of Yellow river and Yangtze rivers (the birthplace of the Chinese culture) in the Neolithic Age. Zhiping, Z. [3] stated that the columns of timber – frame buildings were placed on the stone bases. The author indicated that the connection between the column root and the base relies on gravity and friction like a rubber pad or a ball bearing which allow small deformation but not subjected to bending moment during ground excitations, so that, earthquake energy could be absorbed and released by column root, by preventing the timber – frame from vibration.

In addition to the loads due to the effects of gravity, earthquake loading must be considered when designing structures located in seismically active areas. The philosophy in the conventional seismic design is that structure is designed to resist the lateral loads corresponding to wind and small earthquakes by its elastic action only, and the structure is permitted to suffer damage but not collapse while it is subjected to a lateral load associated with moderate or severe seismic events. For that reason, plastic hinges must be developed in order to dissipate the seismic

energy. The design method based on this philosophy is acceptable to account for the needs for both economic consideration and life safety. However, the development of the plastic hinges relies on the large deformation and high ductility of a structure. The more ductility a structure requires the more damage it suffers. On the other hand, some structures constructed with high investments by the governments and they must remain to function after a major earthquake. Nevertheless, the life-safety based design philosophy is not appropriate for these structures, because serviceability of these structures would probably be lost after a severe earthquake. These structures should be capable to deal with large displacements and accelerations so that they can maintain their functions when excited by a severe ground motion.

Seidensticker [4] stated that the use of seismic isolation as an earthquake hazard mitigation strategy for structures is rapidly receiving interest throughout the world. In addition, there is a growing use of seismic isolation throughout the world for critical facilities such as hospitals, emergency facilities, and buildings with very high-cost equipment (e.g., computers) and as a strategy to reduce loss of life and expensive equipment in earthquakes. Such a design approach is in complete contrast to the conventional seismic design strategy in which the structure and components are provided with sufficient strength and ductility to resist the earthquake forces and to prevent structural collapses or failure.

The potential advantages of seismic isolation and the recent advancements in isolation-system products already have led to the design and construction of over 200 seismically isolated buildings and bridges in the United States. [5]. The 5 structures listed below employ seismic isolation technologies, as a retrofit.

1. Oakland City Hall, California (retrofit): retrofit utilized 42 lead rubber bearings and 69 natural rubber bearings.

2. San Francisco City Hall, California (retrofit): The two-block-long building was isolated by 530 isolators and shock absorbers.
3. Los Angeles City Hall, California (retrofit): City Hall has been isolated by a mechanical system of isolators, sliders, and dampers employing base isolation technology.
4. Airport International Terminal Building, Antalya (retrofit): 341 lead rubber bearings were used, inserted some pot and sliding bearings. Seismic retrofit was completed without interruption of service in the terminal.
5. The Atatürk International Airport Terminal Building, Istanbul (retrofit): Roof of the structure is supported by 130 Friction Pendulum bearings, placed between the roof frame and the concrete columns that rise 7m above the ground level.

### **1.1.2 Seismic Isolations of Steel Roofs**

Roberto Villaverde and Gilberto Mosqueda [6] presented a report that covers the details of and results from analytical and experimental studies conducted with a small-scale laboratory model to assess the feasibility and effectiveness of seismic roof isolation system. Based on their findings, the report is concluded that the proposed roof isolation system (flexible laminated rubber bearings with viscous dampers) has the potential to become a practical and effective way to reduce earthquake damage in low- and medium-rise buildings.

The authors tested a simple five – storey steel frame with and without the proposed vibration absorber system with a pair of shaking tables under sinusoidal

excitations and a recorded earthquake ground motion (The Mexico City record, because of its nearly sinusoidal form). Due to the limitations in the capacity of the equipment made it impossible to test the experimental model under an excitation that would make its beams and columns undergo inelastic deformations, such a question is explored using instead an analytical model of frame.

An inspection of the results reveals that the proposed roof isolation system substantially reduces the response of the studied frame. In the experimental study, the reduction factors were of the order of 30 percent. In the analytical study, the maximum floor displacements are reduced, on average, by 84, 67, 37 and 41 percent when the ground motion is considered with the scale factors of 0.11, 1.1, 3.3 and 11.0 respectively.

The authors stated that the suggested isolation system could only be effective in buildings for which their roof weight represents a significant percentage of their total weight. Since it has been found in previous studies that effective vibration absorber requires a mass of the order of 7 per cent of the total mass of the building where it is installed, this means that without an added mass the proposed isolation system can only be effective for buildings with up to about 15 stories. At the same time, they stated that buildings should have sufficient clearance to permit the unrestricted motion of the bearings.

Roberto Villaverde [7] also presented an article about a roof isolation system, which is performed insertion of flexible laminated rubber bearing between a building's roof and the columns with the addition of viscous dampers connected between the roof and rest of the building. The author stated that roof isolation system reduces the floor displacements and interstory drifts by as much as 83 percent at the end of his analyses.

The advantages of proposed roof isolation system of the author are as follows:

1. Installation of flexible elements and set of dampers between its roof and the columns that support this roof is simple and practical.
2. Roof space is generally kept free and therefore, it may be used for any other installations.
3. There is no need for the use of restraints to avoid an excessive lateral motion, since the dampers themselves supply such a restraint.
4. No significant weight is added to the existing building and there is little disruption involved during its construction for retrofit of the structures.
5. Elastomeric bearings are stiff at small strains, therefore, they will prevent significant displacements under small wind and earthquake loads. On the other hand, they have a low stiffness at high strains; hence, they will show the required flexibility under severe earthquakes.
6. Laminated rubber bearing with viscous damper is self-storing isolator type even after large shear strains. Therefore, self-centering will be performed with this isolator combination.

In addition to elastomeric bearings and viscous dampers combination, lead rubber bearings and friction pendulum systems are commercially used as seismic roof isolators and there are many investigations on them in the literature.

### 1.1.2.1 Elastomeric Bearings

As Kikuchi and Aiken [8] defined, base isolation is a seismic design concept that affords protection to a structure from the damage caused by earthquake. This is achieved by setting some type of flexible support that shifts the period of the structure away from the predominant period of the ground excitation. Elastomeric bearings are well known isolators among these types of flexible supports. The number of seismic isolation applications using elastomeric bearings has grown considerably in recent years.

Most widely used system for structures decoupling from the horizontal components of the ground motion is elastomeric bearings. Maura Imbimbo and James M. Kelly [9] stated that elastomeric bearings are susceptible to buckling as structural columns. This buckling load of a bearing is determined by a linear elastic analysis. The accuracy of this analysis has been verified through tests conducted at the Earthquake Engineering Research Center (EERC). Many experiments were performed to decide the mechanical characteristics of low shape factor (LSF) bearings. These experiments showed that LSF elastomeric bearings bolted to their endplates showed an increase in shear force carrying capacity at large shear strains. This feature of the elastomeric bearings provides shear resistance for bearings subjected to large deformations. Therefore, a very high safety factor is provided against failure under earthquake loads that exceed the design level. Using this feature of isolators would be invaluable for structural engineers for use in highly seismic areas.

The authors also stated that bearing connection to the superstructure is an important factor when analyzing a bearing's behavior. There are two types of commonly used connection: first one is the dowel-type connection for which the bearing is not fixed to the foundation; and the second one is the bolted-type connection for which the bearing is bolted to end plates (Figure 1.4). Dowel-type

bearings are very susceptible to failure while bolted bearings show large horizontal strains without failure.

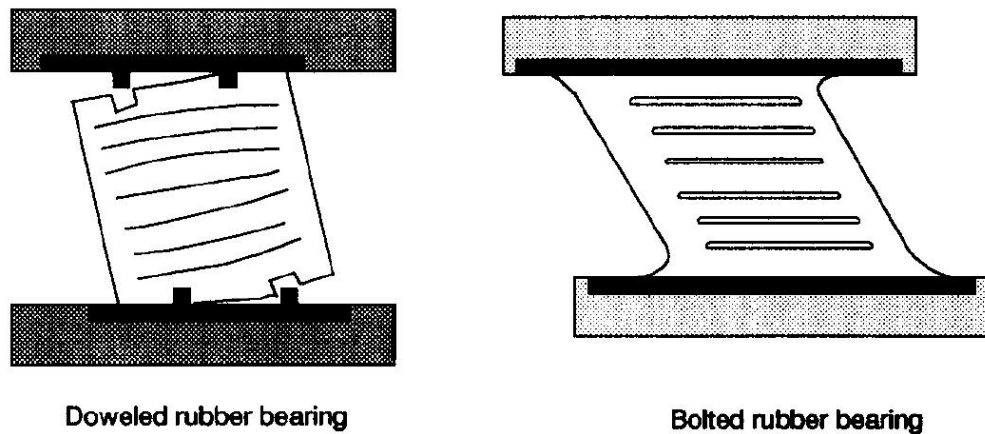


**Figure 1.4** Behaviors of Doweled & Bolted Rubber Bearings At Large Shear

Strains [9] (From *Journal of Engineering Mechanics*)

Imbimbo and Kelly [9] carried out an experiment research at EERC. They performed monotonic shear tests consisted of monotonic horizontal loading conducted an axial loads of  $P = 0$  and  $P = 78.5$  kN. They investigated that the horizontal stiffness of the bearing decreases as the horizontal displacement increases, whereas for high shear strains, the horizontal stiffness increases (Figure 1.5). This stiffening property allows the bearing to be subjected to large deformations without failure. Dowel-type bearings fail before reaching this feature of strain-induced stiffening. Strain – induced stiffening effect is not subject of the this study, but, it is stated that the presence of carbon-black fillers and the additional shear strain due to compression and bending are two main factors which control this effect according to the authors.

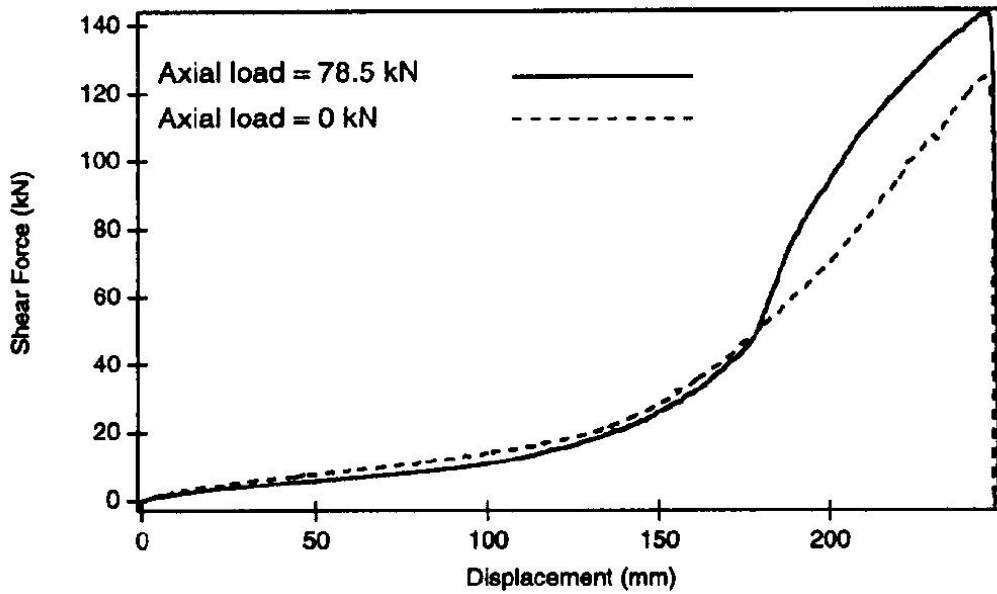


**Figure 1.5** Monotonic Shear Loading Test for  $P = 0$  and  $P = 78.5$  kN [9] (From *Journal of Engineering Mechanics*)

The shape factor,  $S$ , is defined like that it is the ratio of the loaded area to the force-free area for a rubber layer. For example, a square pad of side dimension  $a$  and thickness  $t$ ;  $S = (a \times a) / (4 \times a \times t) = a / (4 \times t)$ . Experiment results show that bearings with high shape factors (generally  $S > 20$ ) perform well in the horizontal direction, while bearings with low shape factor (LSF, generally  $5 < S < 20$ ) perform well in both the horizontal and vertical directions.

Koh and Kelly [10] and Kelly [11] developed linear elastic relationship to predict the buckling load of an elastomeric bearing in case of material nonlinearity. The shear modulus is replaced by a shear modulus-shear strain relationship for the nonlinear elastic response of the rubber, the shear strain being the average shear strain of the bearing due to the compression and bending. They used the following expression for the horizontal stiffness in the linear elastic model:

$$K_H = (G \times A_S / h) \times (1 - P^2 \times (P_S \times P_E)) \quad (1.1)$$

where

$$P_S = G \times A_S = G \times A \times (h / t_r) \quad (1.2)$$

represents the shear stiffness of the bearing and

$$P_E = \pi^2 \times E \times I_s / h^2 = (\pi^2 / h^2) \times E_c \times (I / 3) \times (h / t_r) \quad (1.3)$$

represents the Euler load (the buckling load when shear deformation is neglected) of the bearing. Buckling load:

$$P_{crit} = \sqrt{(P_S \times P_E)} \quad (1.4)$$

where  $G$  is the shear modulus of the rubber,  $A$  is the cross sectional area of the bearing,  $h$  is the total height of the bearing,  $t_r$  is the total height of the rubber,  $I$  is the moment of inertia of the bearing cross section,  $E_c$  is the effective compression modulus provided by  $E_c \approx 6 \cdot G \cdot S^2$  for a circular pad [9] and  $S$  is the shape factor of the bearing. In case of material nonlinearity,  $G$  can be replaced by:

$$G = G(\gamma) \quad (1.5)$$

This can be determined by experimental data.

### 1.1.2.2 Viscous Dampers

Viscous dampers have been widely used in the military and aerospace industry for many years and they have recently been adapted for structural applications in civil engineering. A fluid viscous damper generally consists of a piston within a

damper covering filled with a compound of silicone or similar type of oil, and the piston may contain a number of small orifices through which the fluid may pass from one side of the piston to the other. Thus, fluid viscous damper dissipate energy through the movement of a piston in a highly viscous fluid by the way of fluid orifice. [12]

Jenn-Shin Hwang [13] presented the ideal force output of a viscous damper with an equation:

$$F_D = C \times |\dot{u}|^\alpha \times \text{sgn}(\dot{u}) \quad (1.6)$$

Where  $F_D$  is the damper force,  $C$  is the damping constant (experimentally determined),  $\dot{u}$  is the relative velocity between the two ends of the damper, and  $\alpha$  is the exponent between 0.1 and 1.0 for seismic applications; And  $\text{sgn}(\bullet)$  is the signum function. The damper with  $\alpha = 1$  is called a linear viscous damper in which the damper force is proportional to the relative velocity. The dampers with  $\alpha$  larger than 1 have not been seen often in practical applications. The damper with  $\alpha$  smaller than 1 is called a nonlinear viscous damper which is effective in minimizing high velocity shocks. Figure 1.6 shows the force – velocity relationships of the three different types of viscous dampers. This figure demonstrates the efficiency of nonlinear dampers in minimizing high velocity shocks. For a small relative velocity, the damper with a  $\alpha$  value less than 1 can give a larger damping force than the other two types of dampers.

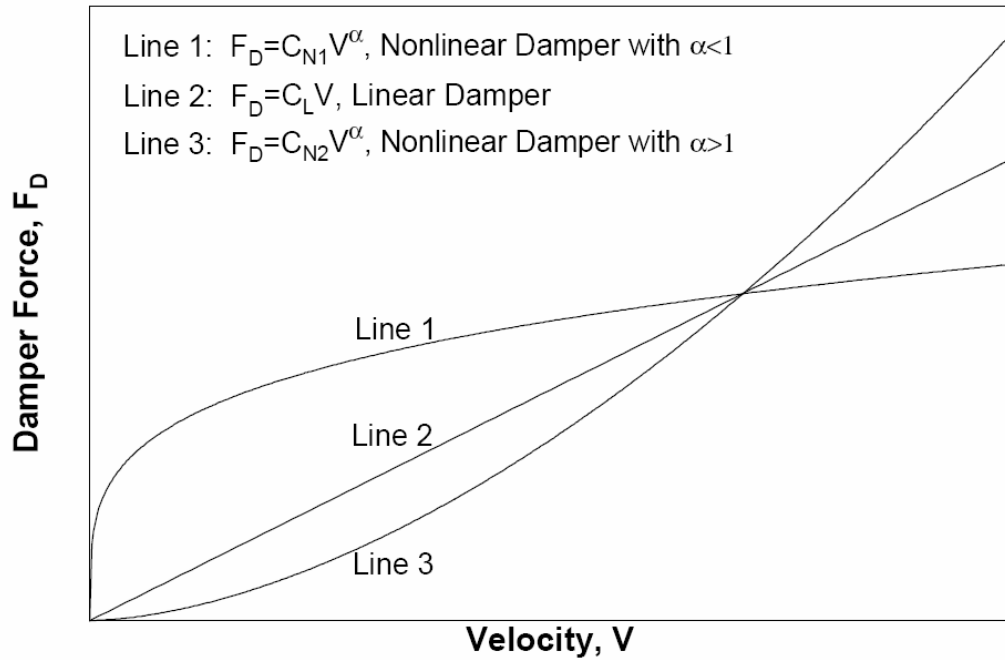


**Figure 1.6** Force-Velocity Relationships of Viscous Dampers [13] (From National Science Council)

Figure 1.7 (a) shows the hysteresis loop of a pure linear viscous behavior. The loop is a perfect ellipse under this circumstance. The absence of storage stiffness, which is needed for restoring force, makes the natural frequency of a structure incorporated with the damper remain the same. This advantage will simplify the design procedure for a structure with supplemental viscous devices. However, if the damper develops restoring force, the loop will be changed from Figure 1.7 (a) to Figure 1.7 (b). In other words, it turns from a viscous behavior to a viscoelastic behavior.

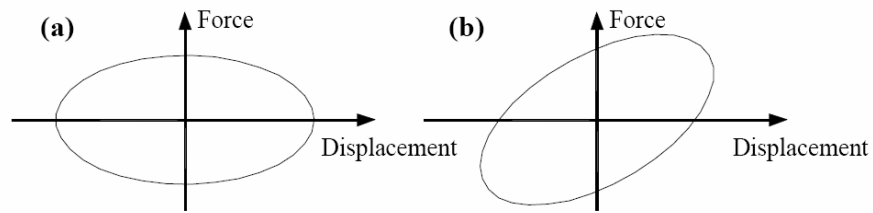


**Figure 1.7** Hysteresis Loops of Dampers with (a) Pure Viscous and (b) Viscoelastic Behavior [13] (From National Science Council)

### 1.1.2.3 Lead Rubber Bearings

Among the laminated rubber bearings, the natural rubber bearing (NRB) which uses natural rubber material has flexibility and small damping. Lead rubber bearing (LRB) is composed of an inserted lead plug in the NRB to provide hysteretic damping. [14]

This type of bearing was first invented in New Zealand in 1975 [15, 16] and Naeim and Kelly [17] stated that it has been widely used in New Zealand, Japan and the United States and buildings isolated with Lead-Plug Bearings performed well during the 1994 Northridge and 1995 Kobe earthquakes.

Buckle, Constantinou, Dicleli and Ghasemi [18] stated that lead-rubber isolators are kind of elastomeric bearings having an energy dissipating central lead core at high displacements of seismic movements. This type of bearing has the same properties for rubber and steel shims vulcanization, except from central lead core. Rubber layers provide horizontal flexibility and steel shims both vertical stiffness and confinement for lead core. In fact, lead core prevents the movement of the superstructure under service loads, on the other hand, lead yields and dissipates seismic energy subjected to the superstructure under seismically

induced lateral displacements. Once the lead core yields, isolator becomes very flexible in the horizontal direction and it absorbs excess energy.

I.N. Doudoumis, F. Gravalas and. Doudoumis [19] describes the bearing's parameters that describe the lateral force – displacement bilinear law are the initial elastic stiffness  $K_u$ , the yielded stiffness  $K_d$ , the characteristic strength  $Q_d$  and the lateral design displacement  $D_d$ . The authors denoted that these properties can also be predicted with remarkable accuracy by using simple analytical formulas, except from the initial elastic stiffness  $K_u$  value which is mainly a function of the fabrication details of the bearing and especially of the confinement of the lead core.

As Yılmaz, Booth and Sketchley [20] indicated, while rubber provides improving load carrying capacity, lateral flexibility and re-centering to the isolator, the lead plug provides required damping and lateral restraint at small displacements for wind or minor earthquake loads.

According to Ryan and Chopra [21], design of elastomeric or lead – rubber bearings is controlled by the expected lateral deformation and axial forces in the bearings. The lateral design is a transition process between flexibility, stability, displacement capacity, and energy dissipation capacity. Although isolation systems are highly nonlinear due to energy dissipation parts of isolators such as high damping fillers or lead cores [22], code methods estimating the lateral deformation depend on equivalent – linear analysis [23].

Ryan, Kelly, and Chopra [24] observed that the yield strength of lead – rubber bearings has also been observed to vary with axial load, such that a lightly loaded bearing may not achieve its theoretical strength. For example, Hwang and Hsu [25] studied on a three – story structure with isolated by lead rubber bearings and the structure was subjected to triaxial ground excitations. They observed that the

bearings isolating heavily loaded columns reached much greater strength and energy dissipation capacity than identical bearings isolating lightly loaded exterior columns.

Effective stiffness according to the bilinear law is defined as follows:

$$K_{\text{eff}} = K_2 + Q / D \quad D \geq D_y \quad (1.7)$$

$D_y$  is the yield displacement. Effective period is given by:

$$T = 2 \times \pi / \sqrt{(w_0^2 + \mu \times g / D)} \quad (1.8)$$

where  $\mu = Q / W$  and  $w_0^2 = \sqrt{(K_2 \times g / W)}$ . The effective damping for  $D \geq D_y$  is defined to be:

$$\beta_{\text{eff}} = 4 \times Q \times (D - D_y) / (2 \times \pi \times (K_2 \times D + Q) \times D) \quad (1.9)$$

where  $D_y = Q / (K_1 - K_2)$  and as a general rule of thumb, elastic stiffness  $K_1$  is taken as  $10 \times K_2$ , so that  $D_y = Q / (9 \times K_2)$ , and as a result [17]:

$$\beta_{\text{eff}} = 4 \times Q \times (D - Q / (9 \times K_2)) / (2 \times \pi \times (K_2 \times D + Q) \times D) \quad D \geq D_y \quad (1.10)$$

#### 1.1.2.4 Friction Pendulum System Isolators

Buckle, Constantinou, Dicleli and Ghasemi [18] state that friction pendulum bearings are sliding – based seismic isolators. A typical friction pendulum isolator composed of stainless steel concave spherical plate, an

articulated slider and a housing plate (Figure 1.8). The authors also state that the side of the articulated slider in contact with the concave spherical surface is coated with a low-friction composite material. Despite this side of the slider, the other side of the slider surface is also spherical, but coated with stainless steel and sits in a spherical cavity also coated with low – friction composite material.

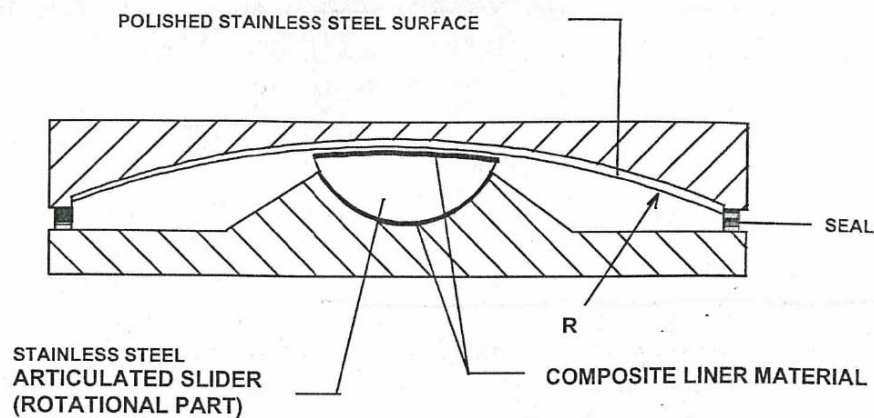


**Figure 1.8** Friction Pendulum Isolator [18] (From MCEER, Federal Highway Administration)

The frictional pendulum system (FPS) has become a widely accepted device for seismic isolation of new buildings, bridges and industrial facilities, as well as for the retrofit of existing structures [26]. The demand for this device depends on the simplicity of the principles that govern its behavior and the self-centering action due to the concavity of the sliding surface. During an earthquake, the slider moves upward on the spherical surface and lifts the structure and dissipating energy by friction between the spherical surface and the slider. Almazàn and Llera [27] denoted that the stainless steel slider is usually cover by a resistant Teflon layer for keeping frictional forces relatively low, assuming a friction coefficient  $\mu = 5\% -10\%$ .

The earthquakes with long predominant periods often produce significant displacement responses in the isolator of base – isolated structures. In view of this, an advanced isolator called the multiple friction pendulum system (MFPS) has been proposed to accommodate large displacements induced by earthquakes with long predominant periods [28]. As shown in Figure 1.9, the MFPS isolator consists of two concave surfaces and a specially designed articulated slider, which is located between these two concave surfaces. Tsai, Chen W.S., Chiang and Chen B.-J. [29] indicated that the displacement capacity for the MFPS isolator is twice that of the traditional FPS isolator with a single concave surface of identical plan dimensions. In addition to this, they stated that the bending moment induced by the sliding displacement for the MFPS isolator is half that of FPS isolator. Furthermore, fundamental frequency of the MFPS isolator is lower than that of the FPS of the same plan size due to the series connection of the doubled sliding surfaces. Hence, the MFPS isolator can be considered to be a much more effective tool for reducing the seismic responses of structures when compared to the traditional FPS isolator. However, the MFPS isolators are out of the scope of this thesis.

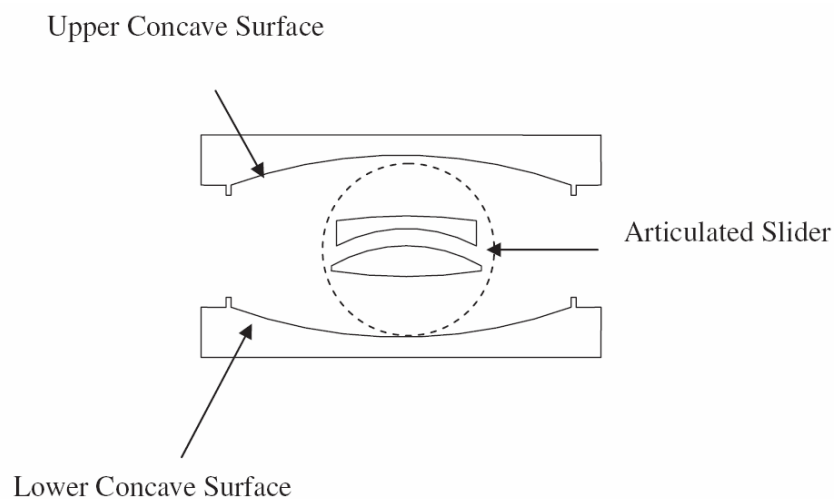


**Figure 1.9** Multiple Friction Pendulum System (MFPS) [28] (*From ASME, Pressure Vessels and Piping Conference*)

The essential properties of sliding isolators are period shift, energy dissipation and the restoring mechanism. Curved surface of FPS incorporates all of these in a single unit [30]. Almazàn and Llera [31] concatenated the most remarkable features of FPS are the simplicity of the system and repeatability of its cyclic behavior, the stability of physical properties and durability, reduced height, the separation between the restoring and dissipating action and the control of the fundamental vibration period and deformation capacity by simple geometric properties.

The restoring force developed by the concave surface of the isolator is given:

$$F = W \times D / R + \mu \times W \times (\text{sgn}\dot{D}) \quad (1.11)$$

R is the radius of curvature. The first term is the restoring force due to the rise of the mass, proving a horizontal stiffness [17]:

$$K_H = W / R \quad (1.12)$$

An isolated structure period T is given:

$$T = 2 \times \pi \times \sqrt{(R / g)} \quad (1.13)$$

Isolated structure period is independent of the carried mass. The second term in the restoring force equation is the friction force between the slider and the concave surface. On the other hand, the coefficient of friction  $\mu$  depends on pressure p and sliding velocity  $\dot{D}$ .

Effective stiffness of friction pendulum system is given:

$$K_{\text{eff}} = W / R + \mu \times W / D \quad (1.14)$$

The damping produced by friction at the sliding surfaces can be given as:

$$\beta = (2 / \pi) \times (\mu / ((D / R) + \mu)) \quad (1.15)$$

### 1.1.3 Bilinear Modeling

Melanoma and Frailly [32] describe characterization of the isolation systems with three different analytical models. These are Elastic Viscous, Bilinear Hysteretic and Wen's Model. On the other hand, considering non – linear isolation systems, most of them may be approximated using bilinear models. Under cyclic loading, the force – displacement law may then be represented by parallelogram – shaped hysteresis loops. Laminated rubber bearings with a lead core, steel energy dissipaters and lead – extrusion dampers demonstrate such a behavior. Even several systems with friction elements, such as friction pendulum systems, variable frequency pendulum isolators and resilient – friction base isolators, may be represented by bilinear models [33].

Breton, Infant, Castellán and Nicosia [34] studied on self – centering capacity of seismic isolation systems and their systems are based on bilinear – force displacement relation. The authors indicate that most of the current isolation devices exhibit a nearly bilinear behavior (Figure 1.10). An ideal bilinear model is fully characterized by three main parameters. These are the strength force  $Q$ , the post – yield stiffness  $K_p$ , and the yield displacement  $u_y$ . The system strength  $Q$  is usually expressed as a portion of the structural weight  $W$  supported by the isolator. The authors stated that typical  $Q$  values range between 3 and 12% of  $W$ , while typical values of the yielding displacement range from 0.2 to 0.5mm for sliding bearings to 10-50mm for LRB and hysteretic bearings. While the initial

stiffness has in general a small effect on the behavior of the isolation system subjected to moderate and strong ground excitations, the post – yield stiffness is an important parameter that is directly related to the self – centering capacity of the device.

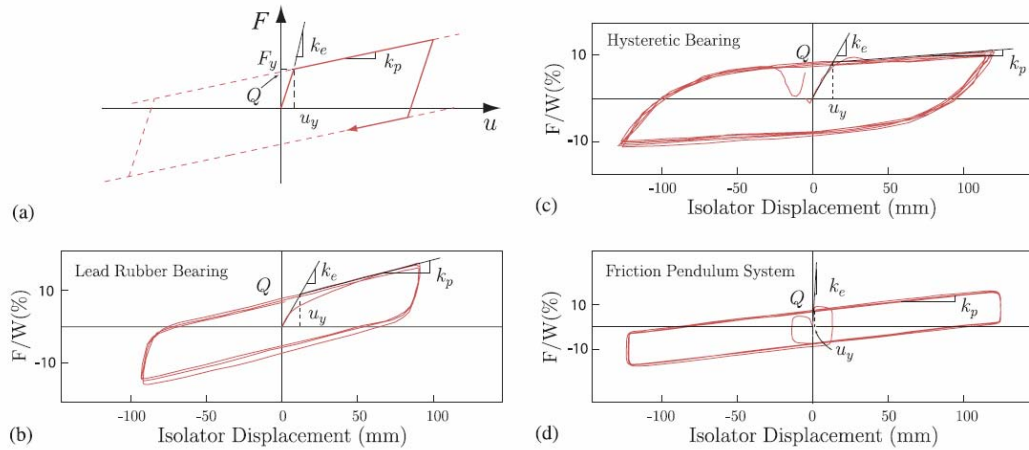


**Figure 1.10** Force – Displacement Responses: (a) idealized bilinear model; (b) lead – rubber isolator; (c) hysteretic bearing; and (d) friction pendulum system

[34]. (From *Structural Control and Health Monitoring*)

Erkus and Johnson [35] performed an analysis based on a sample control design for the base – isolated benchmark building with bilinear bearings (e.g. lead – rubber bearings). The seismic isolation of system consists of 31 rubber bearings and 61 lead – rubber bearings in their analysis. The rubber bearings were modeled with linear stiffness and linear damping properties. The lead – rubber bearings were modeled as with bilinear stiffness and linear damping properties. The bilinear stiffness of the lead – rubber bearings was further modeled as linear stiffness and elastic – perfectly plastic stiffness where linear behavior

corresponded to the rubber and the elastic – perfectly plastic behavior corresponds to the lead.

Seismic isolation design stage requires careful attention to the parameters of the isolators controlling overall behavior of isolated structures. Thus, more reliable parameters of the isolator are required at a preliminary seismic isolation design stage. Park and Otsuka [36] studied on the optimal yield level of bilinear seismic isolation devices. The authors denoted that one of the most important parameters is  $Q_y / W$  (the ratio of the yield force of the isolator  $Q_y$ , and the total weight of the structure  $W$ ) and this parameter is largely related to the structural responses and the absorbing energy of isolators under severe earthquake loadings.

## **1.2 OBJECT AND SCOPE**

Seismic isolation is widely used throughout the world. Applications of this technique have an increasing rate for different structure types, like buildings, bridges, steel – truss roof systems, etc. There are also many applications of seismic isolation in Turkey and Halkapinar Gymnasium is one of these isolated structures. Elastomeric bearings with viscous dampers were chosen isolator types by the designers installed under the bearings of the steel – truss roof of the gymnasium.

Investigation of existing roof isolation system is the first main objective of this study. SAP2000 was used as software tool in the analysis. Because of the non – linearity's of isolators, seven different time – history analysis were included to simulate ground excitation. Structural modal periods, roof support displacements, column moments and shear forces were main parameters for all comparisons in the investigations of analysis. How different isolator types change the system response is the other main objective of this study. Therefore, every analysis is compared with previous analysis results.

Chapter 2 covers investigation of elastomeric bearing and viscous damper's effects on the structural response by changing the isolator support combinations. Hence, effective isolator combination was tried to find by comparing each combination and non – isolation condition as well.

It is also thought that there may be used other isolator types such as lead rubber bearing and friction pendulum systems for seismic isolation of Halkapınar Gymnasium. Therefore, Chapter 3 covers additionally these two types isolator analysis. Design stages and parameters used in the SAP2000 analysis were presented. Due to the non – linear isolation systems using bilinear models, effects of bilinear modeling are also included in this chapter. Firstly, elastic stiffness was taken as constant and different post – yield stiffness values were taken. Then, post – yield stiffness value was taken as constant and different elastic stiffness values were taken.

Finally, the most effective and economic seismic isolator is decided by comparing all results for seismic isolation of Halkapınar Gymnasium steel – truss roof. All comparisons are investigated to find the most effective isolator type in Chapter 4.

## **CHAPTER 2**

### **EFFECTS OF ROOF SUPPORT CONDITIONS ON SYSTEM BEHAVIOR**

#### **2.1 SYSTEM DESCRIPTION**

There are 10 steel truss beams on the roof of the main court of Halkapınar gymnasium (Figure 1.2 & 1.3). All structural members are composed of concrete except from the steel truss roof. C30 and St 37.2 are the chosen material classes for concrete and steel members, respectively. Total weight of the steel truss roof is 940 tons and roof support level is 21.20m from the ground level. Gymnasium has 3 leveled floor stands for tribunes. These platforms are at 3.90m, 8.10m and 15.90m levels from the ground. Mat foundation was designed as a foundation type.

Seismic isolation technique was used to decrease the structural responses occurred due to time – history analyses. Column moments and shear forces are compared with the non – isolated structure at the end of each analysis in this and following chapters. This investigations show that non – isolated structure cause high stresses levels in the columns being supports of the truss roof.

İzmir Halkapınar Gymnasium was located on an area having 110m x 190m in plan. Structure is composed of 15 main parts and a steel roof system (Figure 2.1). All parts are separated from each other by expansion joints.

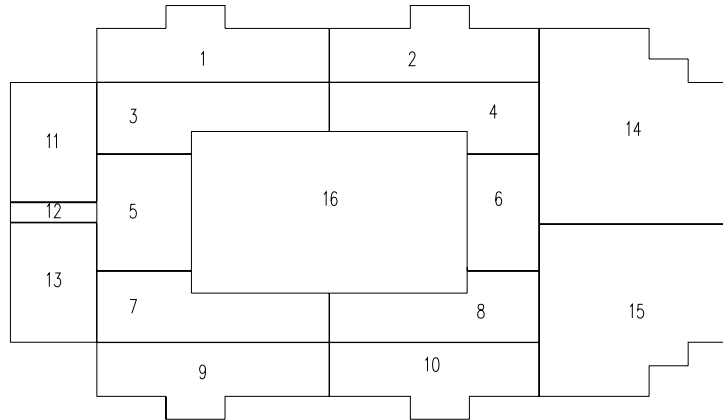


**Figure 2.1** Main Parts of Halkapınar Gymnasium

- |                  |                                     |
|------------------|-------------------------------------|
| 1, 2, 9, 10, 12  | : Entrance of the structure         |
| 3, 4, 5, 6, 7, 8 | : 3 leveled floors of the tribunes. |
| 11, 13           | : workout halls                     |
| 14, 15           | : car park area                     |
| 16               | : roof of gymnasium                 |

Actually, there are three types of column dimensions for the structure. First one is 80cm x 180cm columns located on the axes of the supports of the roof and the columns under tribune platforms (3, 4, 5, 6, 7, 8) have 70cm x 70cm dimensions and 80cm x 80cm dimensions (1, 2, 9, 10). Column application plan is given in Figure 2.2. In Figure 2.2, continues lines show the expansion axes between columns. Due to columns under platforms 3, 4, 5, 6, 7 and 8 are only to carry platform dead and live loads; these columns (70 x 70) were not used in 3D model. On the other hand, parts of the gymnasium 1, 2, 9, and 10 consists of support columns (80 x 80 & 80 x 180) of the roof, therefore, these columns were included in the 3D model analyses.

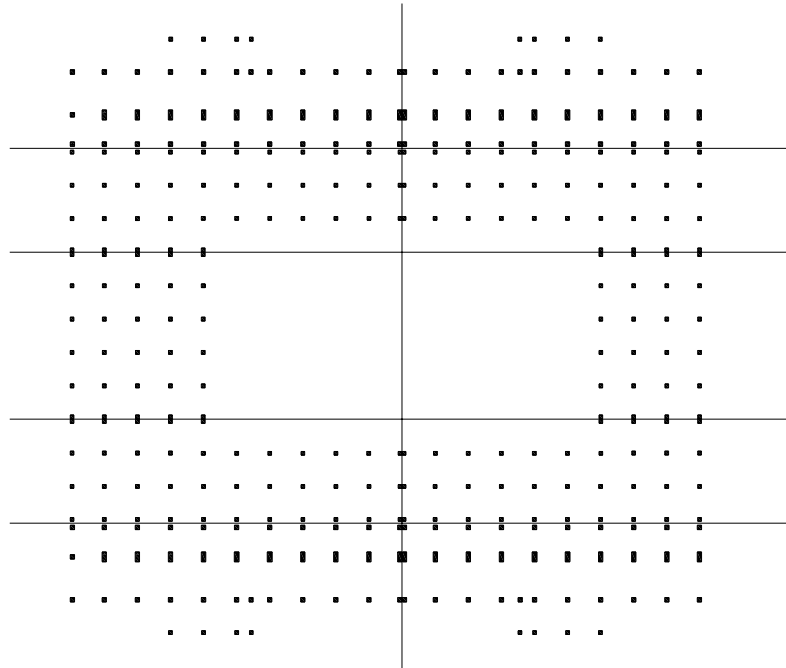


**Figure 2.2** Columns Application plan

When construction stages of the structure is considered, firstly, concrete members of the structure had been cast – in place and then, steel truss beams were assembled in the field and finally, they were installed to the supporting piers. (Figure 2.3)



**Figure 2.3** Installations of Steel Truss Beams

Roof of the gymnasium is composed of steel truss – beams. Each steel truss – beam has 80m span length in plan and each of them is supported by piers with (2x6.11) 12.22m distance interval. Therefore, there are total 10 steel truss – beams on the roof of the structure. As steel truss – beams having two longitudinal steel tubes on the top head and one longitudinal steel tube at the bottom head, they have triangular cross section. There are several interring truss members between top and bottom head of steel truss – beam and these members provide spatial structure to the truss – beams. Height of the triangular cross section is 6m. Distance between two steel tubes at the top head is 6.11m. Purlins are composed of lightweight profiles. (Figure 1.2 & 1.3).

The entire structure except the link elements was modeled with a frame/shell finite element (FE) system (Figure 2.4).

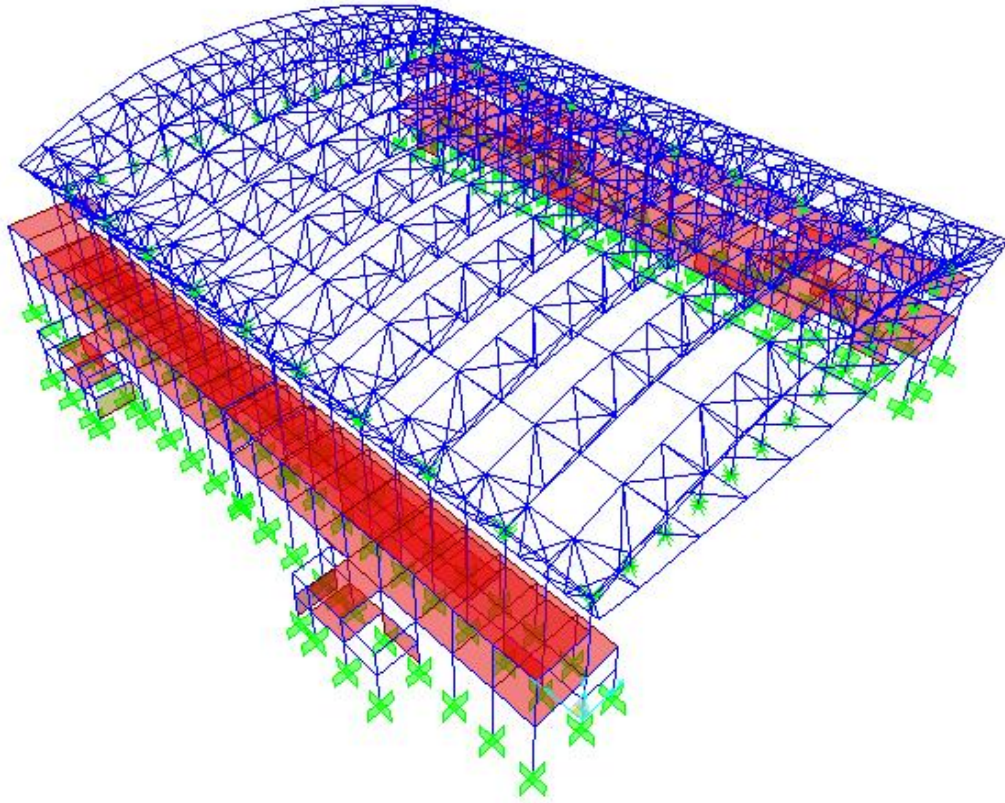


**Figure 2.4** Halkapinar Gymnasium Finite Element (FE) Model

## **2.2 EXISTING ROOF ISOLATIONS**

Steel roof of the gymnasium is separated from the superstructure by seismic isolators. There are 10 main steel truss beams of the roof and each of roof supports is isolated by elastomeric bearing (EB). Furthermore, viscous dampers (VD) are installed for each direction (two pieces at each support) to decrease the earthquake force effects and displacements. These effects will be detailed in the following sections. Therefore, there are 20 EB's and 40 VD's on columns.

The vertical loads, which are mostly due to the dead load of the roof, are carried by normal rubber bearings providing a little amount of energy dissipation for horizontal loads during seismic event (about 5%).

High amount of energy is dissipated by fluid damper (FD) elements anchored in the longitudinal and transversal directions to the piers of the structure.

Two kinds of analysis were performed by the software. First a linear modal analysis was made in order to calculate the principal vibration modes of the structure and its general response behavior. Then the whole structure was analyzed throughout a step-by-step non linear calculation where the non linearity was given by the FD dissipating elements.

The whole structure was modeled and the dynamic analysis was performed with the SAP2000 calculation program.

### **2.2.1 Elastomeric Bearings**

The elastomeric bearings transfer the vertical loads of the superstructure's roof and partially transmit the horizontal loads. The superstructure is in fact seismically isolated through the adoption of fluid dampers, which dissipate energy during a seismic event.

#### **2.2.1.1 Qualities and Specifications of Materials**

##### **2.2.1.1.1 Steel**

The reinforcing plates of the bearings were made of rolled steel EN 10025 types S 275 JR, with the following properties:

- Tensile strength	$\geq 430 \text{ N/mm}^2$
- Yield stress	$275 \text{ N/mm}^2$
- Impact test at $-20^\circ\text{C}$	$\geq 27 \text{ J}$
- Elongation at break	$\geq 21 \%$

### 2.2.1.1.2 Elastomeric

The elastomeric bearings consisted of natural rubber, with the following mechanical properties:

- Hardness Shore	$60 \pm 5$
- Shear modulus	$0.9 \text{ N/mm}^2$
- Bulk modulus	$2000 \text{ N/mm}^2$
- Elongation at break	$450\%$

### 2.2.1.2 Check of Bearings

The check of bearings was performed according to prEN 1337-3:2004 (5.3.3). The geometrical and mechanical properties, forces acting on bearings and displacements are represented in the next formulas.

#### 2.2.1.2.1 Check of Shear Strains

The maximum shear strain  $\varepsilon_{t,d}$  of the elastomeric should not exceed the value 7.0:

$$\varepsilon_{t,d} = K_L (\varepsilon_{c,d} + \varepsilon_{q,d} + \varepsilon_{\alpha,d}) < 7.0 \quad (2.1)$$

Where:

$$\varepsilon_{c,d} \text{ (design strain due to compressive loads)} = 1.5 V / (G A_r S)$$

$$\varepsilon_{q,d} \text{ (design strain due to horizontal movements)} = v_{xy,d} / h_e < 1.0$$

$$\varepsilon_{\alpha,d} \text{ (design strain due to angular rotation)} = (a^2 \alpha_x + b^2 \alpha_y) t_i / (2t_i^3)$$

$$K_L \text{ (type loading factor)} = 1.0$$

#### 2.2.1.2.2 Check of Reinforcing Plates Thickness

To resist induced tensile stresses under load, the minimum thickness of the reinforcing steel plates is given by the expression:

$$t = (K_p \cdot V \cdot t_i \cdot K_h \cdot \gamma_m) / (A_r \cdot f_y) \quad (2.2)$$

Where:

$$K_h \text{ (factor for induced tensile stresses in reinforcing steel plates)} = 1.0$$

$$\gamma_m \text{ (partial safety factor)} = 1.0$$

$$K_p \text{ (correction factor)} = 1.3$$

#### 2.2.1.2.3 Rotational Limitation Conditional

The rotation and the total vertical deflection  $v_{z,d}$  shall satisfy the following formula:

$$v_{z,d} - (a \cdot \alpha_x + b \cdot \alpha_y) / K_{r,d} \geq 0 \quad (2.3)$$

$$\text{Where } K_{r,d} \text{ (rotation factor)} = 3.0$$

#### 2.2.1.2.4 Buckling Stability

The pressure on elastomeric  $V/A_r$  shall satisfy the expression:

$$V/A_r < 2a \cdot G \cdot S / (3 \cdot h_e) \quad (2.4)$$

### 2.2.1.3 Design Loads

Vertical and horizontal forces acting on the elastomeric bearings were calculated in the dynamic and static analysis of the structure, performed with the SAP2000 software.

The design loads used for the elastomeric bearing check are:

$V_p = 900$  kN (obtained from linear static combination)

$V_1 = 950$  kN (plus vertical compressive load due to seismic action)

$H = 110$  kN (average value between 7 accelerograms of horizontal forces V2 and V3)

#### 2.2.1.4 Calculation of Elastomeric Bearings

##### Bearings Type Algabloc NB 350 X 450 X 152

##### Bearing Dimensions :

Overall Width	a	350	mm
Overall Length	b	450	mm
Edge Cover of Elastomer	c	5	mm
Effective Width	$a_e$	340	mm
Effective Length	$b_e$	440	mm
Number of Inner Elastomer Layers	$n_i$	10	
Thickness of an individual inner layer	$t_i$	11	mm
Thickness of an individual outer layer	$t_i'$	2,5	mm
Number of Reinforcing Plates	$n_r$	9	
Thickness of Reinforcing Plates	t	3	mm
Actual Thickness of Elastomer	$h_e$	110	mm
Overall Thickness of Bearing	h	137	mm

### **Design Loads :**

Vertical Permanent Load	$V_p$	900	kN
Vertical Live Load	$V_l$	950	kN
Vertical Design Load Effect	$V$	1850	kN
Longitudinal Horizontal Load	$H_a$	110	kN
Minimum Vertical Design Load	$V_{min}$	900	kN

### **Displacements and Rotations :**

Maximum Rotation Across the Width b	$\alpha_{a,d}$	0,001	rad
Maximum Rotation Across the Length a	$\alpha_{b,d}$	0,001	rad

### **Elastomer Properties :**

Nominal Hardness		60	Shore A
Shear Modulus	$G$	0,9	N/mm <sup>2</sup>
Bearing Horizontal Stiffness	$K_h$	1,29	kN/mm
Total Displacements Due to Horizontal Loads		85,36	mm
Shape Factor	$S$	8,5	
Effective Plan Area	$A_l$	149600	mm <sup>2</sup>
Reduced Effective Plan Area	$A_r$	149600	mm <sup>2</sup>

### **Strain Check :**

Design Strain Due to Compressive Load	$\epsilon_{c,d}$	2,42	
Shear Strain	$\epsilon_{q,d}$	0,71	< 1 OK
Design Strain Due to Angular Rotation	$\epsilon_{\alpha,d}$	0,13	
Type Loading Factor	$K_L$	1	
Total Design Strain	$\epsilon_{t,d}$	3,26	< 7 OK

### **Reinforcing Plates Thickness Check :**

Factor for Induced Tensile Stresses	$K_h$	1	
Stress Concentration Factor	$K_p$	1,3	
Steel Yield Stress	$f_v$	235	N/mm <sup>2</sup>
Minimum Thickness of Plates	$t_s$	1,5	mm < 3,0mm

### **Limiting Conditions :**

Bearing Vertical Direction	$v_c$	0,49	mm
Rotational Limitation Condition		0,22	mm > 0 OK
Buckling Stability		12,37	< 15,764 OK

### **2.2.2 Modeling of the Link Elements**

The isolation system was provided between the piers and the steel roof of the structure. The static scheme may be described as follows (Figure 2.5)

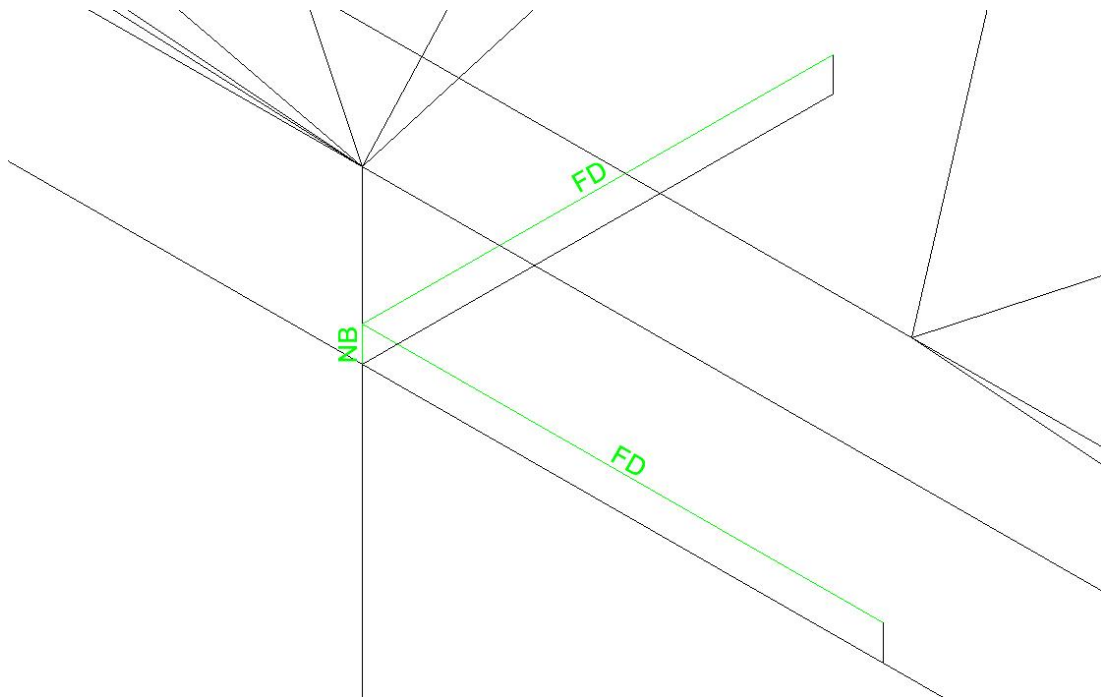


**Figure 2.5** Link Elements

The link elements connecting the roof (superstructure) to the piers were modeled with simple elastic or energy dissipating elements, as described:

The link elements carrying the vertical loads (Rubber bearings) are modeled as simple elastic springs having stiffness in both directions  $K_x = K_y = 1290 \text{ N/mm}$ .

This value can be calculated as follows:

$$\begin{aligned} \text{Rubber bearings have a plan area of rubber } A_r &= 350 \times 450 \text{ mm}^2 \\ &= 157500 \text{ mm}^2 \end{aligned}$$

Shear modulus of rubber compound is  $G = 0,9 \text{ N / mm}^2$

Net height of rubber for each bearing is  $h_g = 110 \text{ mm}$

Horizontal stiffness can be determined as:  $K = A G / h_g = 1290 \text{ N/mm}$ .

The horizontal elements (FD) are modeled with damper units having the following characteristics:

$$F = C v^\alpha, \text{ where}$$

$F$  = axial force acting in FD

$C$  = damping constant = 500kN

$V$  = velocity

$\alpha$  = damping exponent = 0,15

The devices were designed for a maximum velocity of 1m/s. This is equivalent to a maximum force of 500kN. The average load obtained from the time history is 480kN corresponding to a velocity of 0,76 m/s. However, it shall be noted that normally the time history analysis greatly overestimate the velocity. In the time history analysis, the velocity is deducted from the integration of the

motion equations. Direct measurement of the velocity during earthquake normally show lower values of the order of 0,50 m/s in the region considered (no near – fault effect).

### 2.2.2.1 Step by Step Non-Linear Dynamic Analysis

Due to the high non-linear behavior of the FD, the dynamic analysis was carried out using a step-by-step procedure by SAP2000.

Seven functions for ground acceleration were considered acting in the two directions. Table 2.1 shows the names, dates, magnitudes, seismic stations, soil classes, distances from source and peak ground accelerations (PGA) of the earthquakes, which were source for time – history analyses in this study. This data was taken as same as the original design report performed by Yüksel Proje. [37]

**Table 2.1** Seven Response Spectrums Used in Time – History Analyses

Response Spectrum	Date	Earthquake	M <sub>w</sub>	Station	Soil Class	Distance (km)	PGA
290YA	23.11.1980	Campano Lucano	6,9	Sturno	Class A V <sub>s</sub> =1100	32	3.16 m/s <sup>2</sup> (EW)
333XA	24.02.1982	Alkion	6,6	Korinthos- OTE Building	Class C V <sub>s</sub> =234	20	2.25 m/s <sup>2</sup> (N30E)
591YA	26.09.1997	Umbria Marche	5,7	Colfiorito	B	3	2.56 m/s <sup>2</sup> (WE)
879XA	01.10.1985	Dinar	6,4	Dinar Meteoroloji Müdürlüğü	Class C V <sub>s</sub> =234	8	2.67 m/s <sup>2</sup> (SN)
879YA							3.13 m/s <sup>2</sup> (WE)
HSP000	18.10.1989	Loma Prieta	6,9	47524 Hollister - South & Pine	Geomatrix D	28.8 (Cl. to Rupture)	0,371 g
STC090	17.01.1994	Northridge	6,7	90003 Northridge - 17645 Saticoy St	USGS C	13.3 (Cl. to Rupture)	0,37 g

Time-history graphs of these seven functions are as follows. All calculations to get these earthquake loads from the data stated in Table 2.1 were performed by Assoc. Prof. Dr. Kemal Önder Çetin:

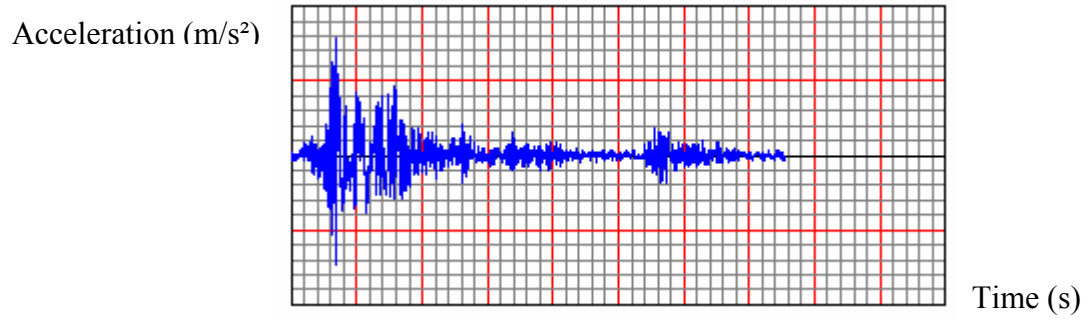


**Figure 2.6** Time-History of 290YA

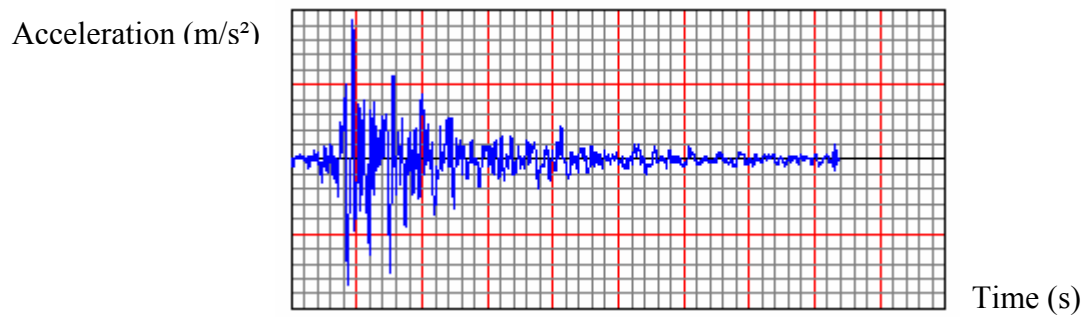


**Figure 2.7** Time-History of 333XA

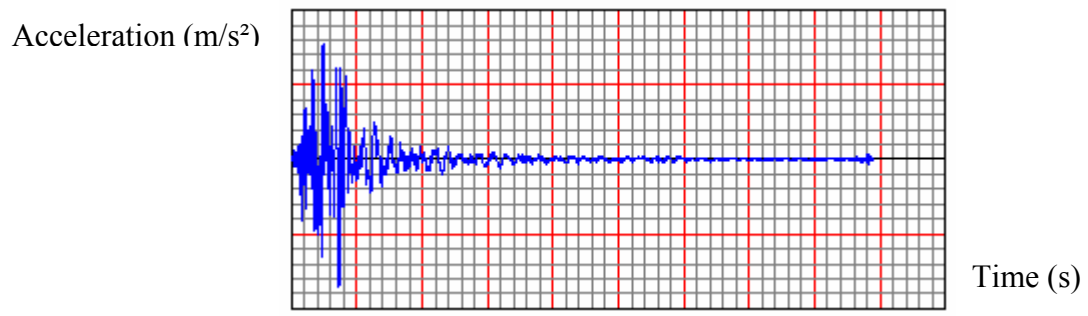


**Figure 2.8** Time-History of 591YA

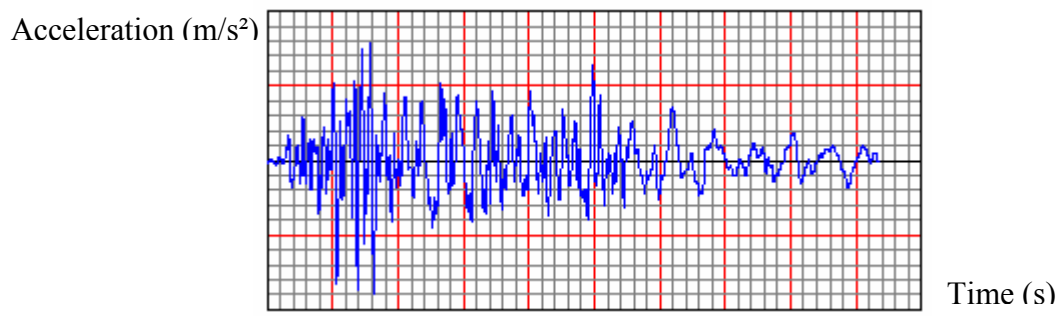


**Figure 2.9** Time-History of 879XA

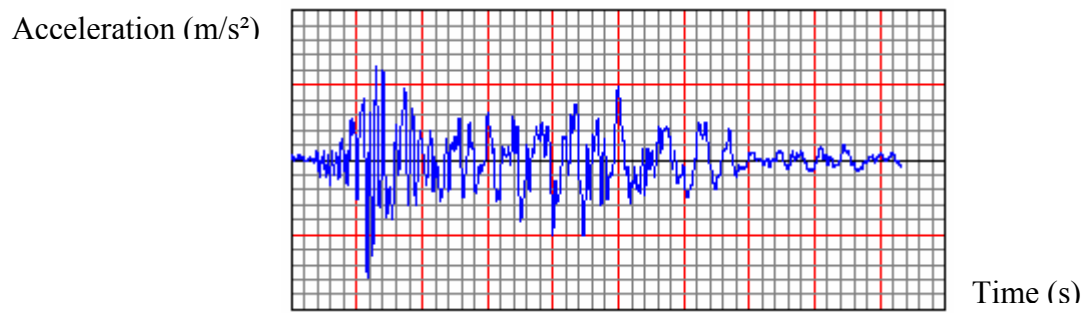


**Figure 2.10** Time-History of 879YA

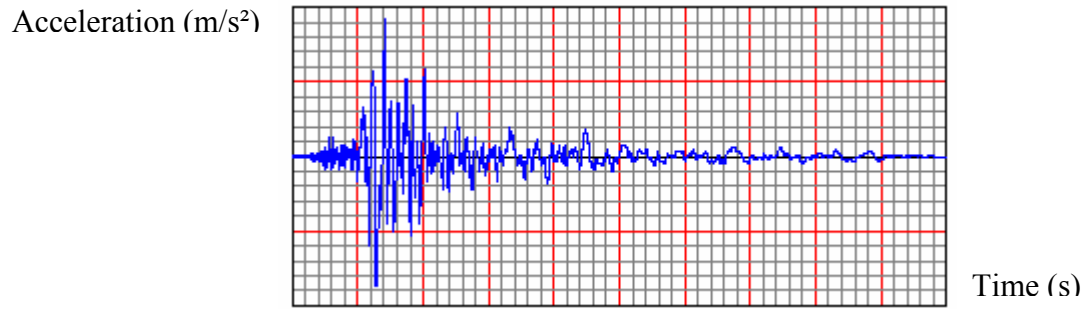


**Figure 2.11** Time-History of HSP000

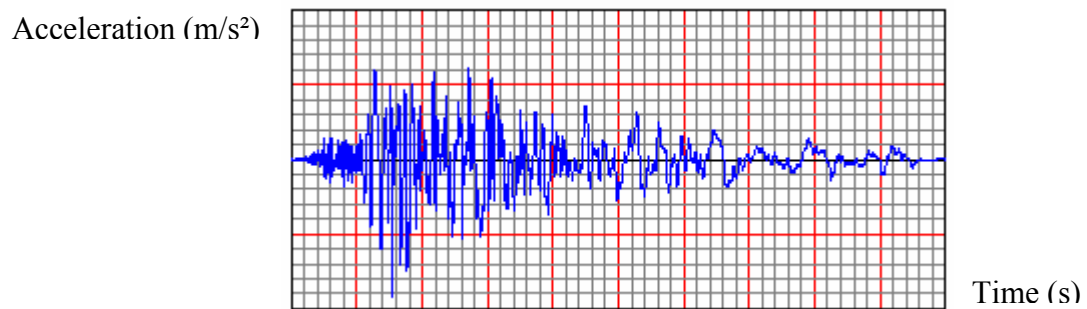


**Figure 2.12** Time-History of STC090

14 time histories were applied to the structure with the combinations in X and Y direction as given in the Table 2.2. Although ASSHTO Guide Specifications for Seismic Isolation Design Guide specifies 100% combination factors for both directions, they were not changed in the analyses to be able to compare analyses results with the original design performed by Yüksel Proje. Designer had followed Turkish Earthquake Code 2006 (Section 2.8.6, Response Quantities of Structural Elements with Principle Axes Nonparallel to Earthquake Directions.) for directional combination rule, because principle axes of some of the elements are not parallel to the orthogonal earthquake directions.

**Table 2.2** 14 Time-History Combinations used in the Model (For Each Direction X and Y).

<b>Time history</b>	<b>Function</b>	<b>Direction</b>	<b>%</b>
290YA_X	290YA	X	100
	290YA	Y	30
290YA_Y	290YA	Y	100
	290YA	X	30
333XA_X	333XA	X	100
	333XA	Y	30
333XA_Y	333XA	Y	100
	333XA	X	30
591YA_X	591YA	X	100
	591YA	Y	30
591YA_Y	591YA	Y	100
	591YA	X	30
879XA_X	879XA	X	100
	879XA	Y	30
879XA_Y	879XA	Y	100
	879XA	X	30
879YA_X	879YA	X	100
	879YA	Y	30
879YA_Y	879YA	Y	100
	879YA	X	30
HSP000_X	HSP000	X	100
	HSP000	Y	30
HSP000_Y	HSP000	Y	100
	HSP000	X	30
STC090_X	STC090	X	100
	STC090	Y	30
STC090_Y	STC090	Y	100
	STC090	X	30

UBC – 97 was applied to scale acceleration records. UBC – 97 states, “*the square root sum of the squares (SRSS) of the 5 percent damped spectrum of the scaled horizontal components shall be constructed for each pair of horizontal ground motions. The motions shall be scaled such that the average value of the SRSS spectra does not fall below 1.3 times the 5 percent damped spectrum of the design basis earthquake (or maximum capable earthquake) by more than 10 percent for periods from 0.5  $T_D$  seconds to 1.25  $T_M$  seconds*”. Therefore,

earthquake records were proportioned such that they do not fall below 1.3 times the 5% damped spectrum of the design basis earthquake by more than 10 percent. Related spectral figures are given in Appendix A.2 performed by Assoc. Prof. Dr. Kemal Önder Çetin.

Scale factors for time – history functions are calculated according to UBC – 97 like this:

$$\lambda = (\text{Nor Normalized Response Spectrum}) / (\text{Normalized Response Spectrum}) \quad (2.5)$$

Time – history analyses can be comparable with normalized response spectrums, performed by Assoc. Prof. Dr. Kemal Önder Çetin, (Appendix A.3) when they are divided by  $\lambda_i$ . Normalized design spectrums,  $S_i$ , can be compared with normalized design spectrum,  $S_D$ , by one by one combination.

$$(\sum \zeta_i S_i) / n > 1.3 \times 0.9 \times S_D \quad T_D < T < T_M \quad (2.6)$$

Where;  $\zeta_i$  = multiplier factor of normalized response spectrum  $S_i$

Scale factors for time – history functions,  $SF_i$ :

$$SF_i = \zeta_i (PGA / \lambda_i) \quad (2.7)$$

Axial forces on the isolators are given in Appendix A.4 at the end of these 14 time-history analysis cases. The maximum values of axial are given in this table for each isolation investigation of this and following chapters.

Local site conditions:

Earthquake Region : 1 (A<sub>0</sub> = 0.40)

Structure Importance Factor : 1.20

Soil Class : 3 (T<sub>A</sub> = 0.15 sec. T<sub>B</sub> = 0.60 sec.)

The peak ground acceleration for all the time histories should be 4.709 m/s<sup>2</sup> (0.40 x 1.20 x 9.81 = 4.709). All the Seven functions used in the dynamic analysis were accordingly amplified (Exp. Function 290YA: 4.709 / 3.16 = 1.49). In the Table 2.3, amplification factors are summarized.

Modal periods of all analyses results were compared with each other in the analyses. Mode shapes of analysis results of this and following chapters are given in Appendix A.5 for first four modes because of that analyses results show similar modal behaviors for higher modes after fourth mode. In addition to this, maximum roof support displacements were also compared. Deformed shapes of the model are given in Appendix A.6 for envelope displacement values of the design isolation case (Two Sided EB+VD) to understand the behavior of the system.

**Table 2.3** Amplification Factors of 7 Time-History Data

N°	Function	Recorded PGA	Units	Multiplying factor	Scaled PGA (m/s <sup>2</sup> )
1	290YA	3.16	m/s <sup>2</sup>	1.4886	4.709
2	333XA	2.25	m/s <sup>2</sup>	2.0907	4.709
3	591YA	2.56	m/s <sup>2</sup>	1.8375	4.709
4	879XA	2.67	m/s <sup>2</sup>	1.7618	4.709
5	879YA	3.13	m/s <sup>2</sup>	1.5029	4.709
6	HSP000	0.371	'g	12.6792	4.709
7	STC090	0.37	'g	12.7135	4.709

## 2.3 DIFFERENT EXISTING ISOLATOR COMBINATIONS

İzmir Halkapınar Gymnasium's steel roof had been isolated by elastomeric bearings (EB) with viscous dampers (VD) in each direction at each support. According to the aim of this study, different seismic isolator types were tried to be investigated, which would be subject of next chapter. Before investigation of different seismic isolator types, existing seismic roof isolation (EB + VD) had been solved. Different isolator combinations on supports were investigated and the most effective existing isolator combination was decided. Then, to be a reference for specific conditions, different support conditions were also investigated in this chapter.

3D model was used in these analyses. EB and VD were modeled for all 3D models as described previous section.

### 2.3.1 Elastomeric Bearing and Viscous Damper (Two Sided)

This analysis represents the existing situation of the structure. There are 10 supports for the roof of the structure at each side, therefore, total 20 EB and, for 2 VD for each direction, total 40 VD exist on the supports of the roof. (Figure 2.13)

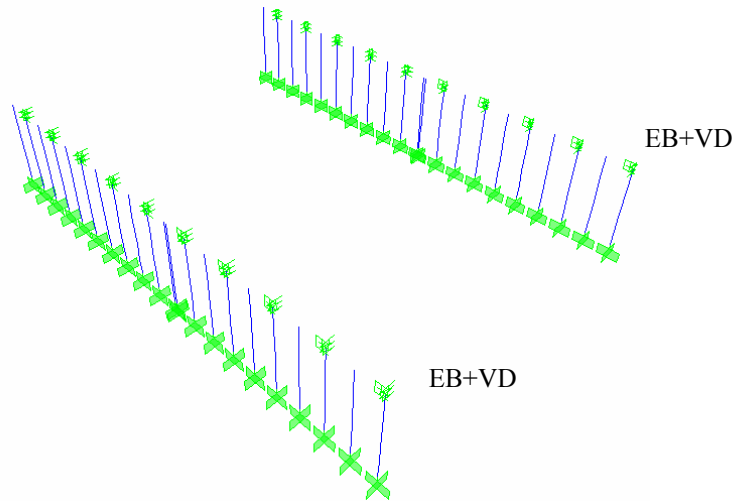


**Figure 2.13** EB + VD (Two Sided)

### 2.3.2 Elastomeric Bearing and Viscous Damper (One Sided)

This analysis is performed to investigate if seismic isolators are needed at each side of the supports. Therefore, total 10 EB and, for 2 VD for each direction, total 20 VD exist on the supports of the roof. (Figure 2.14)

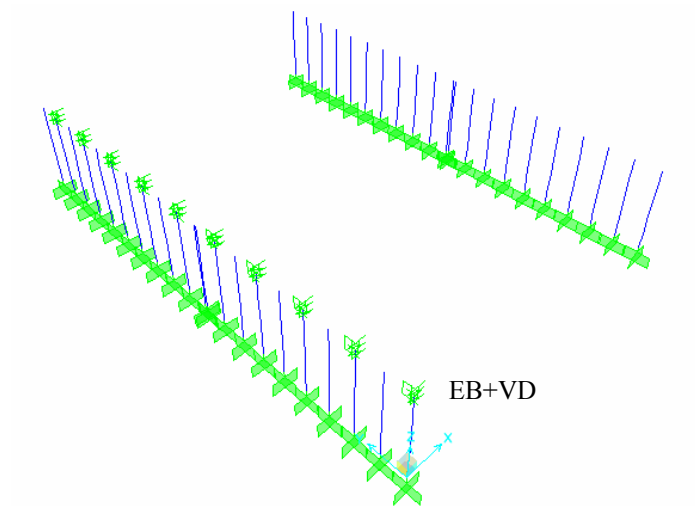


**Figure 2.14** EB + VD (One Sided)

### 2.3.3 Elastomeric Bearings (Two Sided)

This analysis is performed to investigate the effect of elastomeric bearings on the providing displacement capacity to the roof. For this scenario, elastomeric bearings are installed on each side of the supports. Therefore, total 20 EB exist on the model. (Figure 2.15)

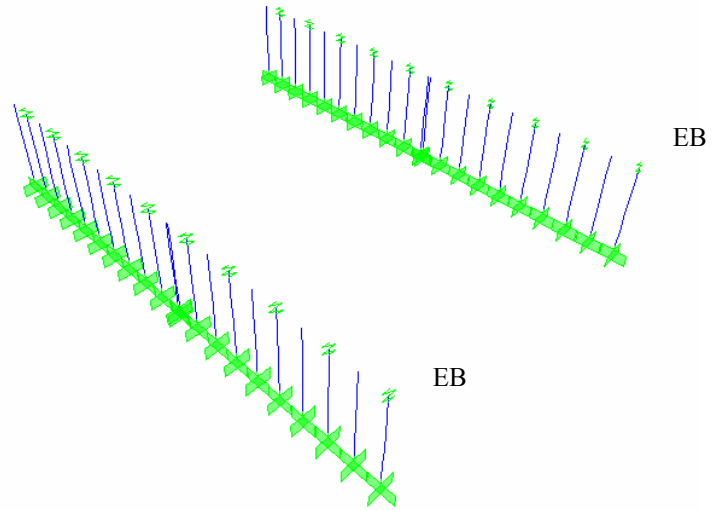


**Figure 2.15 EB (Two Sided)**

### 2.3.4 Elastomeric Bearings (One Sided)

This analysis is studied to see the effect of one side EB on the response of the structure. For this scenario, elastomeric bearings are installed on one side of the supports. Therefore, total 10 EB exist on the model. (Figure 2.16)

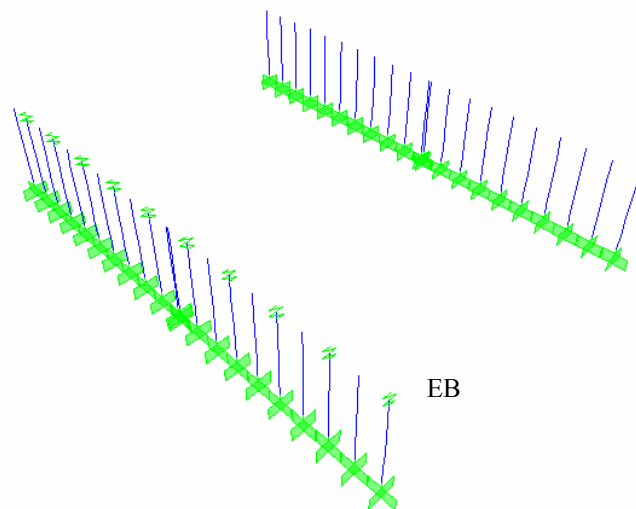


**Figure 2.16 EB (One Sided)**

### 2.3.5 Viscous Dampers (Two Sided)

This scenario is investigated if there would be only VD as isolators on both sides of the supports, the required responses (Higher modes, higher displacements, lower column forces, etc.) would be obtained. Therefore, total 40 VD are installed on each support of the roof. (Figure 2.17)

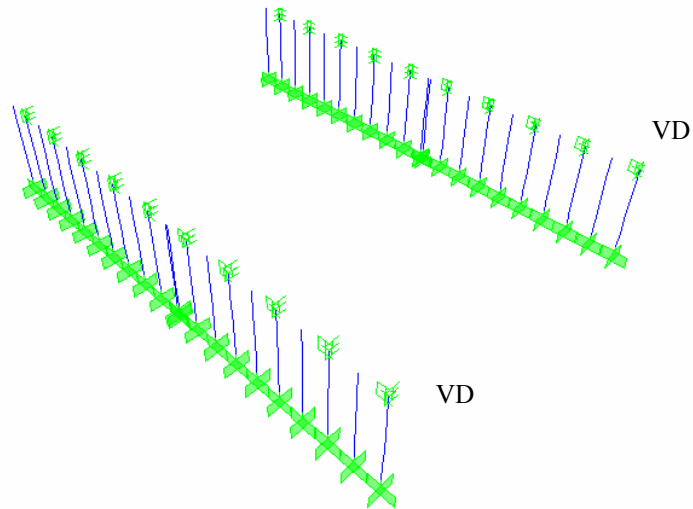
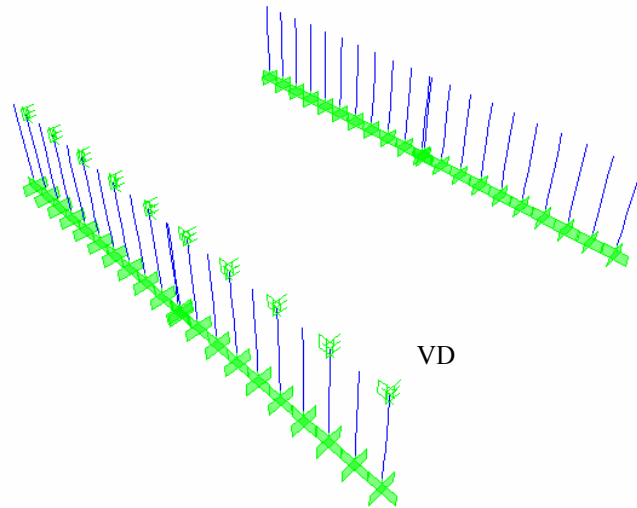


Figure 2.17 VD (Two Sided)

### 2.3.6 Viscous Dampers (One Sided)

This analysis is studied to see the effect of one side VD on the response of the structure. For this scenario, viscous dampers are installed on one side of the supports. Therefore, total 20 VD exist on the model. (Figure 2.18)



**Figure 2.18** VD (One Sided)

### **2.3.7 Non-isolated**

This analysis was performed to investigate if that seismic roof isolation is really needed for Halkapınar gymnasium, or not. This model is also helpful how isolators change the system behavior with respect to the non-isolated roof of the structure.

### **2.3.8 Results of Different Isolation Cases**

All previous isolator combinations were compared with respect to modal periods of the structure, roof support displacements and column responses (moments and shear forces in each direction) for 7 time-history analyses.

#### **2.3.8.1 Comparisons of Modal Periods**

Although 90 modes were used in the analyses, modal periods were compared for the first 10 modes for all comparisons because of the low period

values and having nearly constant decreasing slope on the graphs for higher modes.

When modal periods are compared EB+VD (Two Sided) isolation with EB+VD (One Sided) isolation and Non-isolated supports, it is obvious that EB+VD (Two Sided) isolation increases the modal periods of the structure for first 3 modes. (Figure 2.19)

On the other hand, periods of these three situations coincide with each other at the 4<sup>th</sup> mode and they show nearly the same trend for higher modes. Therefore, it can be said that EB+VD (Two Sided) isolation does not greatly increase modal period values of the structure.

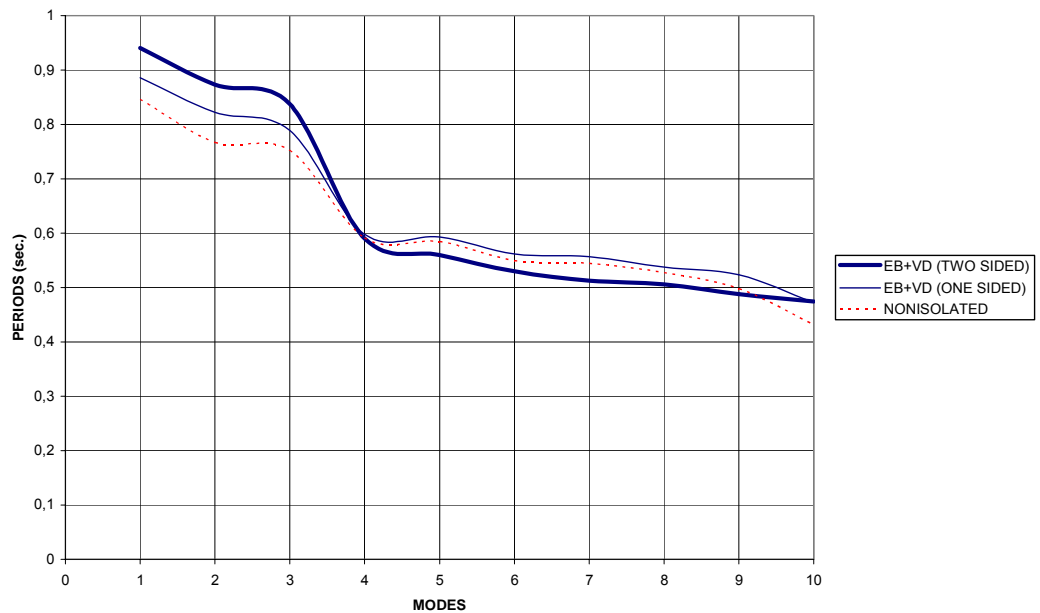


**Figure 2.19** Modal Period Behaviors of EB+VD (Two & One Sided) & Non-Isolated Support Conditions for First 10 Modes.

If only elastomeric bearings are considered as seismic isolators on the supports of the roof of the structure, EB (Two Sided) isolation support condition brings the highest modal period values to the structure with respect to the other support isolation combinations. (Figure 2.20)

Elastomeric bearings on both sides of the structure (EB (Two Sided)) supply nearly 2 times period values of the non-isolated structure's modal periods for the first three modes. As occurred in EB+VD isolation combination, EB (Two Sided), EB (One Sided) and Non-isolated conditions have same period values at the fifth mode. EB (Two Sided) and EB (One Sided) isolation situations shows the nearly same behaviors for higher modes.

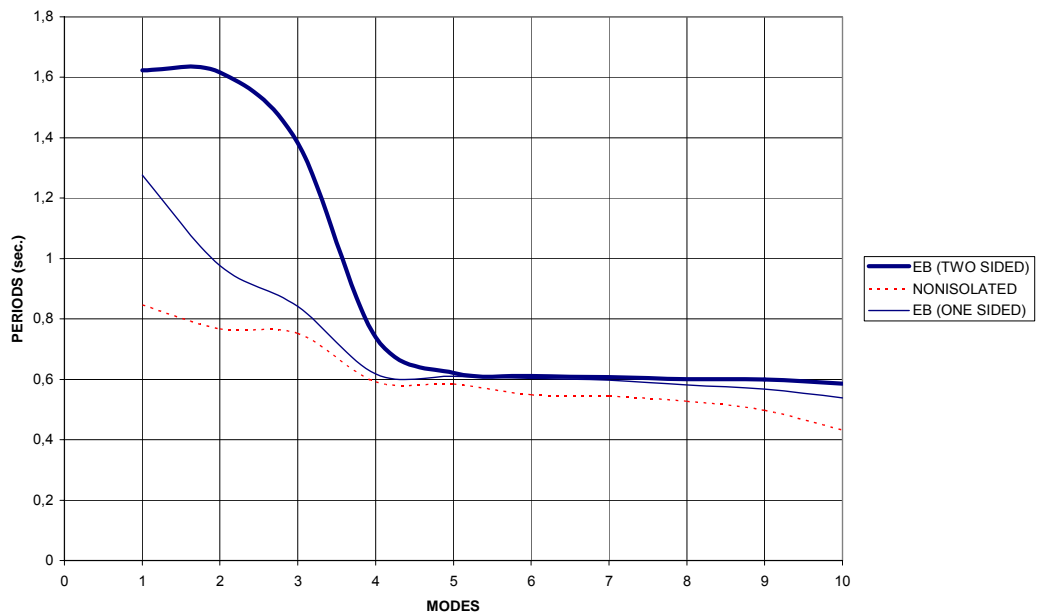


**Figure 2.20** Modal Period Behaviors of EB (Two & One Sided) & Non-Isolated Support Conditions for First 10 Modes.

Viscous dampers do not have any effect on the structure modal periods when they are installed as isolators without elastomeric bearings. VD (One Sided)

isolator combination show the same modal period values with the Non-isolated structure. (Figure 2.21)

VD (Two Sided), VD (One Sided) and Non-isolated support conditions have the same modal period values for the first 4<sup>th</sup> mode. VD (One Sided) also shows the same modal trend with Non-isolated structure and VD (Two Sided) isolator situation has lower modal period values than the non-isolated support condition for higher modes.

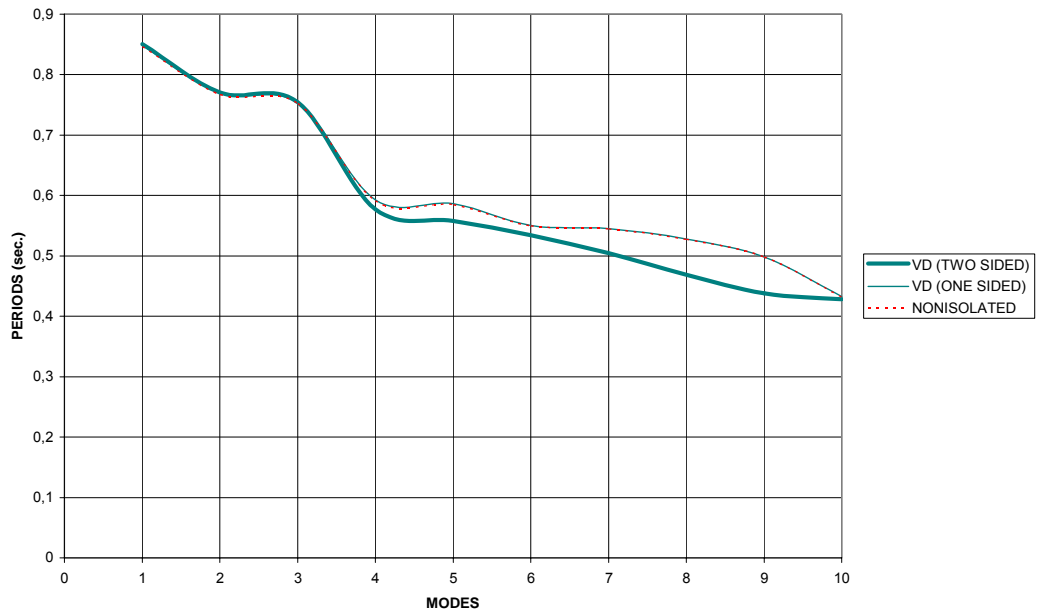


**Figure 2.21** Modal Period Behaviors of VD (Two & One Sided) & Non-Isolated Support Conditions for First 10 Modes.

Although viscous dampers do not have any effect on modal periods of the structure by themselves, when they are used with elastomeric bearings, viscous dampers surprisingly lower the structure modal periods (Figure 2.19 vs. Figure 2.20). The reason of this investigation is not aim of this study, but it can be said that it is probably result of energy absorption feature of the viscous dampers.

### 2.3.8.2 Comparisons of Roof Support Displacements

While roof support displacements are compared, only the columns being supports of the roof of the structure are taken into account and maximum displacement values are compared with each other for different isolator combinations. Displacements are compared separately for X and Y in global directions. For that reason, U1 stands for X direction, U2 stands for Y direction. (Figure 2.22)

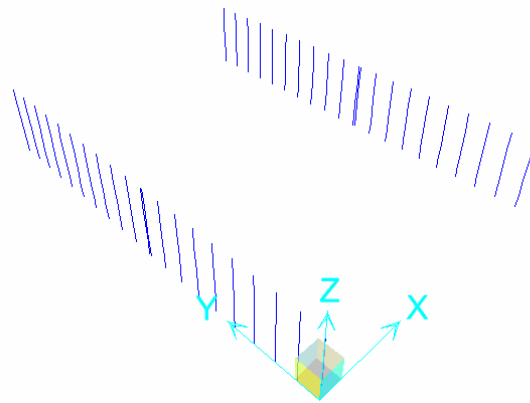


**Figure 2.22** Global Directions

EB+VD (Two & One Sided) increases the displacements in U1 and U2 directions. VD (Two & One Sided) nearly have same effect on the column displacements either two sided or one sided on the structural response, if they are used as only isolators. EB (Two & One Sided) isolators greatly increase the roof support displacements much more than the other isolator combinations. EB (One Sided) isolation shows nearly 4 times the non-isolated displacement in U2 direction. (Figures 2.23 – 2.24)

It is not desired that for columns having larger displacements due to the occurrence of second order moments during an earthquake. Furthermore, when the design spectrums are considered, higher modes would provide less spectral accelerations subjecting to the structure, which means less inertial forces. Therefore, an optimum design is required for higher modal periods and lower support displacements. Although elastomeric bearings provide very high modal period capacity to the structure, they cause excessive support displacements, which are undesirable. On the other hand, viscous dampers do not have any effect on modal periods and show same support displacements for either two sided or one sided when they are used as only isolators. However, elastomeric bearings could lower the support displacements with the help of viscous dampers.

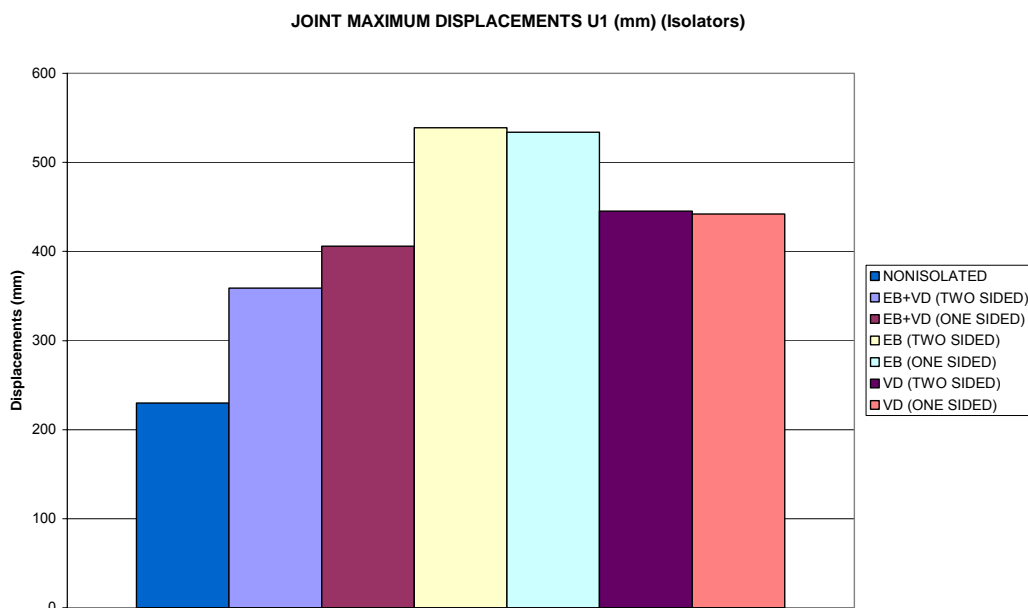


**Figure 2.23** Maximum Roof Support Displacement (U<sub>1</sub> (mm)) For Different Isolator Conditions.

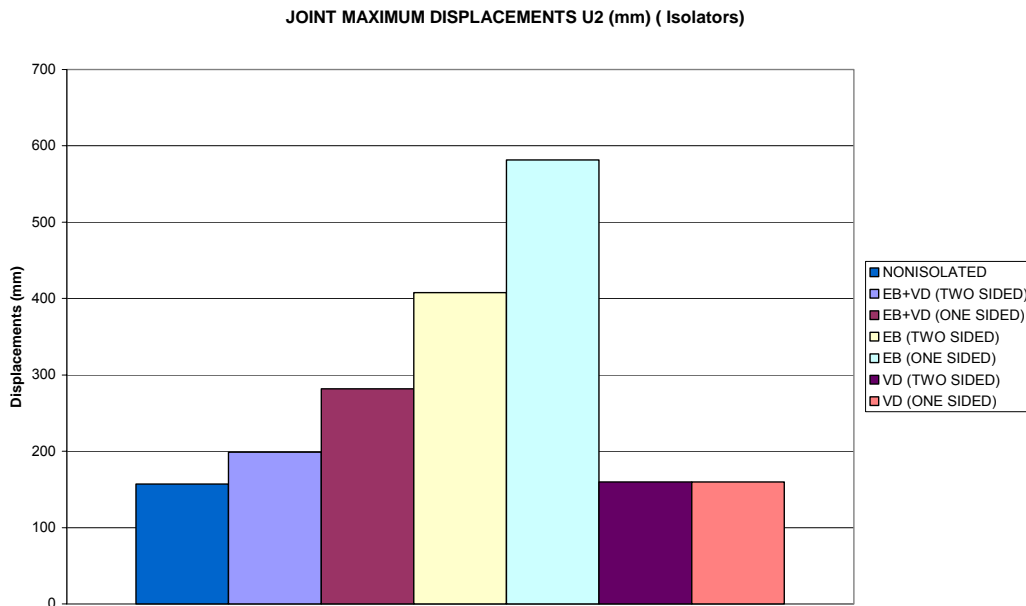


**Figure 2.24** Maximum Roof Support Displacement (U2 (mm)) For Different Isolator Conditions.

As a result, elastomeric bearings have to be used with viscous dampers for not only higher modal periods, but in fact for lower support displacements. At this moment, the question coming into mind is that if elastomeric bearing and viscous dampers should be on both sides of the roof or on only one side of the roof. To answer this question, column responses (Shear forces and moments) are investigated in following section.

### 2.3.8.3 Comparisons of Column Responses (Shear Forces & Moments)

While column responses are compared, only the columns being supports of the roof of the structure are taken into account and maximum shear forces and moment values are compared with each other for different isolator combinations. Shear forces and moments are compared separately for X and Y in local

directions. For that reason, V2 and M2 stand for local X direction; V3 and M3 stand for local Y direction. (Figure 2.25)

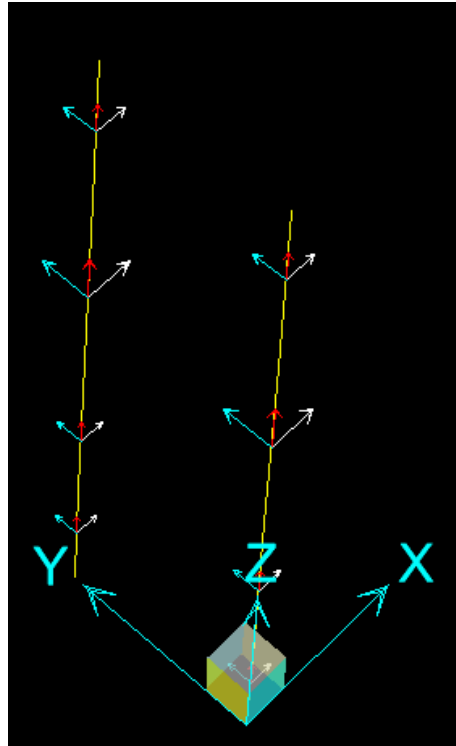


**Figure 2.25** Column Local Directions

(Red : 1, X; White : 2, Y; Blue : 3, Z)

EB+VD (Two & One Sided) isolators reduce the shear forces especially for V2 shear forces. Although EB (Two & One Sided) isolators reduce the shear forces in global X direction, they cause columns to subject higher shear forces in global Y direction. As also can be seen from the following two figures, VD (Two & One Sided) do not any effect to reduce the shear forces for each direction with respect to non-isolated case. (Figures 2.26 – 2.27)

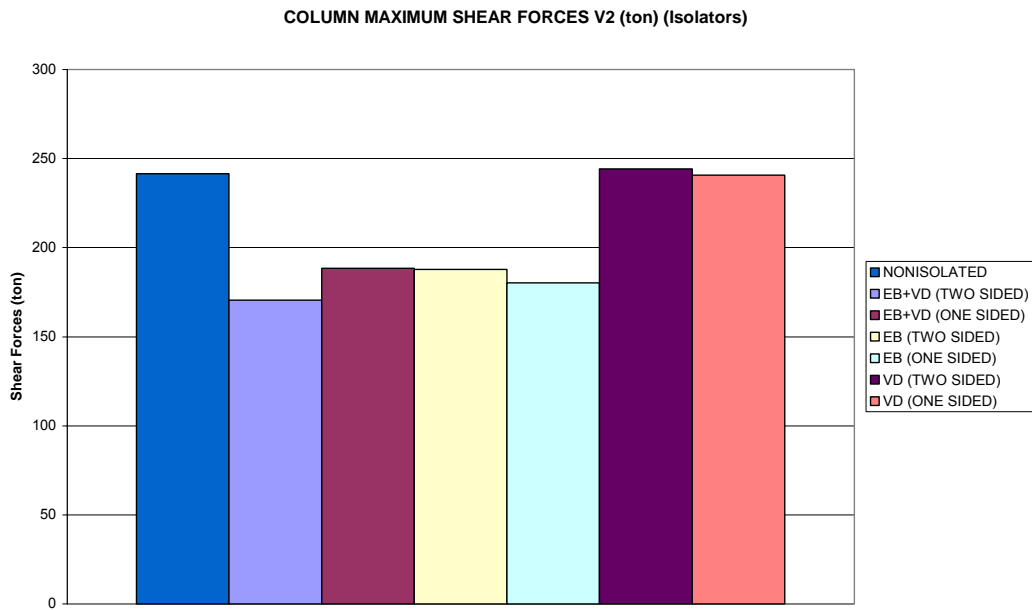


**Figure 2.26** Maximum Column Bottom Shear Forces V2 (ton) For Different Isolator Conditions.

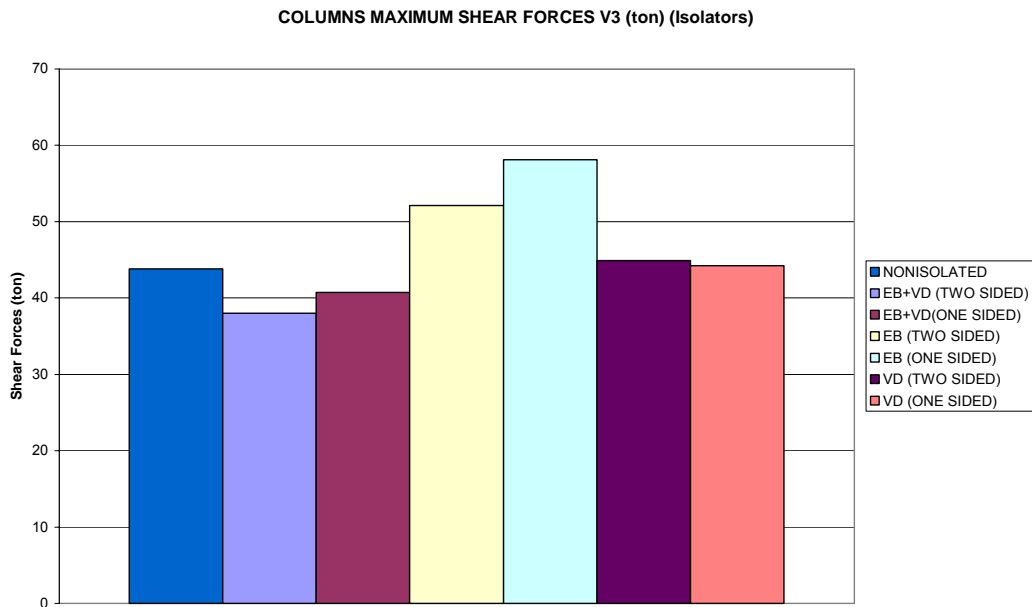


**Figure 2.27** Maximum Column Bottom Shear Forces V3 (ton) For Different Isolator Conditions.

EB+VD (Two Sided) isolation has slightly provide lesser amount of shear forces to the main support columns of the roof of the structure when it is compared with EB+VD (One Sided). These two-isolation conditions also provide nearly same benefit to the structure when column bottom moments are taken into consideration. Both of them lower the M3 column moments that are critical during an earthquake. VD (Two & One Sided) isolation condition do not have any influence on the moment reducing as not having any effect for modal periods, roof support displacements, column bottom shear forces. EB (Two & One Sided) isolation conditions reduce M3 moments much more than the other isolation conditions. On the other hand, they cause greater M2 moments than the non-isolated case. (Figures 2.28 – 2.29)

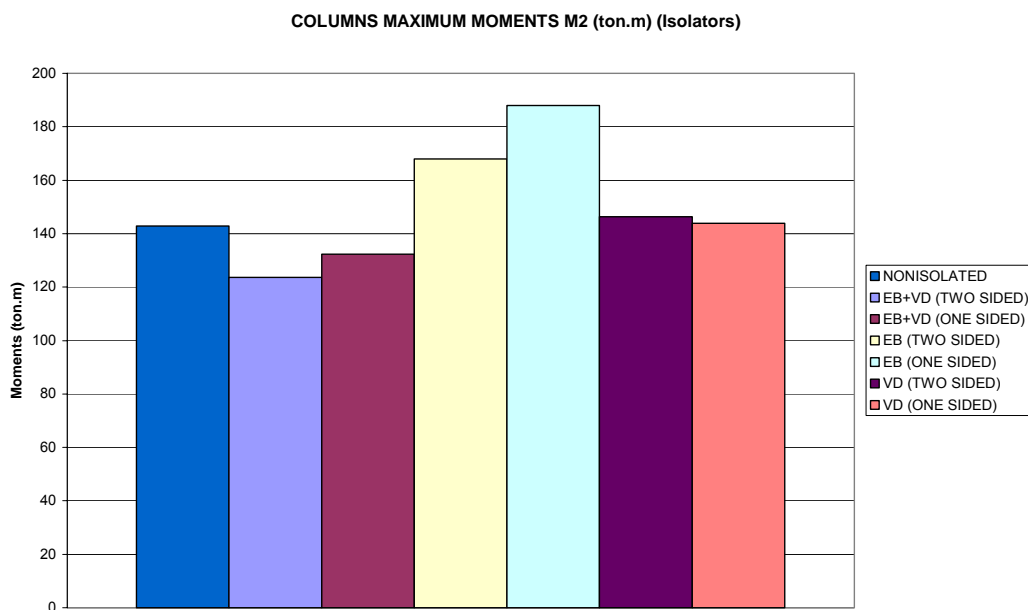


**Figure 2.28** Maximum Column Bottom Moments M2 (ton.m) For Different Isolator Conditions.

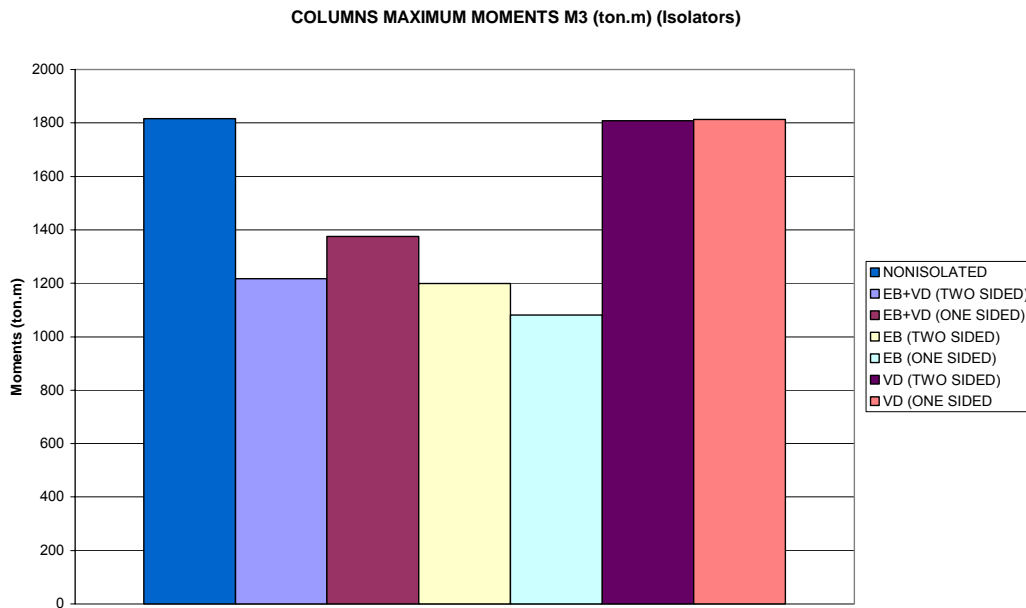


**Figure 2.29** Maximum Column Bottom Moments M3 (ton.m) For Different Isolator Conditions.

As a result of all these analysis, it can be said that elastomeric bearings should be used with viscous dampers to reduce column displacements with the energy absorption feature of viscous dampers. Elastomeric bearing and viscous damper isolation type does not have significant difference when they are installed on both sides of the roof of the structure. Therefore, it can be advised that elastomeric bearing and viscous damper isolation condition can be applied on the only one side of the roof of the structure.

## **CHAPTER 3**

### **DIFFERENT ISOLATOR TYPES and THEIR EFFECTS ON THE SYSTEM BEHAVIOUR**

In the previous section, elastomeric bearing and viscous damper combination was investigated how they changed the response of the structure. In this chapter, another type of elastomeric gained higher damping capacity by the inserted lead core, which is called Lead Rubber Bearing (LRB), was studied. Furthermore, the most popular sliding isolator, Friction Pendulum System (FPS) was also investigated for its effectiveness on the system. Finally, bilinear system modeling was performed by changing its main characteristics to understand the effect of them on the system response.

#### **3.1 LEAD RUBBER BEARING**

Halkapınar Gymnasium was investigated under the effect of Lead-Rubber Isolator. Isolator properties are needed to provide input data for the 3D model. Lead core diameter, isolator diameter, thickness and number of rubber layers, thickness and number of steel reinforcing shims are the main parameters needed to define the isolator in the model.

### 3.1.1 Minimum Required Diameter of Lead Core

The minimum diameter is needed to estimate for resisting wind loading. This required minimum diameter provides to ensure that roof of the gymnasium will not move under the wind load effect.

#### 3.1.1.1 The Wind Force On the Roof of the Gymnasium

The horizontal wind force acting on the roof is calculated as follows;

$$q = 110 \text{ kg/m}^2 \quad (H \approx 21\text{m})$$

Distance between two main steel profiles of the eaves is 6.11m and angle,  $\alpha$ ; between steel profile and horizontal axes is  $47^\circ$ . (Figure 3.1)

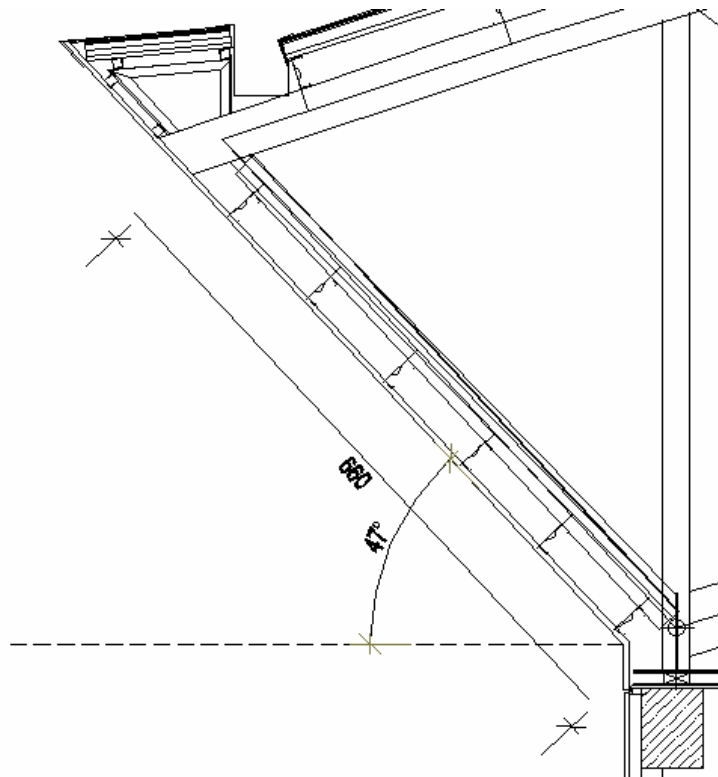


**Figure 3.1** Length and angle of steel profile of eave.

The shape coefficient is calculated according to McGuire, W. and Winter, G. [38] for the pressure side as:

$$C = 1.2 - 0.2 = 1.0 \quad (3.1)$$

$$w L = (1 \times 110 \times (6.11 / 2 + 6.11 / 2)) / 1000 = 0.672 \text{ t / m} \quad (3.2)$$

Length of one steel profile is 6.6m, so that, wind load subjected perpendicularly to one steel profile of eave equals to  $0.672 \times 6.6 = 4.436$  t. There are total 19 steel profiles:

$$19 \times 4.436 = 84.281 \text{ t} \quad (3.3)$$

The shape coefficient is also calculated according to McGuire, W. and Winter, G. [38] for the suction side as:

$$C = 0.5 + 0.2 = 0.7 \quad (3.4)$$

$$w L = (0.7 \times 110 \times (6.11 / 2 + 6.11 / 2)) / 1000 = 0.471 \text{ t / m} \quad (3.5)$$

Length of one steel profile is 6.6m, so that, wind load subjected perpendicularly to one steel profile of eave equals to  $0.471 \times 6.6 = 3.105$  t. There are total 19 steel profiles:

$$19 \times 3.105 = 59.0 \text{ t} \quad (3.6)$$

The horizontal component of the wind load is:

$$\sum wL \times \cos(90 - \alpha) = (59 + 84.281) \times \cos(53) = 86.23 \text{ t} \quad (3.7)$$

The Total weight of the steel truss roof on one-side supports is:

$$W = 940 / 2 = 470 \text{ t} \quad (3.8)$$

Factored wind load acting on the roof of the structure is:

$$F_T = 1.40 \times w \times L = 120.72 \text{ t} \quad (3.9)$$

If it is assumed that the same lead core diameter will be used for all bearings, the required strength,  $Q$  can be calculated by maximum horizontal load effect divided by number of bearings.

Characteristic strength,  $Q$  and yield strength,  $F_y$  are determined by the lead core because of the low – damping feature of elastomeric natural rubber. Minimum required diameter of lead core is calculated according to Buckle, Constantinou, Dicleli and Ghasemi [18] as follows:

$$d_{Lmin} = [(4 \times n \times \Psi \times Q) / (\pi \times (n-1) \times f_{yL})]^{1/2} \quad (3.10)$$

There are two different support conditions in analysis stages of this thesis. One is one side isolated case and the other is two sides isolated case by the isolators. Number of bearings for two side isolated case equals to two-fold number of bearings for one side isolated case. In other words, while total number of bearings is 10 for one side's isolated bearing case, total number of bearings is 20 for two side's isolated bearing case. The calculated horizontal component of total factored wind load is subjected to all bearings.

$Q$ : characteristic strength for one isolator

$$Q = F_T / 20 = 120.72 \times 9.81 / 20 = 59.213 \text{ kN} \quad (3.11)$$

$$\Psi = 2.0 \text{ for service loads (wind)} \quad (3.12)$$

$$n = 8 \text{ for service loads (wind)} \quad (3.13)$$

$$f_{yL} = 11.4 \text{ MPa (effective shear yield stress of lead)} \quad (3.14)$$

$$d_{Lmin} = [(4 \times 8 \times 2 \times 59.213 \times 10^3) / (\pi \times (8-1) \times 11.4)]^{1/2} \approx 123\text{mm} \quad (3.15)$$

$$\mathbf{d_{Lmin} = 123mm} \quad (3.16)$$

### 3.1.2 Lead Core Diameter and Rubber Stiffness

Target values for the effective period and damping ratio should be initially assumed to calculate the cross sectional area of the lead. For that reason, effective period and damping ratio are assumed as follows:

$$T_e = 1.0 \text{ sec.} \quad (3.17)$$

$$\beta_e = 0.3 \text{ (30\% damping ratio)} \quad (3.18)$$

#### 3.1.2.1 Design Displacement

The determination of preliminary design displacement is based on the assumption that all the bearings displacements are the same and the effect of substructure flexibility is neglected.

The new design displacement (according to UBC-97):

$$D_D = (g / (4\pi^2)) \times (C_{VD} \times T_D / B_D) \quad (3.19)$$

Where;

$C_{VD}$  : constant-velocity regions of DBE spectrum. (UBC-97, Table 16-Q)

$$C_{VD} = 0.14 \text{ (for soil type } S_C \text{ and seismic zone 1)} \quad (3.20)$$

$$T_D = 1.0 \text{sec. (Target isolated period)} \quad (3.21)$$

$$B_D = 1.82 \text{ (Damping coefficient according to target damping ratio, 30\%, by using formula: } (1 / B_D) = (0.25) \times (1 - \ln(\beta)), [17]) \quad (3.22)$$

$$D_D = (9810 / (4\pi^2)) \times (0.14 \times 1.0 / 1.82) = 19 \text{mm} \quad (3.23)$$

### 3.1.2.2 Required Effective Stiffness of the Isolators

All the bearings have the same effective stiffness, therefore, the effective stiffness of each individual bearing is calculated as:

$$K_e = (W / (n_b \times g)) \times (2 \times \pi / T_e)^2 \quad (3.24)$$

W : weight of the steel truss roof on one side bearing

g : gravitational acceleration

$n_b$  : number of bearings

$T_e$  : effective period (target period)

$$K_e = (470 \times 9.81 \times 10^3 / (10 \times 9810)) \times (2 \times \pi / 1.0)^2 \approx 1855 \text{ N/mm} \quad (3.25)$$

### 3.1.2.3 Initial Required Characteristic Strength (Seismic Resistance) of the

#### Lead Core and Final Diameter of the Lead Core

Initial required strength of the lead core for the seismic resistance can be calculated by neglecting yield displacement,  $D_y$  in the equation (due to the lack of final characteristic strength,  $Q$ , of the lead core) as follows:

$$Q_i = (1/2) \times \pi \times \beta_e \times K_e \times D_d = (1/2) \times \pi \times 0.30 \times 1855 \times 19 = 16.608 \text{ kN} \quad (3.26)$$

$$\begin{aligned} d_L &= [(4 \times n \times \Psi \times Q) / (\pi \times (n-1) \times f_{yL})]^{1/2} \\ &= [4 \times 10 \times 1 \times 16608 / (\pi \times (10-1) \times 11.4)]^{1/2} = 45\text{mm} \end{aligned} \quad (3.27)$$

If it is checked calculated diameter of lead core with the minimum required lead core diameter against service loads (wind), it is seen that minimum required diameter is much greater than calculated value. Therefore, it is advised to use wind-locking devices at each bearing. As a result, calculated diameter governs as design diameter of lead core:

$$d_L = 50\text{mm} \quad (3.28)$$

Initial required strength of the lead core is calculated by using equation as:

$$\begin{aligned} Q_i &= [(n-1) / (n \times \Psi)] \times f_{yL} \times (\pi \times d_L^2 / 4) \\ &= [(10-1) / (10 \times 1)] \times 11.4 \times (\pi \times 50^2 / 4) = 20.145 \text{ kN} \end{aligned} \quad (3.29)$$

$$\Psi = 1.0 \text{ for dynamic (seismic) loads} \quad (3.30)$$

$$n = 10 \text{ for dynamic (seismic) loads} \quad (3.31)$$

### 3.1.2.4 Initial Post-Elastic Stiffness of the Bearing and Final Characteristic

#### Strength (Seismic Resistance) $Q_i$ of the Lead Core

Initial post-elastic stiffness of the bearing is calculated as:

$$K_{d,i} = K_e - Q_i / D_d = 1855 - 20145 / 19 = 795 \text{ N/mm} \quad (3.32)$$

The yield displacement,  $D_y$  of bearing is given by:

$$D_y = Q_i / (K_u - K_d) \quad (3.33)$$

Where,  $K_d$  is post elastic stiffness and  $K_u$  is elastic loading or unloading stiffness.  $K_u$ , elastic stiffness equals to  $n$  times  $K_d$ , post elastic stiffness. “ $n$ ” is a coefficient and has values 10 for dynamic loads, 8 for service loads (wind and braking loads) and 5 for slowly applied loads (environmental effects, such as thermal expansion) [18].

$$K_u = n \times K_d = 10 \times 795 = 7950 \text{ N/mm (n=10 for dynamic loads)} \quad (3.34)$$

$$D_y = Q_i / (K_u - K_d) = 20145 / (7950 - 795) = 2.82 \text{ mm} \quad (3.35)$$

Final characteristic strength,  $Q$  of the lead core:

$$\begin{aligned} Q &= (\pi \times \beta_e \times K_e \times D_d^2) / (2 \times (D_d - D_y)) \\ &= (\pi \times 0.3 \times 1855 \times 19^2) / (2 \times (19 - 2.82)) = 19.5 \text{ kN} \end{aligned} \quad (3.36)$$

$$\mathbf{Q = 19.5 \text{ kN}} \quad (3.37)$$

Initial required characteristic strength of the lead core is close enough to final calculated characteristic strength value. Therefore, core diameter of 140 mm is acceptable.

### 3.1.2.5 Final Post-Elastic Stiffness of the Bearing

The final post elastic stiffness is calculated as:

$$K_d = K_e - Q / D_d = 1855 - 19500 / 19 = 830 \text{ N/mm} \quad (3.38)$$

The minimum restoring force requirements may be expressed by the following equation (AASHTO Guide Specification for Seismic Isolation Design, 1999):

$$K_d \geq W / (40 \times n_b \times D_d) = 470 \times 9.81 \times 10^3 / (40 \times 10 \times 19) = 607 \text{ N/mm} \quad (3.39)$$

$$K_d = 830 \text{ N/mm} \geq 607 \text{ N/mm} \quad \text{OK} \quad (3.40)$$

### 3.1.2.6 Contribution of the Rubber, to the Post-Elastic Stiffness

The contribution of the rubber,  $K_r$  can be calculated by using the factor  $f$  for the effect of lead on post-elastic stiffness ( $f$  is generally taken as equal to 1.1, [18]).

$$K_r = K_d / f = 830 / 1.1 = 755 \text{ N/mm} \quad (3.41)$$

### 3.1.3 Isolator Diameter and Rubber Thickness

Bonded plan area of the bearing is formulated according to AASHTO 1998, (article 14.7.5.3.2-1), as follows:

$$A_b = P / f_c = 470 \times 9.81 \times 10^3 / (10 \times 11) = 41915 \text{ mm}^2 \quad (3.42)$$

(Divided by 10 for each bearing)

Where;

$P$  : Total axial load (N)

$f_c$  : Allowable compressive stress = 11.0 MPa

The bonded diameter,  $d_b$ , of a lead rubber bearing with a central lead core diameter,  $d_L$  is calculated as:

$$d_b = (4 \times A_b / \pi + d_L^2)^{1/2} \quad (3.43)$$

The total rubber diameter is obtained by adding the thickness of the rubber cover around the bearings.

$$d = d_b + 2 \times c \quad (3.44)$$

Where;

$c$  : thickness of the rubber covers (5mm in general).

$$d_b = (4 \times A_b / \pi + d_L^2)^{1/2} = (4 \times 41915 / \pi + 50^2)^{1/2} \approx 240 \text{ mm} \quad (3.45)$$

But, it is taken as 350mm due to buckling instability.

$$d = d_b + 2 \times c = 350 + 10 = 360 \text{ mm} \quad (3.46)$$

$$A_b = \pi \times (d_b^2 - d_L^2) / 4 = \pi \times (350^2 - 50^2) / 4 = 94248 \text{ mm}^2 \quad (3.47)$$

Total rubber thickness is given by

$$T_r = G \times A_b / K_r \quad (3.48)$$

Where;

$G$  : Shear modulus of rubber,  $G_r = 0.62 \text{ MPa}$

$A_b$  : Bonded plan area

$K_r$  : Rubber stiffness

$$T_r = G \times A_b / K_r = 0.62 \times 94248 / 755 = 77 \text{ mm} \quad (3.49)$$

### 3.1.4 Thickness of Rubber Layers

The thickness of rubber layers will be determined from the shape factor. It is needed to calculate overlap area  $A_r$  between top- bonded and bottom-bonded areas of elastomer in a displaced elastomeric isolator. (See figure. 3.2)

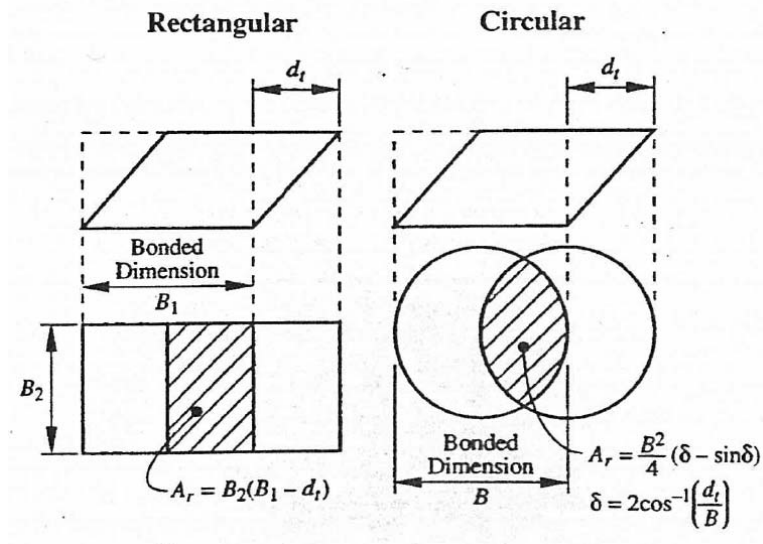


**Figure 3.2** Overlap Areas  $A_r$ , [18] (From AASHTO 1999)

Overlap area can be calculated as shown in figure 3.2 at total displacement as follows:

$$A_r = (d_b^2 / 4) \times (\delta - \sin \delta) \quad (3.50)$$

Where;

$$\delta = 2 \times \cos^{-1} (D_d / d_b) = 2 \times \cos^{-1} (19 / 350) = 3.00 \text{ rad} \quad (3.51)$$

$$A_r = (d_b^2 / 4) \times (\delta - \sin\delta) = (350^2 / 4) \times (3.00 - \sin 3.00) = 87553 \text{ mm}^2 (3.52)$$

The required shape factor S, to satisfy limits on compression strain,  $\gamma_c$ , can be calculated by using following equations:

For  $S \leq 15$  :

$$S = [3 \times P \pm (9 \times P^2 - 32 \times (\gamma_c \times A_r \times G)^2 \times k')^{1/2}] / (8 \times \gamma_c \times A_r \times G) \times k' \quad (3.53)$$

For  $S > 15$  :

$$S = [(\gamma_c \times A_r \times K) / (12 \times P)] \pm [((\gamma_c \times A_r \times K) / (12 \times P))^2 - K / (8 \times G \times k')]^{1/2} \quad (3.54)$$

Where;

P : Vertical load resulting from the combination of dead load plus live load using a load factor  $\gamma = 1$

$k'$  : material constant for elastomer,  $k' = 0.73$

K : Bulk modulus of elastomer,  $K = 2000 \text{ MPa}$

G : Shear modulus of elastomer,  $G_r = 0.62 \text{ MPa}$

In addition to the equations for required shape factor above, there is one more equation for the restriction for shape factor in AASHTO 1998, equation 14.6.5.3.2.1:

$$S \geq P / (1.66 \times G \times A_b) \quad (3.55)$$

$$\gamma_c = 2.0 \text{ (Maximum shear strain due to compression limit = 2.5)} \quad (3.56)$$

$$A_b = 94248 \text{ mm}^2 \quad A_r = 87553 \text{ mm}^2 \quad (3.57)$$

$$P = (470 \times 9.81 \times 10^3) / 10 = 461070 \text{ N} \quad (3.58)$$

If it is assumed that shape factor is less than 15;

$$S = [3 \times (461070) \pm [9 \times (461070)^2 - 32 \times (2.0 \times 87553 \times 0.62)^2 \times 0.73]^{1/2}] / (8 \times 2.0 \times 87553 \times 0.62 \times 0.73) = 4.20 \quad (3.59)$$

$$S \geq P / (1.66 \times G \times A_b) = 461070 / (1.66 \times 0.62 \times 94248) = 4.75 \quad (3.60)$$

Therefore, minimum value for S is 4.75.

Maximum layer thickness is given in the following layer shape factor equation, defined for circular lead plug rubber:

$$S = (d_b^2 - d_L^2) / (4 \times d_b \times t_i) \quad (3.61)$$

$$t_i = (d^2 - d_L^2) / (4 \times d \times S) = (360^2 - 50^2) / (4 \times 360 \times 4.75) = 18.6 \text{ mm} \quad (3.62)$$

Any thickness being smaller than this value can be used as individual layer thickness. But, 6 mm layer thickness will be used to provide stability at large horizontal displacements. 6 mm layer thickness will provide higher shape factor and higher load capacity at large displacements.

Maximum recommended thickness is 9 mm that is required for adequate confinement of the lead core [18].

$$\text{Number of rubber layers} = 24 \quad (3.63)$$

$$\text{For the top and bottom cover thickness} = 3 \text{ mm} \quad (3.64)$$

$$\text{Total rubber thickness} = 6 \times 24 + 3 \times 2 = 150 \text{ mm.} \quad (3.65)$$

$$\mathbf{T_r = 150 \text{ mm}} \quad (3.66)$$

### 3.1.5 Isolator Stability Check

#### 3.1.5.1 Factor of Safety against Buckling Instability

High factor of safety against instability is advised for all isolators when they are subjected to dead and live loads without any lateral deformation. AASHTO 1999 requires a factor of 3.0 for these situations in article 12.3. [18].

$$FS = P_{cr} / P \quad (3.67)$$

$$S = (d^2 - d_L^2) / (4 \times d \times t_i) = (360^2 - 50^2) / (4 \times 360 \times 6) \approx 15 \quad (3.68)$$

$$\begin{aligned} E_c &= 1 / [ (1 / (6 \times G \times S^2)) + (4 / (3 \times K))] \\ &= 1 / [ (1 / (6 \times 0.62 \times 15^2)) + (4 / (3 \times 2000))] = 537 \text{ MPa} \end{aligned} \quad (3.69)$$

$$I = \pi \times (d_b^4 - d_L^4) / 64 = \pi \times (350^4 - 50^4) / 64 = 736.311 \times 10^6 \text{ mm}^4 \quad (3.70)$$

$$P_{cr} = [ (\pi^2 \times E_c \times I \times G \times A) / (3 \times T_r^2) ]^{1/2}$$

$$= [(\pi^2 \times 537 \times 736.311 \times 10^6 \times 0.62 \times 94248) / (3 \times 150^2)]^{1/2}$$

$$= 1838009 \text{ N} \quad (3.71)$$

$$FS = 1838009 / 461070 = 3.99 > 3.0 \text{ OK} \quad (3.72)$$

### 3.1.5.2 Isolator Condition in Deformed State

Stability is also required that 1.2 times dead load plus axial load due to overturning caused by seismic loads while deformed to 1.5 times the total design displacement (D) for a 475 – year event with acceleration greater than 0.19g, or 2.0 times the total design displacement (D) for a 475 – year event with accelerations less than or equal to 0.19g according to AASHTO 1999 in article 12.3.

Since  $A = 0.48g > 0.19g$ , critical load in deformed state should be calculated at a displacement equal to  $1.5 D_d$ .

$$D_d = 19 \text{ mm} \quad (3.73)$$

$$d_b = 350 \text{ mm} \quad (3.74)$$

$$\delta = 2 \times \cos^{-1} (1.5 \times D_d / d_b) = 2 \times \cos^{-1} (1.5 \times 19 / 350) = 2.98 \text{ rad} \quad (3.75)$$

$$A_r = (d_b^2 / 4) \times (\delta - \sin\delta) = (350^2 / 4) \times (2.98 - \sin 2.98) = 86292 \text{ mm}^2 \quad (3.76)$$

$$P_{cr}' = P_{cr} \times A_r / A_b = 1838009 \times 86292 / 94248 = 1682844 \text{ N} \quad (3.77)$$

$$P_D = 461070 \text{ N (dead load)} \quad (3.78)$$

$$P_{SL} = 0 \text{ (axial load due to overturning caused by seismic loads)} \quad (3.79)$$

$$P_{cr}' = 1682844 > 1.2 \times P_D + P_{SL} = 553284 \text{ N} \quad \text{OK} \quad (3.80)$$

### 3.1.6 SAP2000 Input Values for Lead Rubber Bearing

Nonlinear time-history analysis was performed by SAP2000 version 9.0.1. Therefore, only the required parameters will be given for lead rubber bearing type. Mass of the isolators is negligible when mass of the roof of the gymnasium considered. The parameters required for link properties at both directions are as follows:

It is needed that effective stiffness and effective damping at all directions for linear analysis cases. Both of them were calculated in section 3.2.4, so that, they are:

Effective Stiffness : 1855 kN/m

Effective Damping : 0.3

Stiffness (elastic behavior), yield strength of lead and post – yield stiffness ratio (non – linear behavior) values are needed at 2 and 3 local directions for non-linear analysis cases. These values are as follows:

Stiffness : 8300 kN / m (Elastic Stiffness)

Yield Strength : 11.4 Mpa = 11400 kN / m<sup>2</sup>

Post Yield Stiffness Ratio : 0.1 ( $K_2 / K_1$ )

Shear deformation value for this type of friction isolator can be taken as 0.

Lead rubber bearing is flexible at horizontal direction and stiffer at vertical direction as all isolators. Therefore, axial stiffness was taken as thousand of horizontal effective stiffness for all analysis cases (1855000kN/m).

## **3.2 ISOLATOR COMBINATIONS OF LRB**

There were two analysis cases through out this thesis, one was one side isolated case and the other was two side isolated case. This investigation was always carried out to see that either two side isolated case was needed or one side isolated case enough to reduce seismic forces subjected to the system. The results of these analyses were compared with each other and non – isolated case.

### **3.2.1 Lead Rubber Isolator (Two Sided)**

This analysis represents the comparison tool for existing situation of the structure. The arising question for this analysis case is that what the response of the structure would be, if lead rubber bearings were used instead of elastomeric bearing with viscous damper. There are 10 supports for the roof of the structure at each side, therefore, total 20 lead rubber bearing exist on the supports of the roof.

### **3.2.2 Lead Rubber Isolator (One Sided)**

This analysis was performed to investigate if seismic isolators were needed at each side of the supports. Therefore, total 10 lead rubber bearings were used on the supports of the roof in the analyses.

### **3.2.3 Results of Isolator Combinations**

All previous isolator combinations were compared with respect to modal periods of the structure, roof support displacements and column responses (moments and shear forces in each direction) for 7 time-history analyses as performed in chapter 2. Results of two and one sided elastomeric bearing with viscous dampers and non – isolated case of section 2, two sided LRB and one sided LRB are the comparison tools for this section.

### 3.2.3.1 Comparisons of Modal Periods

Modal periods were compared for the first 10 modes for all comparisons because of the low period values and having nearly constant decreasing slope on the graphs.

When modal periods of EB+VD (Two & One Sided) isolation, LRB (Two Sided) and LRB (One Sided) are compared with Non-isolated supports, it is obvious that isolation techniques increase the modal periods of the structure for the first 4 modes. (Figure 3.3)

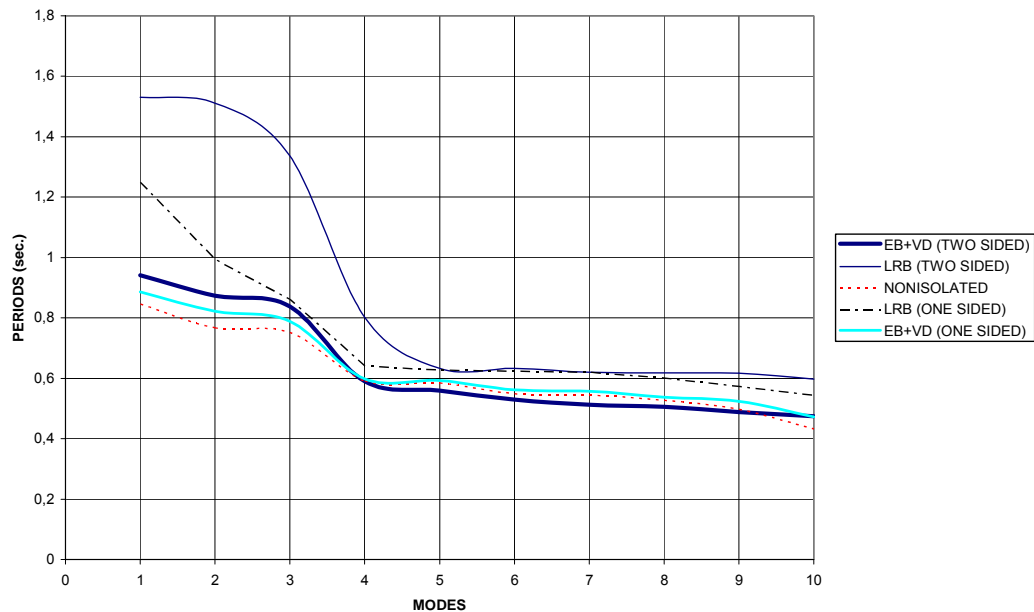


**Figure 3.3** Modal Period Behaviors of EB+VD (Two & One Sided), LRB (Two & One Sided) & Non-Isolated Support Conditions for First 10 Modes.

On the other hand, periods of EB+VD (Two & One Sided) and non - isolated situations coincide with each other at the fourth mode and they show nearly the same trend for higher modes as the LRB (Two & One Sided) isolation

situations. LRB (Two Sided) has the highest modal period values for the first 5 modes. But, it is seen that LRB (Two Sided) and LRB (One Sided) have nearly same modal period values for higher modes.

### **3.2.3.2 Comparisons of Roof Support Displacements**

While roof support displacements were compared, maximum displacement values were compared with each other for different isolator combinations. Displacements were compared separately for X and Y in global directions. For that reason, U1 stands for X direction, U2 stands for Y direction. (Figure 2.20)

EB+VD (Two & One Sided) do not increase the displacements in U1 as much as LRB (Two & One Sided) increase the displacements with respect to non – isolated case. On the other hand, all the isolator techniques also increase the displacement of the roof in U2 direction. While EB+VD (Two Sided) does not change the displacement values in U1 and U2 direction significantly, LRB (Two & One Sided) have the maximum displacement value in U1 direction with respect to other three isolation techniques. (Figures 3.4 – 3.5)

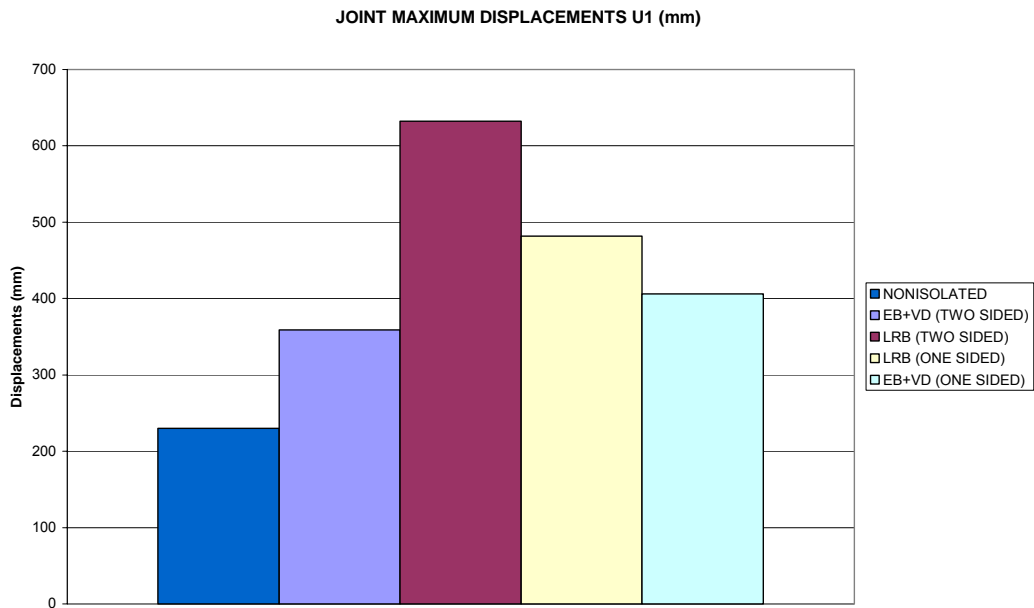


**Figure 3.4** Maximum Roof Support Displacements (U1 (mm))For Different Isolator Conditions.

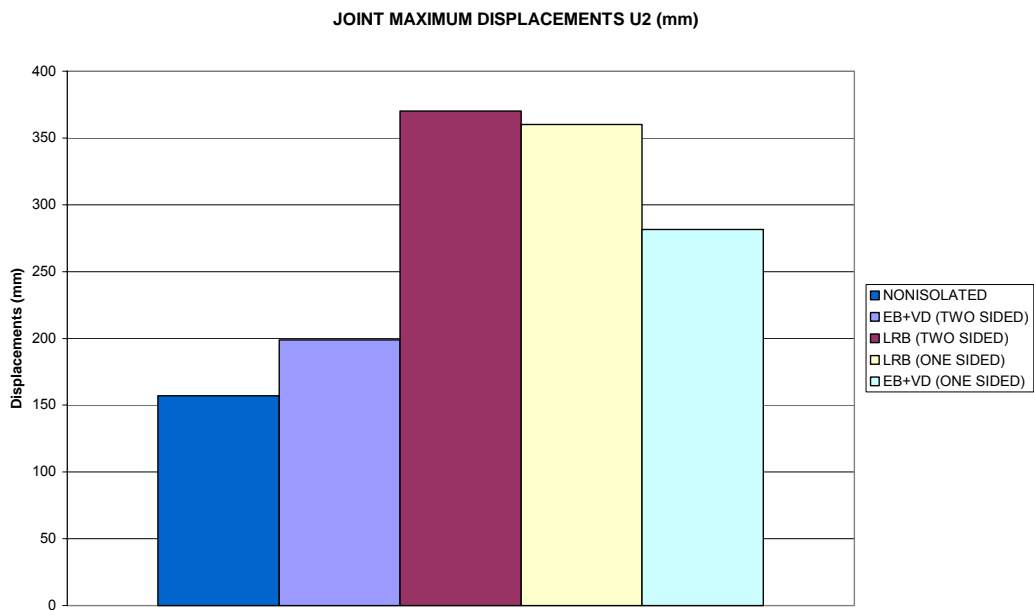


**Figure 3.5** Maximum Roof Support Displacements (U2 (mm))For Different Isolator Conditions.

EB+VD (Two Sided) does not increase the displacement values of the roof in U1 and U2 directions as much as other isolation techniques.

### **3.2.3.3 Comparisons of Column Responses (Shear Forces & Moments)**

While column responses were compared, only the columns being supports of the roof of the structure were taken into account and maximum shear forces and moment values were compared with each other for different isolator combinations. Shear forces and moments were compared separately for X and Y in local directions. For that reason, V2 and M2 stand for local X direction, V3 and M3 stand for local Y direction. (Figure 2.23)

EB+VD (Two & One Sided) isolation techniques significantly reduces the column bottom shear forces in X direction, and they reduces the column bottom shear forces in Y direction with respect to LRB isolation solution. On the other hand, LRB isolation conditions (Two & One Sided) do not change the column shear forces subjected to the structure according to seven different time – history analysis cases for X direction. Furthermore, they increase shear forces in other direction. (Figure 3.6 – 3.7)



**Figure 3.6** Maximum Column Bottom Shear Forces V2 (ton) For Different Isolator Conditions.

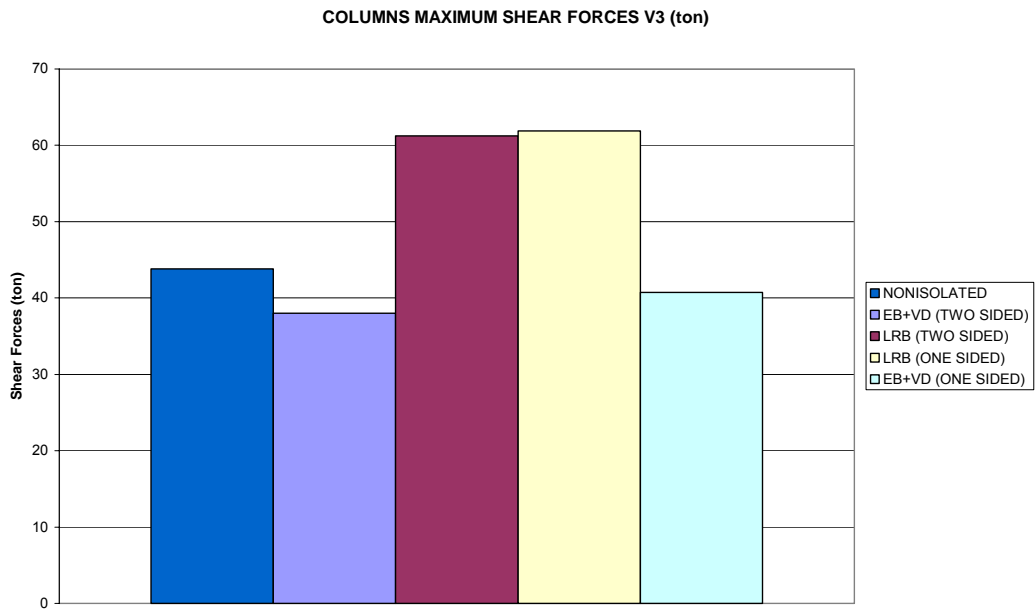


**Figure 3.7** Maximum Column Bottom Shear Forces V3 (ton) For Different Isolator Conditions.

As column bottom shear forces, column bottom moments in both directions show similar results for mentioned isolation techniques. While the EB+VD (Two & One Sided) isolation cases reduces the column moments, LRB (Two & One Sided) do not reduces them. Furthermore, LRB (Two & One Sided) isolation case slightly increases the column moments with respect to non – isolated structure. (Figure 3.8 – 3.9)

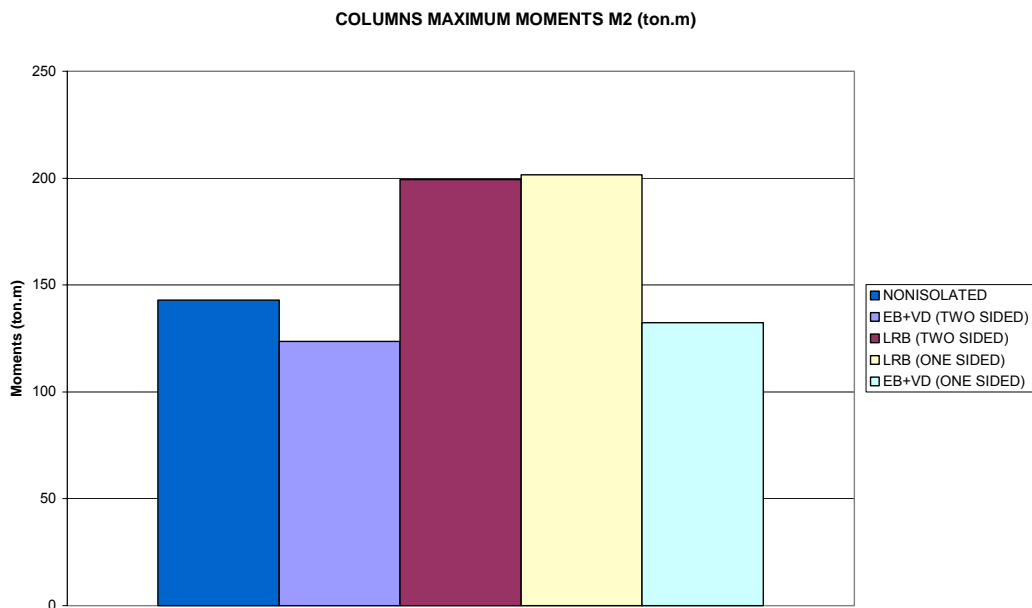


**Figure 3.8** Maximum Column Bottom Moments M2 (ton.m) For Different Isolator Conditions.

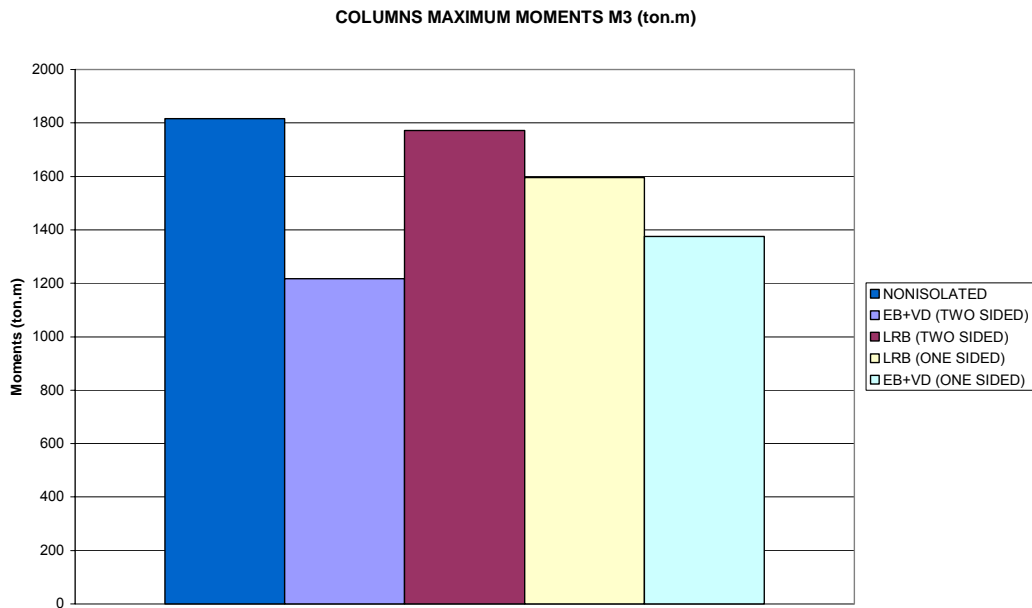


**Figure 3.9** Maximum Column Bottom Moments M3 (ton.m) For Different Isolator Conditions.

### 3.3 FRICTION PENDULUM ISOLATOR

Halkapınar Gymnasium was also investigated by using friction pendulum isolators. Firstly, isolator properties were obtained to provide input data for the 3D model. Dynamic friction coefficient, radius of concave surface and displacement capacity of the isolator were the main required parameters to define the isolator in the model.

#### 3.3.1 Minimum Required Friction Coefficient

The minimum required friction coefficient should be calculated to get the design friction coefficients,  $\mu_{\max}$  and  $\mu_{\min}$ , of friction pendulum isolators for resisting wind forces subjected to the roof of the structure. This minimum limitation to the friction coefficient of sliding isolators provides the roof of the

structure will not react under the effect of wind forces for serviceability conditions.

### 3.3.1.1 The Wind Force On the Roof of the Gymnasium

The horizontal wind force acting on the roof was calculated in section 3.1.1.1 as follows;

$$q = 110 \text{ kg/m}^2 \quad (H \approx 21\text{m}) \quad (3.81)$$

Distance between two main steel profiles of the eaves is 6.11m and angle,  $\alpha$ , between steel profile and horizontal axes is  $47^\circ$ . (Figure 3.1)

The shape coefficient is calculated according to McGuire, W. and Winter, G. [38] for the pressure side as:

$$C = 1.2 - 0.2 = 1.0 \quad (3.82)$$

$$w L = (1 \times 110 \times (6.11 / 2 + 6.11 / 2)) / 1000 = 0.672 \text{ t / m} \quad (3.83)$$

Length of one steel profile is 6.6m, so that, wind load subjected perpendicularly to one steel profile of eave equals to  $0.672 \times 6.6 = 4.436 \text{ t}$ . There are total 19 steel profiles:

$$19 \times 4.436 = 84.281 \text{ t} \quad (3.84)$$

The shape coefficient is also calculated according to McGuire, W. and Winter, G. [38] for the suction side as:

$$C = 0.5 + 0.2 = 0.7 \quad (3.85)$$

$$w L = (0.7 \times 110 \times (6.11 / 2 + 6.11 / 2) / 1000 = 0.471 \text{ t / m} \quad (3.86)$$

Length of one steel profile is 6.6m, so that, wind load subjected perpendicularly to one steel profile of eave equals to  $0.471 \times 6.6 = 3.105 \text{ t}$ . There are total 19 steel profiles:

$$19 \times 3.105 = 59.0 \text{ t} \quad (3.87)$$

The horizontal component of the wind load is:

$$\sum wL \times \cos (90 - \alpha) = (59 + 84.281) \times \cos (53) = 86.23 \text{ t} \quad (3.88)$$

The Total weight of the steel truss roof on one-side supports is:

$$W = 940 / 2 = 470 \text{ t} \quad (3.89)$$

Factored wind load acting on the roof of the structure is:

$$F_T = 1.40 \times w L = 120.72 \text{ t} \quad (3.90)$$

The minimum required friction coefficient is then calculated as:

$$\mu = 120.72 / (940 \times 1.60) = 0.08 = 8.0 \% \quad (3.91)$$

$$\mu_{\min, \text{req}} \approx 8.0\% \quad (3.92)$$

### 3.3.2 Minimum and Maximum Friction Coefficient

Minimum and maximum friction coefficients need to be determined because of the temperature changes, aging, loading history and contamination. The minimum value of friction coefficient is required to calculate maximum

isolator displacement and the maximum value of friction coefficient is required to calculate loads transmitted to the substructure.

### 3.3.2.1 Initial Lower and Upper Bound Friction Coefficients

Buckle, Constantinou, Dicleli and Ghasemi [18] stated that the friction coefficient in the first cycle is approximately 20% higher than the average coefficient of friction from all the cycles in a test involving 3-5 cycles of displacement. The average value of friction coefficient of all cycles is target design coefficient.

$$\mu_L = 8.0\% \qquad \mu_U = 1.2 \times 8.0 = 9.6\% \qquad (3.93)$$

### 3.3.2.2 System Property Modification Factors

System property modification factors are used to take into account for different variations of isolator properties during the life of the isolator. There are two main modification factors. One them is minimum value of the system property modification factor ( $\lambda_{\min}$ ). AASHTO Guide Specifications (AASHTO 1999) sets  $\lambda_{\min}$  equal to unity. On the other hand, maximum value of the system property modification factor  $\lambda_{\max}$  is calculated by the product of six different factors:

$$\lambda_{\max} = (\lambda_{\max,t}) \times (\lambda_{\max,a}) \times (\lambda_{\max,v}) \times (\lambda_{\max,tr}) \times (\lambda_{\max,c}) \times (\lambda_{\max,scrag}) \quad (3.94)$$

where;

$\lambda_{\max,t}$  : to account for the effect of temperature (Appendix A.1.1)

$\lambda_{\max,a}$  : to account for the effect of aging (Appendix A.1.2)

$\lambda_{\max,v}$  : to account for the effect of velocity (equals to unity unless established otherwise by test)

$\lambda_{\max,tr}$  : to account for the effect of travel and wear (Appendix A.1.3)

$\lambda_{\max,c}$  : to account for the effect of contamination (Appendix A.1.4)

$\lambda_{\max,scrag}$  : to account for the effect of scragging (equals to unity for sliding isolators)

$\lambda_{\max,t}$  = 1.2 (Unlubricated PTFE (Poly tetrafluoroethylene) for a minimum air temperature of -6.2°C in Izmir. This value was taken from <http://izmir.meteor.gov.tr/istasyonlar/seferihisar.htm>) (3.95)

$\lambda_{\max,a}$  = 1.2 (because of humidity of the İzmir) (3.96)

$\lambda_{\max,v}$  = 1.0 (should be controlled by tests) (3.97)

$\lambda_{\max,tr}$  = 1.0 (cumulative travel <1005m for Unlubricated PTFE) (3.98)

$\lambda_{\max,c}$  = 1.0 (sealed bearings with the stainless steel surface facing down for Unlubricated PTFE) (3.99)

$\lambda_{\max,scrag}$  = 1.0 (for sliding isolators) (3.100)

### 3.3.2.3 System Property Adjustment Factor

Adjustment factor ( $f_a$ ) is taken into account due to that the conditions for system modification factors will not occur at the same time. Therefore, this factor can be called reduction factor of system modification factors  $\lambda$ . According to the structure importance adjustment factors differs as shown in table-3.1.

**Table 3.1** System Property Adjustment Factors [18] (From AASHTO 1999)

Structure Importance	Adjustment Factor, $f_a$
Critical	1.00
Essential	0.75
Other	0.66

$$\lambda_{adj} = 1 + f_a (\lambda_{max} - 1) \quad (3.101)$$

$$f_a = 0.66 \quad (3.102)$$

$$\lambda_t = 1.0 + (1.2 - 1.0) \times 0.66 = 1.132 \quad (3.103)$$

$$\lambda_a = 1.0 + (1.2 - 1.0) \times 0.66 = 1.132 \quad (3.104)$$

$$\lambda_v = 1.0 \quad \lambda_{tr} = 1.0 \quad \lambda_c = 1.0 \quad (3.105)$$

$$\lambda_{scrag} = 1.0 \quad (3.106)$$

$$\lambda_{min} = 1.0 \quad (3.107)$$

$$\lambda_{max} = 1.132 \times 1.132 \times 1.0 \times 1.0 \times 1.0 \times 1.0 = 1.2814 \quad (3.108)$$

#### 3.3.2.4 Minimum and Maximum Probable Friction Coefficient

$$\mu_{min} = 1.0 \times 8.0 = 8.0\% \quad \mu_{max} = 1.2814 \times 9.6 = 12.30\% \quad (3.109)$$

### 3.3.3 Radius of Concave Surface

Before calculation of radius of concave surface, we need to determine minimum lateral force requirement, expected displacement and required damping ratio.

The AASHTO Guide Specification for Seismic Isolation Design specifies a minimum required second slope ( $K_d$ ) such that:

$$K_d \geq 0.025 W/D \quad (3.110)$$

This requirement for  $K_d$  also means that the period  $T_d$  must satisfy that:

$$T_d \leq 40 (D/g)^{1/2} \quad (3.111)$$

The minimum stiffness according to the AASHTO Guide Specification for Seismic Isolation Design should provide that the difference between the magnitude of the restoring force at design displacement and at 50% of the design displacement is larger than the weight acting on the bearings divided by a factor of 80 to meet self-centering requirements.

The period when sliding is given by:

$$T = 2\pi \sqrt{R/g} \quad (3.112)$$

Comparing equations for  $T_d$  and  $T$ , previous AASHTO requirement is satisfied when:

$$R \leq 40 D_d \quad (3.113)$$

where;

R : the radius of the concave surface

$D_d$  : design displacement of the friction pendulum isolator

If it is assumed that a target displacement as 30mm, the maximum value for R can be calculated as:

$$R_{\max} = 40 \times 30 = 1200\text{mm} \quad (3.114)$$

If it is assumed that a target damping ratio of 30% and a design displacement 30mm, and using a friction coefficient of 8.0%, the minimum radius, R can be calculated from equivalent viscous damping ratio,  $\beta_e$ , equation:

$$\beta_e = (2 / \pi) \times (\mu / (\mu + D / R)) \quad (3.115)$$

$$0.30 = (2 / \pi) \times [0.08 / (0.08 + 0.030 / R)] \implies R_{\min} = 335\text{mm} \quad (3.116)$$

The friction pendulum bearings are manufactured a standard radius of 1020mm and 1550 mm within the range of interest. As previously showed, period of friction pendulum isolator is directly proportional square root of concave surface radius of isolator. Therefore, smaller radius will have smaller displacement due to the less period value. Thus,

$$R = 1020 \text{ mm} \quad (3.117)$$

The corresponding period can be calculated according to the equation as previously stated:

$$T = (2\pi) \times \sqrt{(R / g)} = 2\pi \times \sqrt{(1020/9810)} \approx 2.0 \text{ sec.} \quad (3.118)$$

This period value is less than the 6 second limit imposed by ASSHTO Guide Specification for Seismic Isolation Design. Therefore, radius of 1020mm provides the minimum lateral restoring force requirements.

### 3.3.4 Preliminary Seismic Design Displacement

The determination of preliminary design displacement is based on the assumption that all the bearing displacements are the same and the effect of substructure flexibility is neglected. It is an iterative procedure, therefore it is, firstly, assumed as a design displacement 30mm as previously assumed for the determination of the radius of concave surface.

- Equivalent (effective) stiffness of the structure:

$$K_e = \mu W_s / D_d + W_s / R = 0.08 \times (4700 \times 10^3) / 30 + 4700 \times 10^3 / 1020 = 17141 \text{ kN/m} \quad (3.119)$$

- Damping produced by friction at the sliding surface:

$$\beta_e = (2/\pi) \times [\mu / (\mu + D_d / R)] = (2/\pi) \times (0.08 / (0.08 + 30 / 1020)) = 0.46 \quad (3.120)$$

When the damping ratio,  $\beta$ , becomes greater than 30%, damping factor B becomes unreliable and a nonlinear time history analysis is recommended in these situations [18]. Equivalent damping ratio is taken as 30% and corresponding damping factor, B equals to 1.82.

- Effective period of vibration:

$$T_e = (2\pi) \times \sqrt{[W_s / (K_e \times g)]} = (2\pi) \times \sqrt{[4700 \times 10^3 / (17141 \times 9810)]} = 1.05 \text{ sec.} \quad (3.121)$$

- The new design displacement (according to UBC-97):

$$D_D = (g/(4\pi^2)) \times (C_{VD} \times T_D / B_D) \quad (3.122)$$

where;

$C_{VD}$ : constant-velocity regions of the DBE spectrum. (UBC-97, Table 16-Q)

$$C_{VD} = 0.14 \text{ (for soil type } S_C \text{ and seismic zone 1)} \quad (3.123)$$

$$T_D = 1.49 \text{ sec. (Isolated period corresponding DBE level responses)} \quad (3.124)$$

$$B_D = 1.82 \text{ (damping coefficient corresponding DBE level responses)} \quad (3.125)$$

$$D_D = (9810/(4\pi^2)) \times (0.14 \times 1.49 / 1.82) = 29 \text{ mm} \quad (3.126)$$

When it is compared that the initial assumed design displacement 30mm with the calculated preliminary seismic design displacement 29mm very close agreement exists. With this close agreement, required friction pendulum isolator properties are obtained, Further, time history analysis of the Halkapinar gymnasium can be performed with the following SAP2000 input values.

### 3.3.5 SAP2000 Input Values for Friction Isolator

Nonlinear time-history analysis was performed by SAP2000 version 9.0.1. Therefore, only the required parameters will be given for friction isolator type. Mass of the isolators is negligible when mass of the roof of the gymnasium considered. The parameters required for link properties are as follows:

It is needed that effective stiffness and effective damping at 2 and 3 local directions for linear analysis cases. Both of them were calculated in section 3.2.4, so that, they are:

Effective Stiffness : 17141kN/m

Effective Damping : 0.3

Stiffness, friction coefficients (slow and fast), rate parameter and radius of concave surface values are needed at 2 and 3 local directions for non-linear analysis cases. These values are as follows:

Stiffness :  $W / R = 470 \times 9.81 / 1.02 = 4520\text{kN/m}$

Friction Coefficient (slow) : 2.0% (Accepted)

Friction Coefficient (fast) :  $\mu_{\min} = 8.0\%$  (For Modes, Displacements)  
 $\mu_{\max} = 12.30\%$  (For Reactions)

Rate Parameter : 35 (Accepted)

Radius of Sliding Surface : 1.020m

Shear deformation value for this type of friction isolator can be taken as 0.

Stiffness value taken in local 1 (axial) direction taken as follows:

$$K_1 = A \times E / (2 \times H) \quad (3.127)$$

$$A = \pi \times D_s^2 / 4 \text{ (Area of Slider)} = \pi \times 1^2 / 4 = 0.785 \text{ m}^2 \quad (3.128)$$

$$E = 2 \times 10^8 \text{ kN/m}^2 \text{ (Elastic Modulus of Steel)} \quad (3.129)$$

$$H = 60 \text{ cm (Height of Bearing / Accepted)} \quad (3.130)$$

$$K_1 = 130833333 \text{ kN / m} \quad (3.131)$$

### **3.4 ISOLATOR COMBINATIONS OF FPS**

The standard two analysis cases through out this thesis, one and two sided isolated cases, were also combination of this section analysis. This investigation was always carried out to see that either two side isolated case was needed or one side isolated case was enough to reduce seismic forces subjected to the system. The results of these analyses were compared with each other, EB+VD (Two & One Sided) and non – isolated cases.

#### **3.4.1 Friction Pendulum System (Two Sided)**

This analysis represents the comparison tool for existing situation of the structure. The arising question for this analysis case is that what the response of the structure would be, if friction pendulum is used instead of elastomeric bearing with viscous damper. There are 10 supports for the roof of the structure at each side, therefore, total 20 friction pendulum bearings exist on the supports of the roof.

#### **3.4.2 Friction Pendulum System (One Sided)**

This analysis was performed to investigate if seismic isolators were needed at each side of the supports. Therefore, total 10 friction pendulum bearings exist on the supports of the roof.

### **3.4.3 Results of Isolator Combinations**

All previous isolator combinations were compared with respect to modal periods of the structure, roof support displacements and column responses (moments and shear forces in each direction) for 7 time-history analyses as performed in chapter 2. Results of two and one-sided elastomeric bearing with viscous dampers and non – isolated case of section 2, two sided FPS and one sided FPS were the comparison tools for this section.

#### **3.4.3.1 Comparisons of Modal Periods**

Modal periods were compared for the first 10 modes for all comparisons, because the structural response is mainly determined by initial modes.

Friction pendulum system increases the structure period very slightly with respect to non – isolated structure for the first two periods. Furthermore, periods of the gymnasium are decreased for higher modes of friction pendulum isolators (Two sided). One sided friction pendulum bearing shows nearly the same behavior with the non – isolated roof of the structure as EB+VD (One sided). (Figure 3.10)

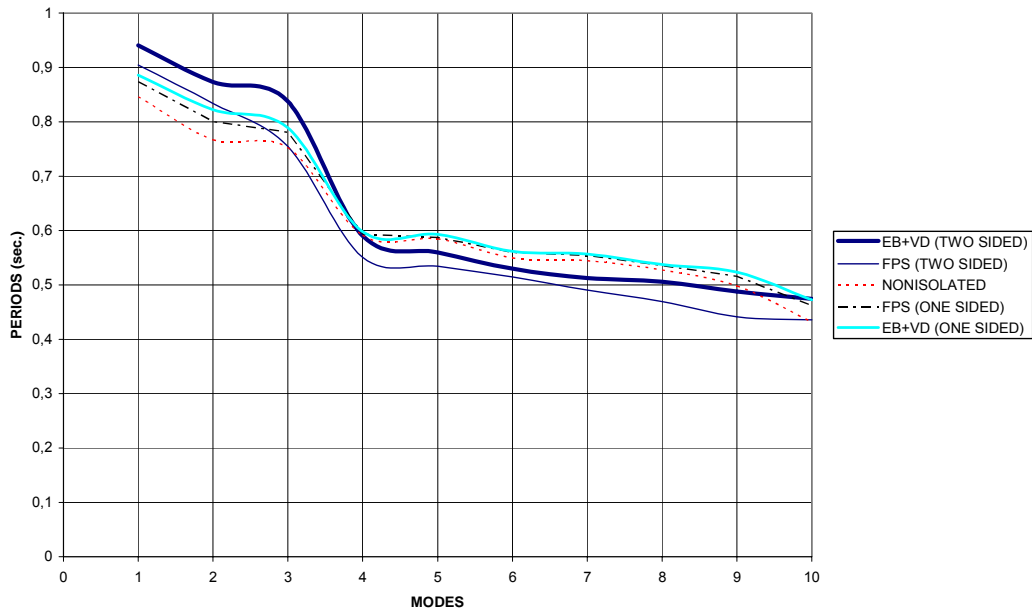


**Figure 3.10** Modal Period Behaviors of EB+VD (Two & One Sided), FPS (Two & One Sided) & Non-Isolated Support Conditions for First 10 Modes.

Seismic isolators are expected to increase the structure periods to get fewer amounts of seismic forces with increasing in damping. Nevertheless, two sided friction pendulum isolator shows less period values than the non – isolated case for given FPS configuration. In other words, horizontal stiffness is not enough reduced to gain higher modal values.

### 3.4.3.2 Comparisons of Roof Support Displacements

While roof support displacements were compared, maximum displacement values were compared with each other for different isolator combinations. Displacements were compared separately for X and Y in global directions. For that reason, U1 stands for X direction, U2 stands for Y direction (Figure 2.20). Minimum friction coefficient was used in the roof displacement analysis.

Two-sided FPS greatly reduced the displacements in U1 direction, while it increased the displacements in U2 direction. On the other hand, one-sided FPS significantly changed the displacement values for U1 and U2 directions, in addition to this, it increased the maximum roof displacement three times of the non – isolated case in U2 direction. (Figures 3.11 – 3.12)

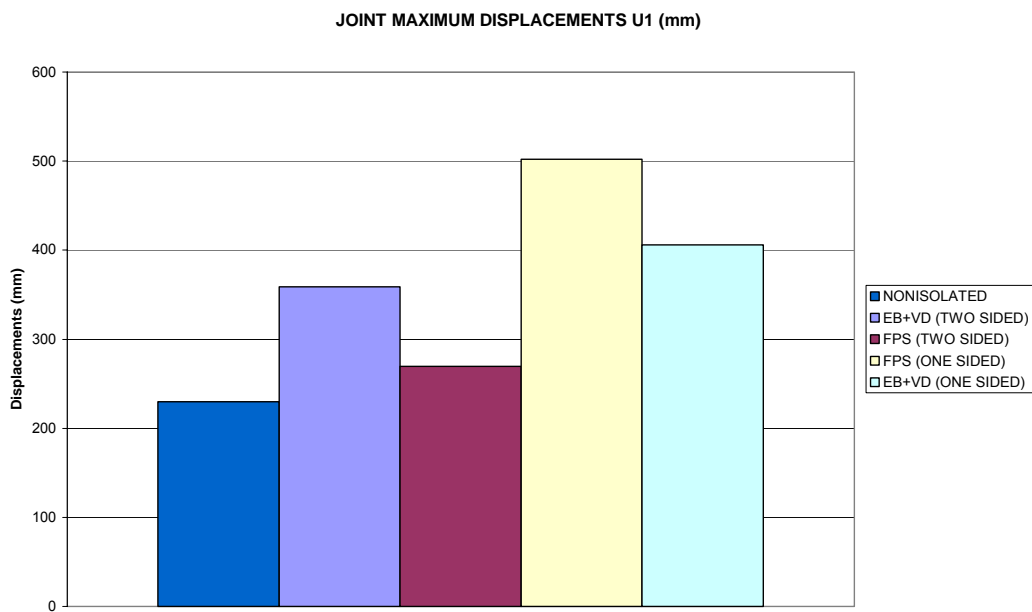


**Figure 3.11** Maximum Roof Support Displacements (U1 (mm))For Different Isolator Conditions.

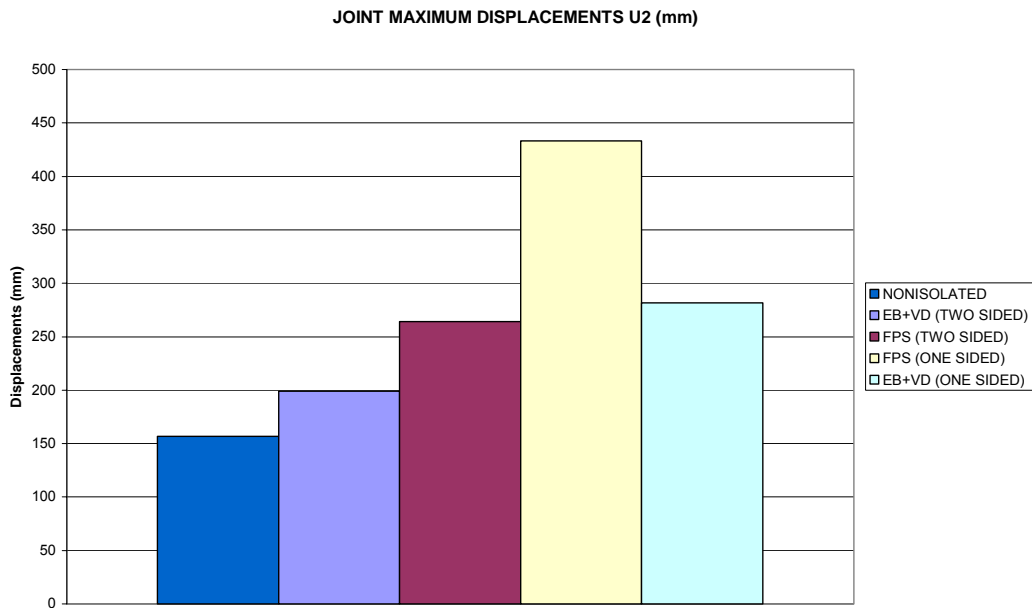


**Figure 3.12** Maximum Roof Support Displacements (U2 (mm))For Different Isolator Conditions.

One-sided FPS is not desirable for the isolation of gymnasium roof because of the maximum roof displacement values in U2 direction for above FPS parameters.

### 3.4.3.3 Comparisons of Column Responses (Shear Forces & Moments)

While column responses were compared, only the columns being supports of the roof of the structure were taken into account and maximum shear forces and moment values were compared with each other for different isolator combinations. Shear forces and moments were compared separately for X and Y in local directions. For that reason, V2 and M2 stand for local X direction, V3 and M3 stand for local Y direction (Figure 2.23). Maximum friction coefficient was used in the column responses analysis.

While two and one-sided FPS reduces the column bottom shear forces in V2 direction, they do not efficiently change this response in V3 direction when they are compared with non – isolated case. Two and one sided EB+VD and FPS isolators shows nearly the same values for V2 column shear forces. (Figures 3.13– 3.14)

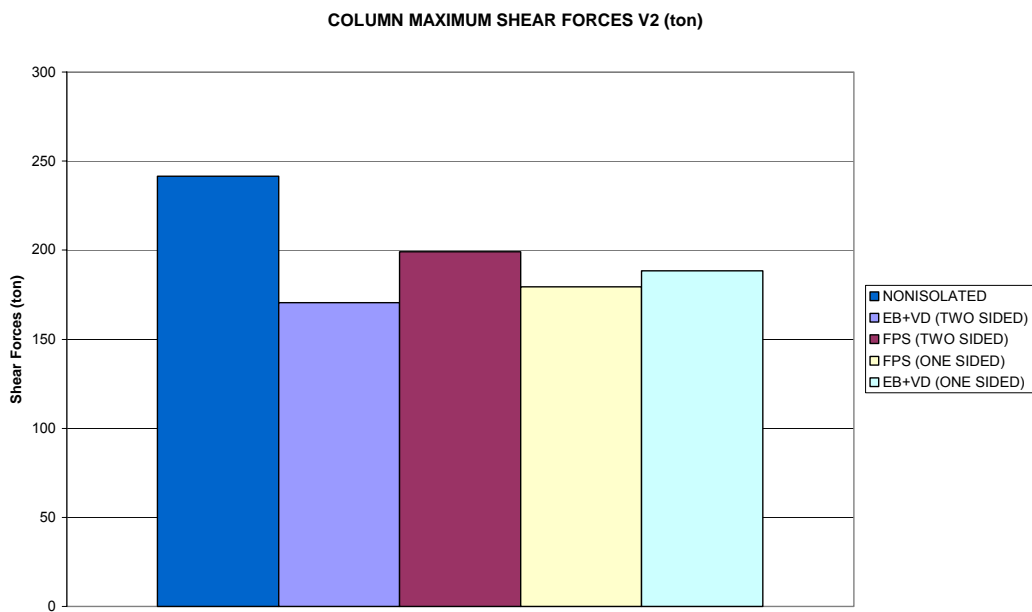


**Figure 3.13** Maximum Column Bottom Shear Forces V2 (ton) For Different Isolator Conditions.

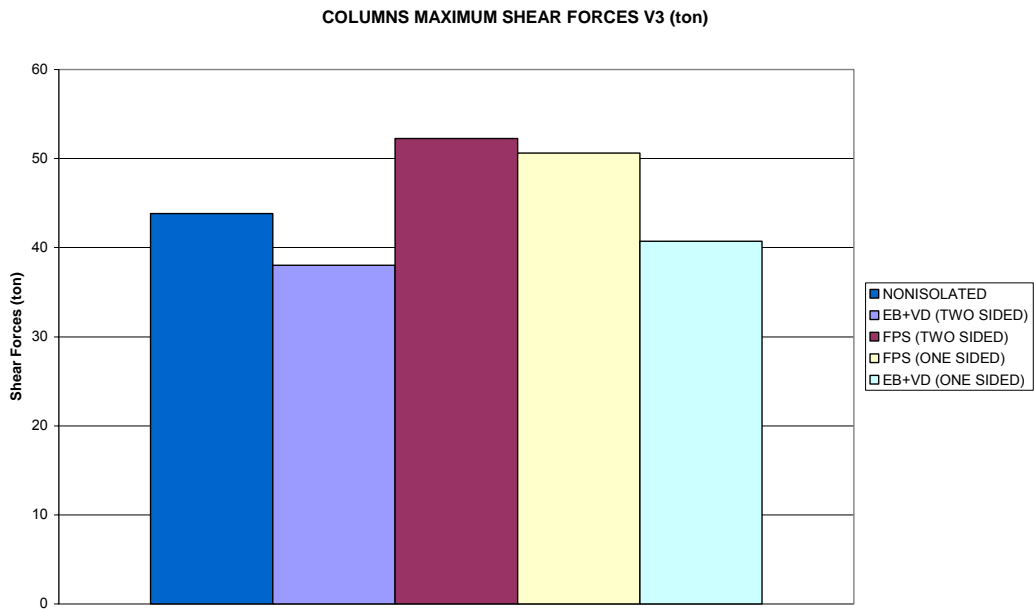


**Figure 3.14** Maximum Column Bottom Shear Forces V3 (ton) For Different Isolator Conditions.

Two and one sided FPS do not efficiently change the column bottom M2 moments as in the case of V3 shear forces of two and one sided FPS. On the other hand, they reduce the column bottom M3 moments as much as two and one-sided EB+VD. (Figures 3.15– 3.16)

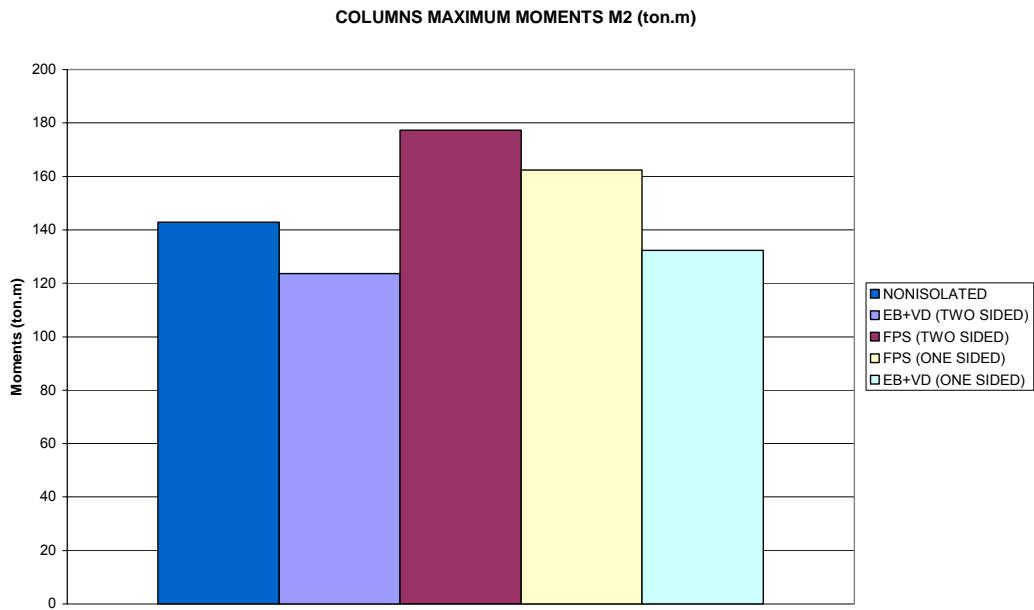


**Figure 3.15** Maximum Column Bottom Moments M2 (ton.m) For Different Isolator Conditions.

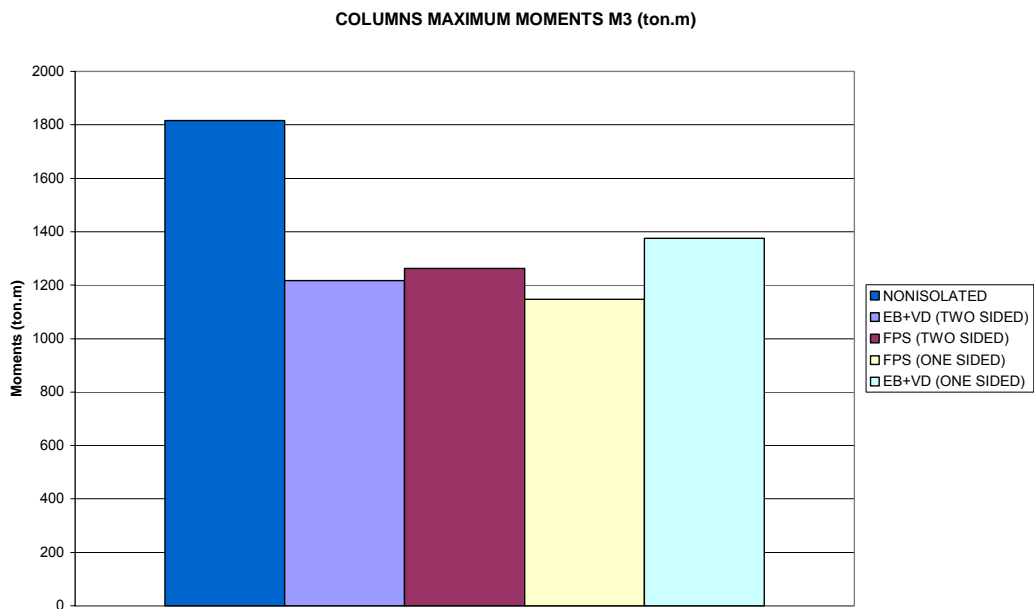


**Figure 3.16** Maximum Column Bottom Moments M3 (ton.m) For Different Isolator Conditions.

### 3.5 BILINEAR MODELLING

Berton, Infanti, Castellano and Hikosaka [34] indicate that most of the current isolation devices exhibit a nearly bilinear behavior. An ideal bilinear model is fully characterized by three main parameters. These are the strength force  $Q$ , the post – yield stiffness  $K_d$ , and the yield force  $F_y$ . (Figure 3.2)

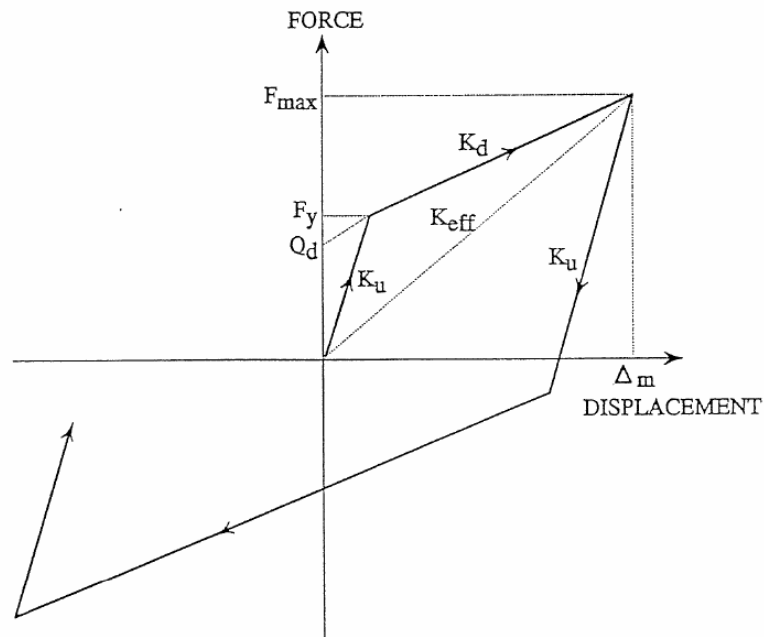


**Figure 3.17** Characteristics of Bilinear Isolation Bearings (*From AASHTO Guide Specifications for Seismic Isolation Design, Figure C4.*)

Where;

- $Q_d$  : Characteristic strength
- $F_y$  : Yield force
- $F_{max}$  : Maximum force
- $K_d$  : Post – elastic stiffness
- $K_u$  : Elastic (unloading) stiffness

$K_{\text{eff}}$  : Effective stiffness  
 $\Delta_m$  : Maximum bearing displacement

In this section, it was tried to investigate effects of bilinear characteristics on system behavior. There are two main parameters, which dominates the bilinear behavior. These are elastic stiffness,  $K_u$ , and post – elastic stiffness,  $K_d$ , of the bilinear modeling.

Two more studies were also performed on the 3D model of Halkapınar Gymnasium. One parameter kept constant while the other was changing. Analyze type – 1 consisted of the condition that when post – elastic stiffness,  $K_d$ , was taken as a constant value, elastic stiffness,  $K_u$ , was changing and analyze type – 2 was vice versa of analyze type – 1 which means that when elastic stiffness was taken as a constant value, post – elastic stiffness was changing. These two analyze type is also given in figure 3.3 and figure 3.4, respectively. Post – elastic stiffness,  $K_d$ , represents the non – linear portion of bilinear behavior. Therefore, non – linear time history analysis was performed during the two analyses to cover the post – elastic stiffness by SAP2000.

The general investigation method of this thesis is also valid for this section. One side isolated and two side isolated cases were performed during the analyze Type – 1 and Type – 2.

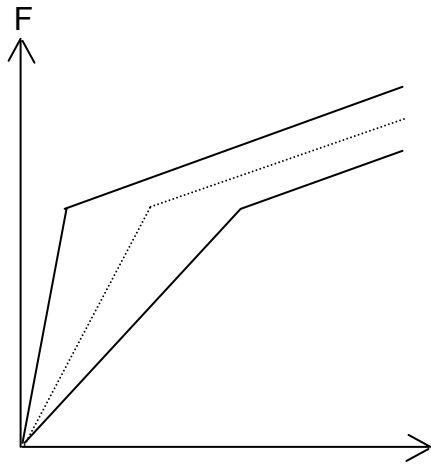


**Figure 3.18** Type-1 Analysis

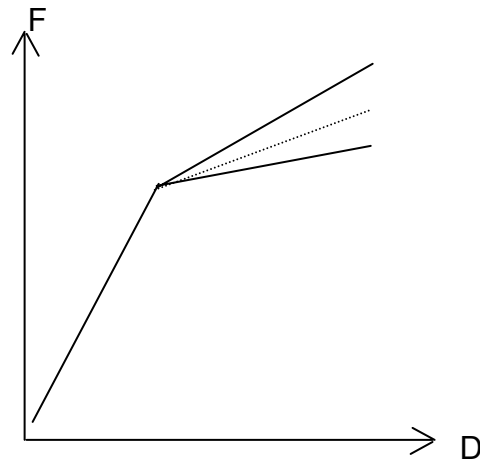


**Figure 3.19** Type-2 Analysis

Bilinear analysis combinations were compared with respect to modal periods of the structure, roof support displacements and column responses (moments and shear forces in each direction) for 7 time-history analyses as performed in section 3.1. Two sided and one sided analyze type - 1, two sided and one sided analyze type – 2 and non – isolated case were the comparison tools for this section.

Halkapınar Gymnasium SAP2000 3D model requires some bilinear curve parameters to be able to define the isolator in the system. These required parameters were taken from chapter 3.1 Lead – Plug bearing analyses. Therefore, calculation steps of these values are not again given here and only the analysis results are going to be presented. Because, obtaining system behavior under different bilinear characteristics is the main target of this section.

There are five main parameters required for analyses. Two of them, effective stiffness and effective damping, are for linear analysis cases and three of them, stiffness, yield strength and post – elastic stiffness ratio, are for non – linear analysis cases. Actually, stiffness of non – linear analysis case represents the elastic portion of bilinear model. On the other hand, Post – elastic stiffness

represents the non-linear portion of bilinear model and post – elastic stiffness ratio is obtained by post – elastic stiffness ratio divided by elastic stiffness. Bilinear parameters of actual case are as follows:

For linear analysis cases:

Effective Stiffness : 1855kN/m

Effective Damping : 0.3

For non – linear analysis cases:

Stiffness : 8300kN / m (Elastic Stiffness)

Yield Strength : 11.4 Mpa = 11400 kN / m<sup>2</sup>

Post – Elastic Stiffness Ratio : 0.1 ( $K_d / K_u$ )

### **3.5.1 Analyze Type – 1 (Elastic Stiffness Changing, Post – Elastic Stiffness Constant)**

Analyze type – 1 covers the all the parameters being constant except from the stiffness for non – linear analysis case. 100 is scale factor used in the analyses for elastic stiffness of linear portion bilinear model. Due to post – elastic stiffness being constant, post – elastic stiffness ratios were also scaled with the same factor in the model. The investigation of general support combinations was also valid for this section. In other words, two sides isolated and one side isolated combinations are two comparison cases with the models in section 3.1. The bilinear parameters changing in the analyses are as follows for both X and Y global directions.

- For scale factor with 100 :

Stiffness : 830000kN / m (Elastic Stiffness)

Post – Elastic Stiffness Ratio : 0.001 ( $K_d / K_u$ ) (To keep  $K_d$  constant)

### **3.5.2 Analyze Type – 2 (Elastic Stiffness Constant, Post – Elastic Stiffness**

#### **Changing)**

Analyze type – 2 covers the all the parameters being constant except from the post – elastic stiffness for non – linear analysis case. 0.01 is the scale factor used in the analyses for post – elastic stiffness of non – linear portion bilinear model. Due to elastic stiffness of bilinear model being constant, only the post – elastic stiffness ratios were scaled with these factors. The investigation of general support combinations was also valid for this section. In other words, two sides isolated and one side isolated combinations are two comparison cases with the models in section 3.1. The bilinear parameter changing in the analyses is as follows for both X and Y global directions.

- For scale factor with 0.01 :

Post – Elastic Stiffness Ratio : 0.001 ( $K_d / K_u$ )

### **3.5.3 Comparisons of Modal Periods**

All isolation cases increase the modal periods of the structure for the first five modes. However, two sided isolated cases show the same modal behaviors between themselves and one-sided isolated cases also show the same modal behaviors between themselves. (Figure 3.5)

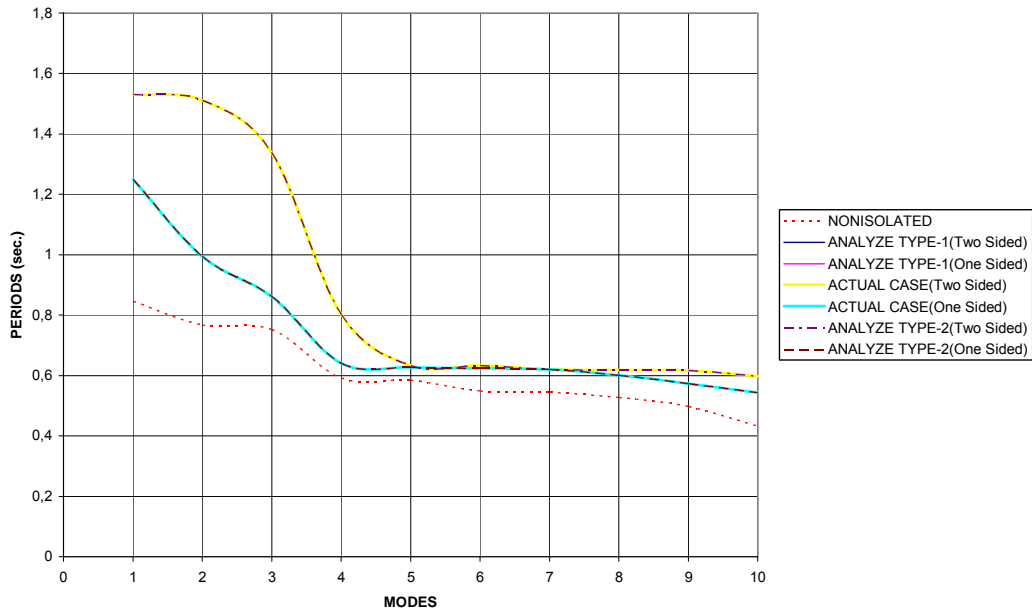


**Figure 3.20** Modal Period Behaviors of Analyze Type-1 & Type-2 (Two & One Sided) and Actual Case (Two & One Sided) Support Conditions

Two sided isolation conditions increase the structure period more than the one sided isolation conditions for the first five modes. Changing in elastic stiffness and post – yield elastic stiffness of non – linear portion of bilinear curve does not have any effect on the system modal responses.

### 3.5.4 Comparisons of Roof Support Displacements

All of the isolation cases using for comparison increases the roof support displacements in both directions U1 and U2. Analyze type – 2 (Two & One Sided) do not show any difference from the actual case for both roof support displacements. This means that isolator had never reached yield displacement in the analysis. On the other hand, Analyze type – 1 (Two & One Sided) case reduces the roof support displacements in both directions U1 and U2 for especially two-sided isolated case. (Figure 3.6 - 3.7)

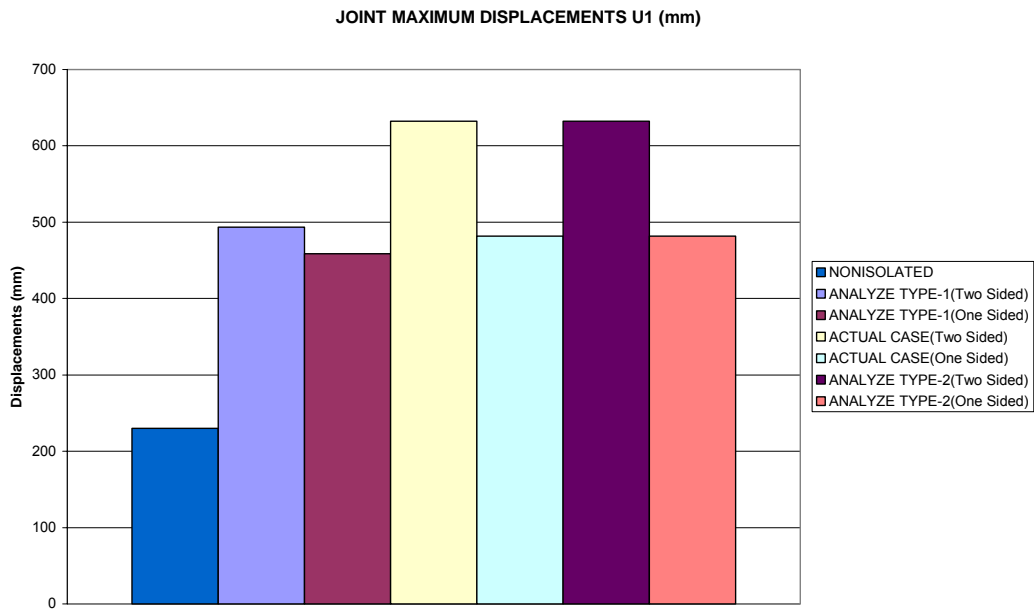


**Figure 3.21** Maximum Roof Support Displacements (U1 (mm))For Different Isolator Conditions.

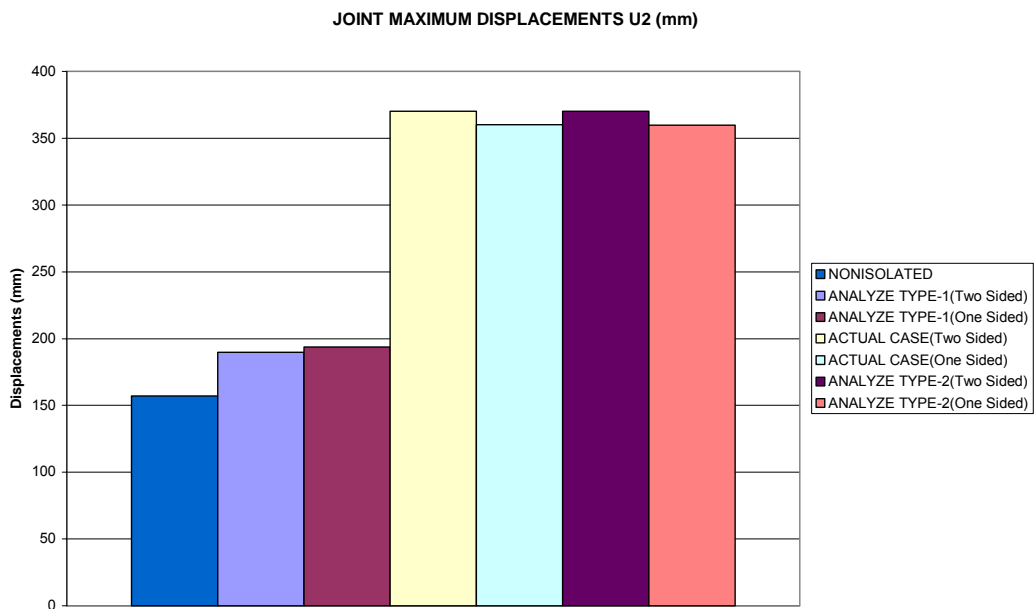


**Figure 3.22** Maximum Roof Support Displacements (U2 (mm)) For Different Isolator Conditions.

The reason why analyze type – 1 (elastic stiffness changing) affects the system displacement response with respect to actual case, while analyze type – 2 (post – elastic stiffness changing) does not have any effect on them, is isolator displacements falls in the elastic range of bilinear curve.

### **3.5.5 Comparisons of Column Responses (Shear Forces & Moments)**

While column responses were compared, only the columns being supports of the roof of the structure were taken into account and maximum shear forces and moment values were compared with each other for different isolator combinations. Shear forces and moments were compared separately for X and Y in local directions. For that reason, V2 and M2 stand for local X direction, V3 and M3 stand for local Y direction. (Figure 2.23)

Analyze type – 2 (Two & One Sided) do not change system response with respect to actual case for column bottom shear forces of V2 and V3. In other words, post – elastic stiffness does not change the shear forces subjected to the columns under seven different time history analyses. As previous section, isolators do not reach their yield displacement limits. Therefore, only the analyze type – 1 (Two & One Sided) affects the system response due to displacements being in the range of elastic range. Furthermore, while post – elastic stiffness being kept constant, increase in elastic stiffness leads to increase in column bottom shear forces for X direction. (Figure 3.8 - 3.9)

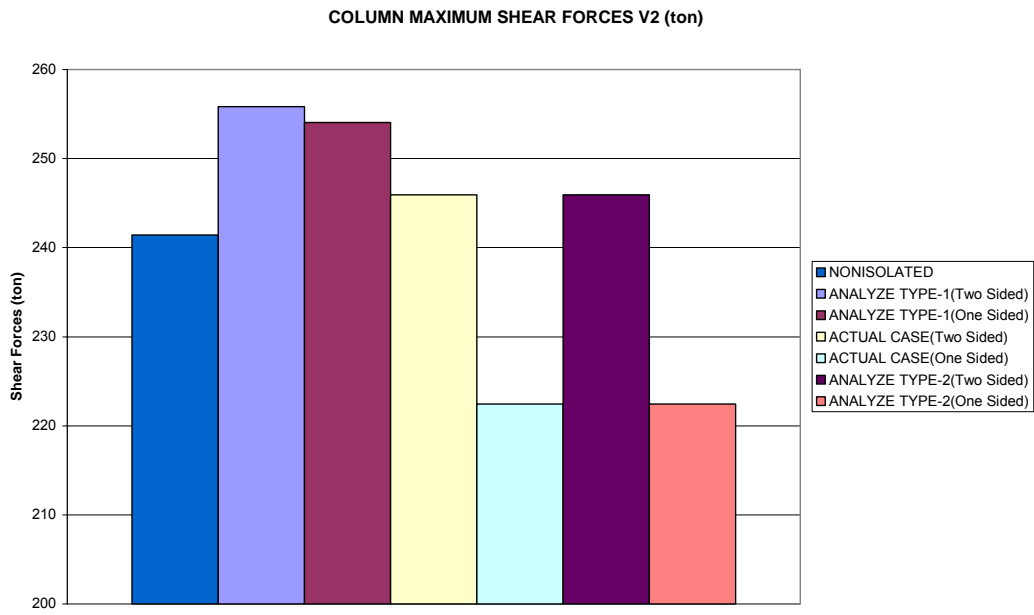


**Figure 3.23** Maximum Column Bottom Shear Forces V2 (ton) For Different Isolator Conditions.



**Figure 3.24** Maximum Column Bottom Shear Forces V3 (ton) For Different Isolator Conditions.

Analyze type – 1 (Two & One Sided) cases increase the column bottom moments of M3 and decrease them of M2 with respect to actual case of bilinear curve as they cause same response for column bottom shear forces. On the other hand, Analyze type – 2 (Two & One Sided) cases do not cause any change in column bottom moments of M2 and M3 when they are compared with actual case of bilinear curve. This result is mainly due to the isolator displacements that did not reach yield limit. (Figure 3.10 - 3.11)

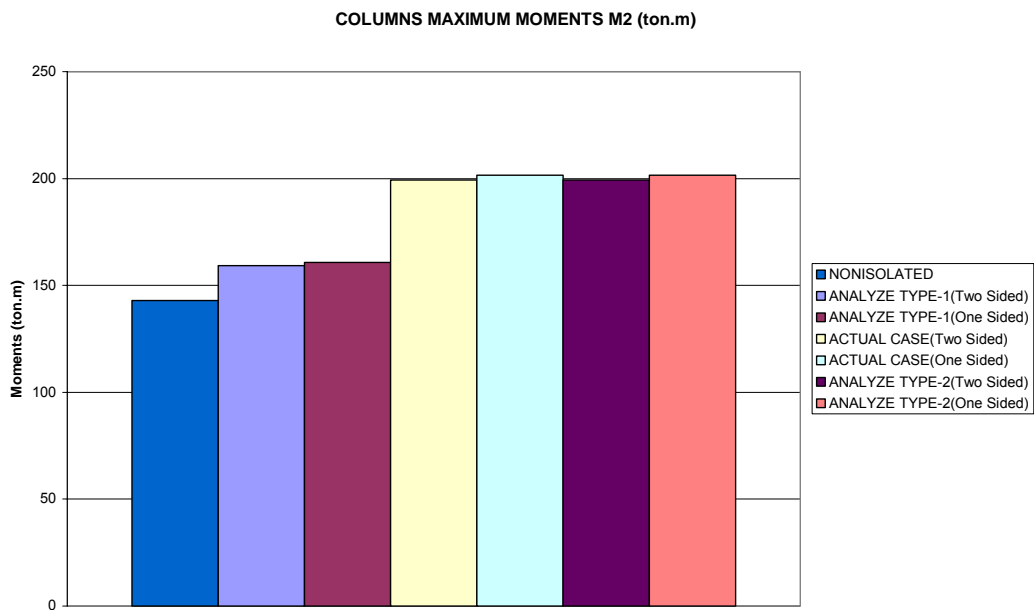


**Figure 3.25** Maximum Column Bottom Moments M2 (ton.m) For Different Isolator Conditions.

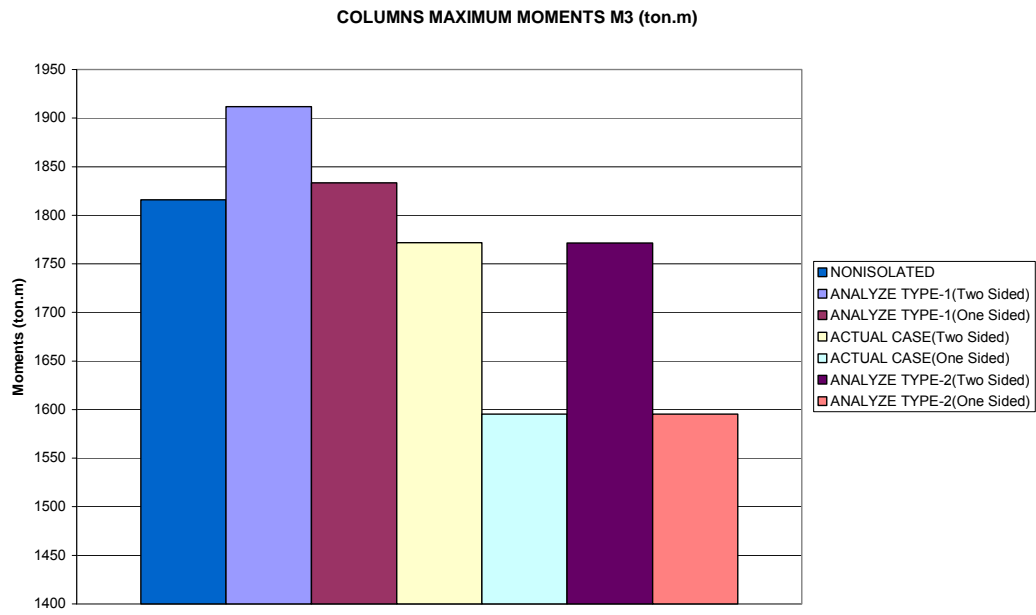


**Figure 3.26** Maximum Column Bottom Moments M3 (ton.m) For Different Isolator Conditions.

## CHAPTER 4

### CONCLUSIONS AND RECOMMENDATIONS

#### 4.1 SUMMARY

Seismic isolation has been widely used in Turkey on bridges and roof of the structures for last years. Elastomeric bearings with or without reinforcing sheets are more widely used for supports of pre – cast beams of bridges than the other supports of the structures, because, elastomeric bearings are well known and practically installed seismic isolators between isolation techniques. However, different isolator types are also being used on supports of, especially, roof of the structures, such as airports, gymnasiums etc with the development of knowledge of seismic isolators. On the other hand, there are a lot of parameters that should be defined more accurately with certain code restrictions and therefore, seismic isolation needs to be defined more accurately by the codes. There is not any code related to seismic isolators in Turkey. In general, international codes are used as guides for Turkish civil engineers such as AASHTO Guide Specifications for Seismic Isolation Design, UBC – 97, FEMA – 273 etc. This is also related to researches performed on seismic isolation as either experimental or analytical. Therefore, this study is aimed to investigate effects of seismic isolators and their support combinations on a real life structure, Halkapınar Gymnasium. First, existing seismic roof isolation, elastomeric bearings with viscous dampers, was investigated to get the effects of each member of this isolation configuration. Then, other more widely used isolator types, Lead Rubber Bearing and Friction Pendulum Systems were also investigated to see how changes the structural response with respect to existing roof isolation and non – isolated case. Finally,

the bilinear behavior, which is the behavior of most of the isolators, was studied by changing the two main parameters that are elastic and post – elastic stiffness of the bilinear curves. All analyses were compared within themselves and existing isolators of Halkapınar gymnasium, elastomeric bearings with viscous dampers. Furthermore, non – isolated case was used to examined either isolation type is needed or needless.

The general philosophy of seismic isolation is to make the structures more flexible when they are subjected to ground excitations. Therefore, it is expected the structures to gain high displacement capacities without any collapse or serviceability interruption. On the other hand, the structural system ends with failure if plastic hinges are designed in order to supply required energy absorption for this level of displacements. Therefore, excessive energy is absorbed by kinetic energy of movements and thermal loss of isolators. So that, less amount of earthquake forces is subjected to structures. For that reason, modal behaviors were firstly investigated for each section in this thesis. Modal behaviors of the structures also sign to the flexibility of the stiffness of the systems. Then, roof support maximum displacements were compared within each section to see the feasibility of seismic isolation solution. Finally, structural responses, column bottom shear forces and moments, were compared with respect to non – isolated case and existing roof seismic isolation, elastomeric bearings with viscous dampers, if the seismic isolation alternative is effective or not.

Bilinear model is accepted as a general behavior of seismic isolators in the literature. Effects of two main parameters, consisting of bilinear curve were also included into the investigations of this thesis.

## 4.2 CONCLUSIONS

Similar to analysis cases, author wishes to present the conclusions also in two parts. Because, while first part stands for existing roof isolation system and its investigation, second part stands for alternative seismic isolation solutions.

### 4.2.1 Elastomeric Bearing with Viscous Dampers

Elastomeric bearing with viscous dampers increases the structural period of the gymnasium either they are installed two sided or one sided. But, they show the same period value with non – isolated structure at mode number of 5. Viscous dampers do not have any effect on the modal behavior of the structures when they are installed as only isolators. On the other hand, when elastomeric bearings are used as seismic isolators, gymnasium modes are greatly improved, especially at two-sided elastomeric bearing isolation. Importance of viscous dampers comes into scene at this moment, because modal periods are reduced by them. In other words, viscous dampers lower the roof support displacements of the elastomeric bearing isolation conditions.

Structural responses are reduced by elastomeric bearings with viscous dampers, when the results are compared with non – isolated condition. Elastomeric bearings provide structural responses to decrease for one direction and cause to increase for other direction in terms of column bottom shear forces and moments. Viscous dampers do not have any effect on the responses at the end of time – history analyses, if they are used as only isolators.

Finally, all of these analyses show that elastomeric bearings become effective when they are used together with viscous dampers. If slight reduction of system performance can be accepted, one-sided elastomeric bearing with viscous damper can be advised as an economical solution for Halkapınar Gymnasium. However, One-sided isolation cases make the structure to unsymmetrical

configuration, which is reason for torsions in columns. Therefore, two-sided elastomeric bearing with viscous dampers is the most feasible solution for Halkapınar.

#### **4.2.2 Other Isolator Types and Bilinear Behavior**

Lead rubber bearing and friction pendulum isolators were studied as an alternative isolation solution of elastomeric bearing with viscous dampers. Lead rubber bearing and friction pendulum isolator were designed for Halkapınar gymnasium steel roof by considering code restrictions.

Lead rubber bearings provide higher modal period values than the elastomeric bearing with viscous damper isolator. In other words, two and one sided lead rubber bearings let higher modal periods than two and one-sided EB+VD, respectively. On the other hand, when structural responses are considered, both two and one sided lead rubber bearings do not change the non – isolated model behavior as effectively as elastomeric bearings with viscous dampers do, in terms of column bottom shear forces and moments with the designed lead rubber bearing.

Friction pendulum isolator did not have enough flexibility in horizontal direction with the given details. Because, one-sided FPS did not change the modal behavior of the non – isolated system and two-sided FPS showed less mode period values than the non – isolated structure for higher modes. While two sided FPS lowers the roof support displacement in short direction of plan, one-sided FPS increases the displacements in other long direction of the plan. Two and one-sided FPS increased the column responses only in one direction and they did not change the column bottom shear forces and moments in other direction, although two and one sided EB+VD reduced the column responses in both directions.

Bilinear modeling is the accepted isolator behavior in the literature. The two main parameters, elastic stiffness and post – elastic stiffness, were search tools to investigate bilinear effect on the structural response. One of them was taken as constant while the other one was factored. Difference did not occur in modal behavior within each support condition, two sided and one sided respectively. This is due to the structural analysis program uses the linear analysis features of bilinear parameters, effective stiffness, to find modes of the system. Increase in elastic stiffness reduced the roof support displacements as expected. Although post – elastic stiffness was reduced with respect to actual case, it did not cause any change to roof support displacements. This can be explained by roof support displacements of defined bilinear curve falls on the elastic range at the end of time – history analyses. Therefore, analysis case – 2 showed the same column responses with the actual case. Furthermore, increase in elastic stiffness of bilinear curve resulted in increase column bottom shear forces and moments.

#### **4.3 RECOMMENDATIONS**

The followings are recommended for the future studies:

- Investigate the behavior of bilinear curve by changing yielding force or maximum displacements
- Investigate effects of parameters of friction pendulum bearings on the structural responses
- Investigate if it is possible to model roof of the systems in two dimensional models or simple models to understand the isolator's behaviors.

## REFERENCES

- [1] Akyüz U. (2006), Seismic Base Isolation (CE 793) Lecture Notes.
- [2] MAURER SÖHNE, “Maurer Seismic Isolation Systems, Products and Technical Information”, 2007, pp.3.
- [3] Zhiping, Z., ICOMOS “ International Wood Committee”, web page: “[www.icomos.org/iwmc/seismic/Zhiping.pdf](http://www.icomos.org/iwmc/seismic/Zhiping.pdf)”
- [4] Seidensticker, R.W., “Testing, licensing, and code requirements for seismic isolation systems”, Technical Report, Argonne National Lab., IL (USA), 2001 May 13, pp.1.
- [5] NEHRP Recommended Provisions for Seismic Regulations for New Buildings and Other Structures, Part 2: Commentary (FEMA 450-2/2003 edition).
- [6] Villaverde, R., Mosqueda, G., “Aseismic Roof Isolation System: Analytic and Shake Table Studies”, Earthquake Engineering and Structural Dynamics, Vol. 28, 1999, pp. 217-234.
- [7] Villaverde, R., “Roof Isolation System to Reduce the Seismic Response of Buildings: A Preliminary Assessment”, Earthquake Spectra, Vol. 14, No 3, August 1998, pp. 521-531.
- [8] Kikuchi, M., Aiken, I.D., “An Analytical Hysteresis Model for Elastomeric Seismic Isolation Bearings”, Earthquake Engineering and Structural Dynamics, Vol. 26, 1997, pp. 215-231.
- [9] Imbimbo, M, Kelly, J.M., “Influence of Material Stiffening on Stability of Elastomeric Bearings at Large Displacements”, Journal of Engineering Mechanics, September 1998, pp. 1045-1049
- [10] Koh, C. G., and Kelly, J. M., “Effects of Axial Load on Elastomeric Isolation Bearings.” Rep. No. UCB/EERC-86-12, Earthquake Engrg., 1986
- [11] Kelly, J. M., “Earthquake-Resistant Design with Rubber, 2<sup>nd</sup> ed.”, Springer-Verlag, London, 1996.

- [12] Yantao, X., Xue H., “Time-History Analysis of Earthquake Response on Structure with Non-Linear Fluid Viscous Damper”, pp.2-3
- [13] Hwang, J., S., “Seismic Design of Structures with Viscous Dampers”, International Training Programs for Seismic Design of Building Structures Hosted by National Center for Research on Earthquake Engineering Sponsored by Department of International Programs, National Science Council, 2002, pp. 12-13.
- [14] Abe, M., Yoshida, J., Fujino, Y., “Multiaxial Behaviors of Laminated Rubber Bearings and Their Modeling. I: Experimental Study”, *Journal of Structural Engineering*, ASCE, DOI: 10.1061 / (ASCE) 0733 / 9445 (2004) 130:8 (1119). August 2004, pp. 1119.
- [15] Robinson, W. H., and Tucker, A. G. (1977), “A Lead-Rubber Shear Damper”, *Bull. New Zealand Natl. Soc. Earthq. Eng.*, Vol. 8, No3, pp. 151-153.
- [16] Robinson, W. H., and Tucker, A. G. (1983), “Test Results for Lead-Rubber Bearings for the William M. Clayton Building, Toe Toe Bridge, and Waiotukupuna Bridge”, *Bull. New Zealand Natl. Soc. Earthq. Eng.*, Vol. 14, No1, pp. 21-33.
- [17] Naeim F., Kelly J. M., “Design of Seismic Isolated Structures: From Theory to Practice”, John Wiley & Sons, Inc., 1999, pp. 49-50.
- [18] Buckle, I.G., Constantinou, M., C., Dicleli, M., Ghasemi, H., “Seismic Isolation of Highway Bridges”, MCEER, Federal Highway Administration, August 21, 2006, pp. 39, 53, 105-141.
- [19] Doudoumis, I.N., Gravalas, F., Doudoumis, N.I., “Analytical Modeling of Elastomeric Lead – Rubber Bearings With the Use of Finite Element Micro models”, 5<sup>th</sup> GRACM International Congress on Computational Mechanics Limassol, 29June – 1July, 2005, pp. 1-8.
- [20] Yılmaz Ç., Booth, E., Sketchley, C., “Retrofit of Antalya Airport International Terminal Building, Turkey Using Seismic Isolation”, 1st European Conference on Earthquake Engineering and Seismology, Geneva, Switzerland, 3-8 September 2006, pp.1259.
- [21] Ryan, K.L., Chopra, A.K., “Estimating Bearing Response in Symmetric and Asymmetric – Plan Isolated Building with Rocking and Torsion”, *Earthquake Engineering and Structural Dynamics*, 24 February 2006, John Wiley & Sons, Ltd., 1009-1036
- [22] Skinner, R.J., Robinson, W.H., McVerry, G.H., “An Introduction to Seismic Isolation”, Wiley; New York, 1993.

- [23] International Code Council. International Building Code, Falls Church, V.A., 2000.
- [24] Ryan, K.L., Kelly, J.K., Chopra, A.K., “Nonlinear Model for Lead – Rubber Bearings Including Axial – Load Effects”, Journal of Engineering Mechanics, ASCE, December 2005, pp. 1270-1278.
- [25] Hwang, J.S., Hsu, T.Y., “Experimental Study of Isolated Building under Triaxial Ground Excitations.”, Journal of Structural Engineering, 2000, 126 (8), pp.879-886.
- [26] Mokha, A., Amin, N., Constantinou, M., Zayas, V., “Seismic Isolation Retrofit of Large Historic Buildings”, Journal of Structural Engineering, ASCE 1996, 122, pp. 298-308.
- [27] Almazàn, J.L., Llera, J.C.D.L., “Analytical Model of Structures with Frictional Pendulum Isolators”, Earthquake Engineering and Structural Dynamics, 2002, 31, pp. 305-332.
- [28] Tsai, C.S., Chiang, T.C., Chen, B.J., “Seismic Behavior of MFPS Isolated Structure under Near – Fault Sources and Strong Ground Motions with Long Predominant Periods”, ASME Pressure Vessels and Piping Conference, Seismic Engineering, Chen J.C.(ed.), Cleveland, Ohio, USA, 20-24 July, 2003, 466, pp. 73-79.
- [29] Tsai, C.S., Chen, W.S., Chiang, T.C., Chen, B.J., ”Component and Shaking Table Tests for Full – Scale Multiple Friction Pendulum System”, Earthquake Engineering and Structural Dynamics, 2006, 35, pp. 1653-1675.
- [30] Murnal, P., Sinha, R., “Earthquake Resistant Design of Structures Using the Variable Frequency Pendulum Isolator”, Journal of Structural Engineering, July 2002, 128, pp.870-880.
- [31] Almazàn, J.L., Llera, J.C.D.L., “Physical Model for Dynamic Analysis of Structures with FPS Isolators”, Earthquake Engineering and Structural Dynamics, 2003, 32, pp. 1157-1184.
- [32] Malangone, P., Ferraioli, M., “A Modal Procedure for Seismic Analysis of Non – Linear Base – Isolated Multistory Structures”, Earthquake Engineering and Structural Dynamics, 1998, 27, pp. 397-412.
- [33] Fragiaco, M., Rajgelj, S., Cimadam, F., “Design of Bilinear Hysteretic Isolation Systems”, Earthquake Engineering and Structural Dynamics, 2003, 32, pp. 1333-1352.

- [34] Berton, S., Infanti, S., Castellano, M.G., Hikosaka, H., “Self – Centering Capacity of Seismic Isolation Systems”, Structural Control and Health Monitoring, 20 August 2006, pp. 1-20.
- [35] Erkus, B., Johnson, E.A., “Smart Base – Isolated Benchmark Building Part III: A Sample Controller for Bilinear Isolation”, Structural Control and Health Monitoring, 2006, 13, pp. 605-625.
- [36] Park, J.G., Otsuka, H., “Optimal Yield Level of Bilinear Seismic Isolation Devices” Earthquake Engineering and Structural Dynamics, 1999, 28, pp. 941-955.
- [37] Agostino, M., Çelebi, N., Varol, B., “Halkapınar Gymnasium Structural Dynamic Report”, ALGA S.p.A., Yüksel Proje Uluslararası A.Ş., June 2005.
- [38] McGuire, W., Winter, G, “Structural Analysis and Design Series”, Prentice Hall International Series in Theoretical and Applied Mechanics, 1968, pp.1087-1089.

## APPENDIX

### A.1 SYSTEM PROPERTY MODIFICATION FACTORS FOR SLIDING ISOLATORS

**Table A.1.1** Maximum Values for Temperature  $\lambda$  – factors for Sliding Isolators ( $\lambda_{max,t}$ )

Minimum Temperature for Design		Unlubricated PTFE	Lubricated PTFE	Bimetallic Interfaces
°C	°F			
21	70	1.0	1.0	To be established by test
0	32	1.1	1.3	
-10	14	1.2	1.5	
-30	-22	1.5	3.0	

**Table A.1.2** Maximum Values for Aging  $\lambda$  – factors for Sliding Isolators ( $\lambda_{max,a}$ )<sup>1</sup>

Environment/ Condition	Unlubricated PTFE		Lubricated PTFE		Bimetallic Interfaces <sup>4</sup>	
	Sealed	Unsealed <sup>2</sup>	Sealed	Unsealed <sup>2</sup>	Sealed	Unsealed <sup>2</sup>
Normal	1.1	1.2	1.3	1.4	2.0	2.2
Severe <sup>3</sup>	1.2	1.5	1.4	1.8	2.2	2.5

- Notes:
1. Values are for 30 year exposure of stainless steel. For chrome – plated carbon steel, multiply values by 3.0
  2. Unsealed conditions assumed to allow exposure to water and salt, thus promoting further corrosion.
  3. Severe environments include marine and industrial environments.
  4. Values for bimetallic interfaces apply to stainless steel – bronze interfaces.

**Table A.1.3** Maximum Values for Travel and Wear  $\lambda$  – factors for Sliding Isolators ( $\lambda_{max,tr}$ )

Cumulative Travel		Unlubricated PTFE	Lubricated PTFE	Bimetallic Interfaces
Ft	M			
<3300	<1005	1.0	1.0	To be established by test
$\leq$ 6600	$\leq$ 2010	1.2	1.0	To be established by test
>6600	>2010	To be established by test	To be established by test	To be established by test

**Table A.1.4** Maximum Values for Contamination  $\lambda$  – factors for Sliding Isolators ( $\lambda_{max,c}$ )

	Unlubricated PTFE	Lubricated PTFE	Bimetallic Interfaces
Sealed with stainless steel surface facing down	1.0	1.0	1.0
Sealed with stainless surface facing up <sup>1</sup>	1.1	1.1	1.1
Unsealed with stainless surface facing down	1.1	3.0	1.1
Unsealed with stainless surface facing up	Not allowed	Not allowed	Not allowed

Notes: 1. Use factor of 1.0 if bearing is galvanized or painted for 30 – year lifetime.

## A.2 DESIGN SPECTRUMS

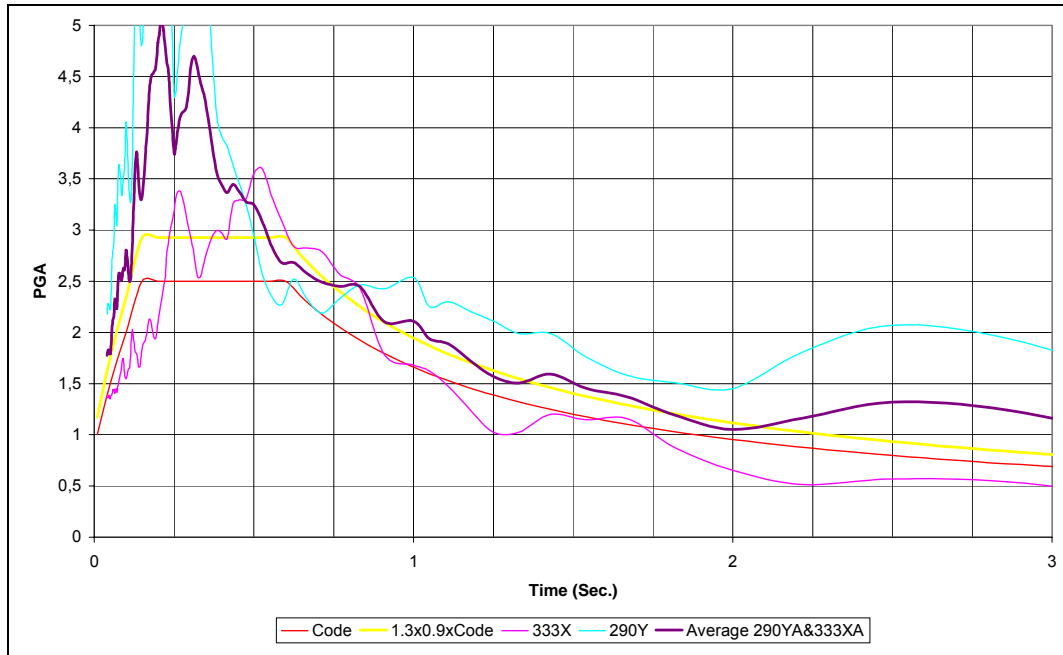


Figure A.2.1 Spectrum Comparisons of 290Y & 333X

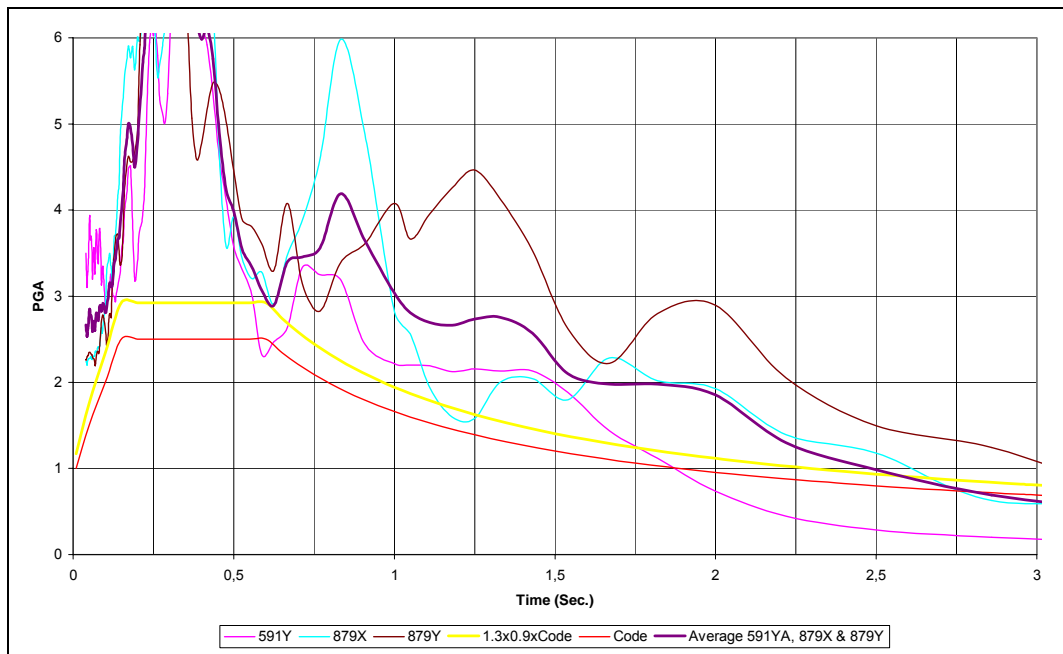
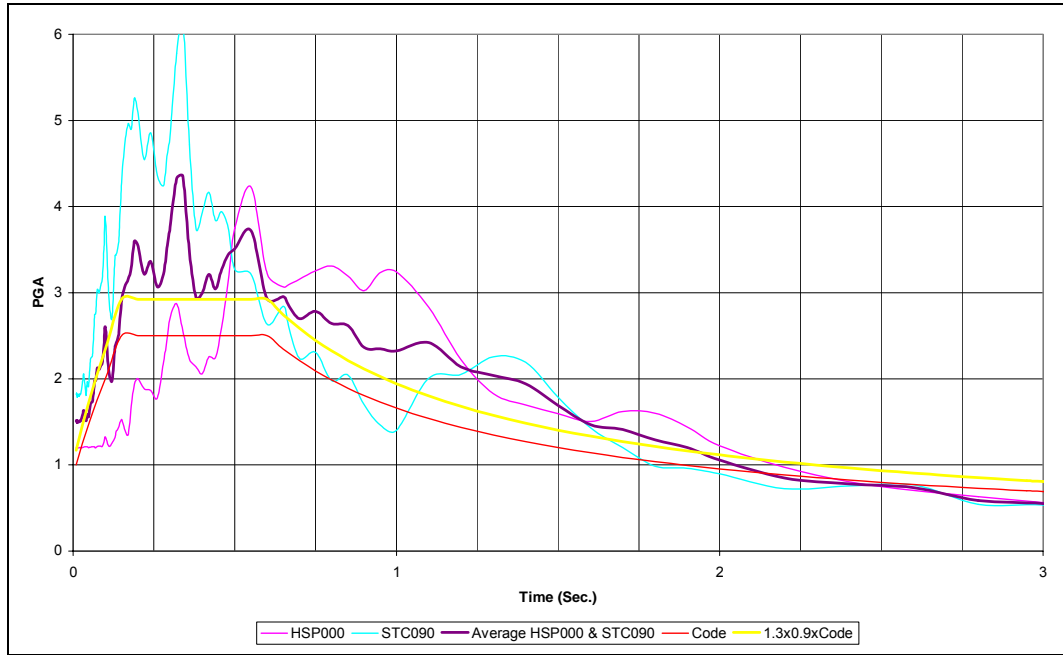
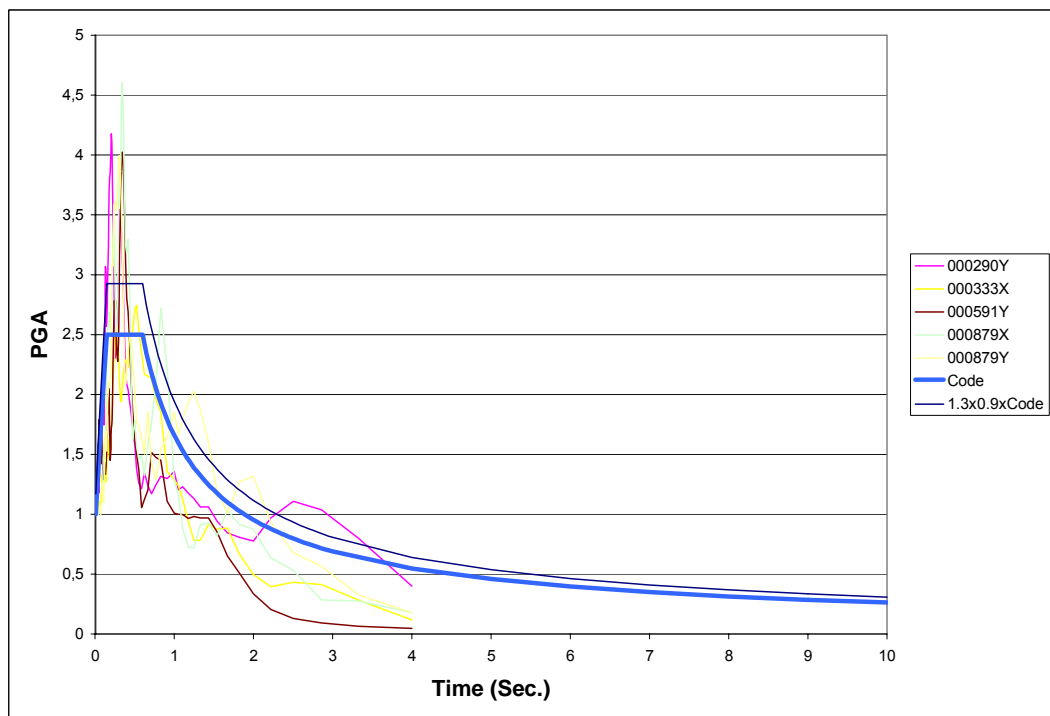


Figure A.2.2 Spectrum Comparisons of 591Y, 879X & 879Y



**Figure A.2.3** Spectrum Comparisons of HSP000 & STC090



**Figure A.2.4** Design Spectrums - 1

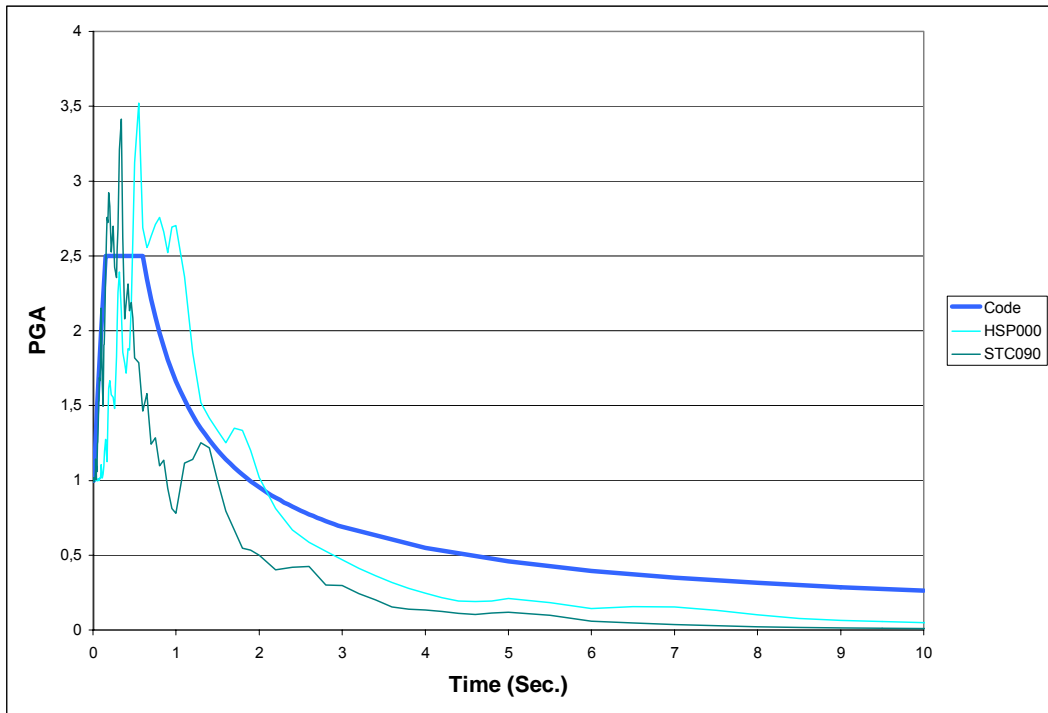


**Figure A.2.5** Design Spectrums - 2

### A.3 NORMALIZED RESPONSE SPECTRUMS

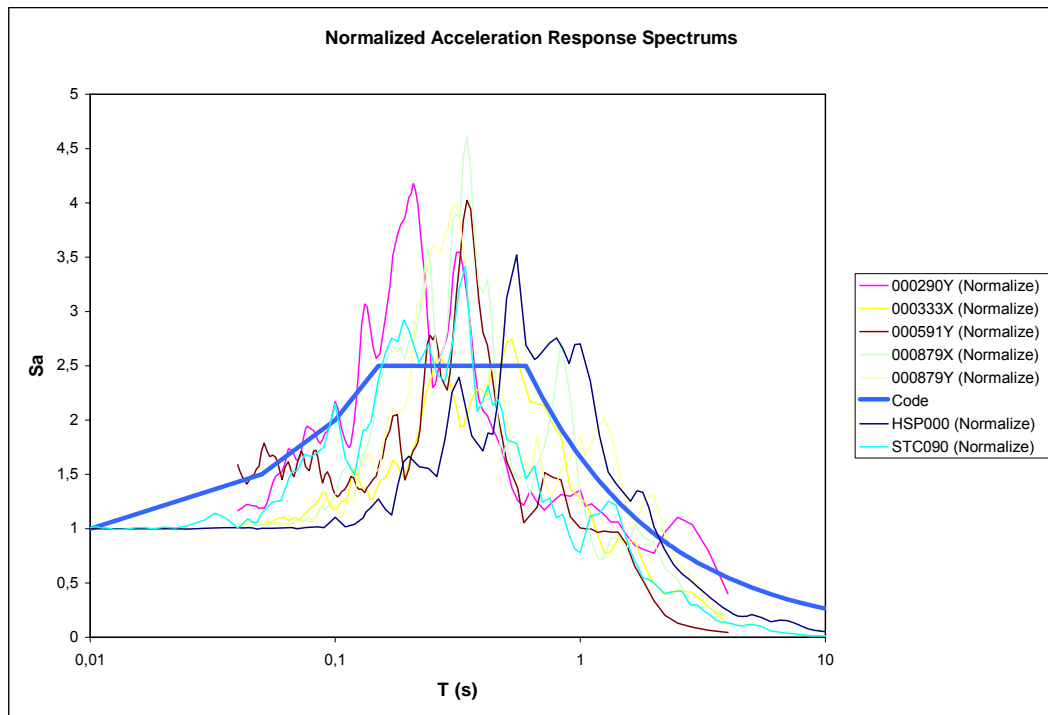
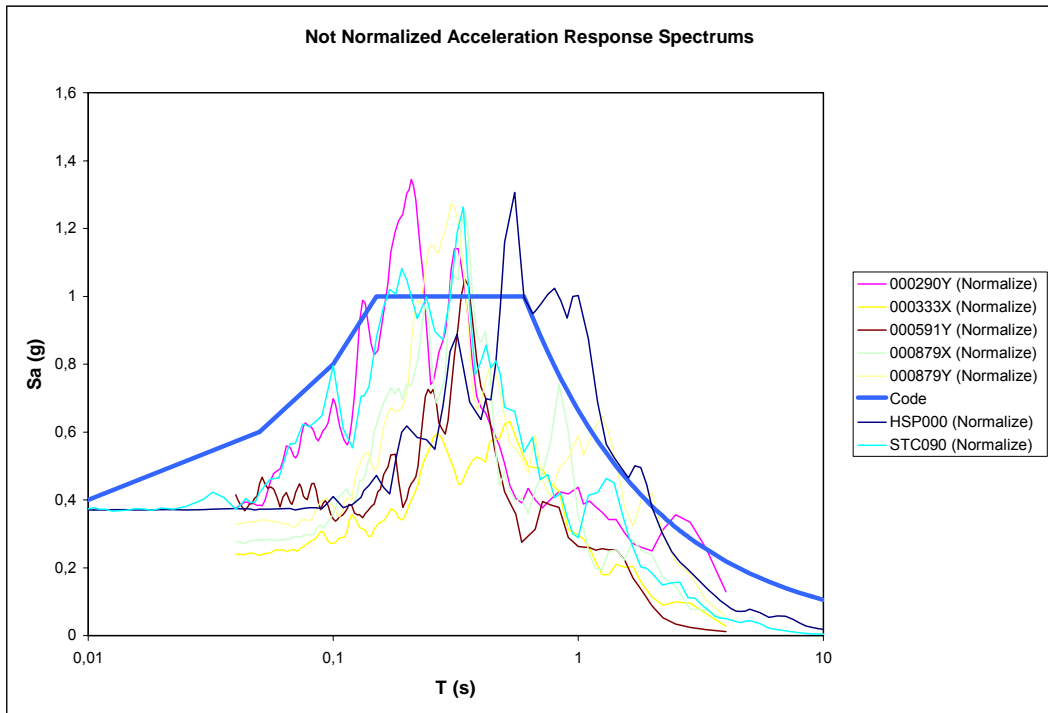
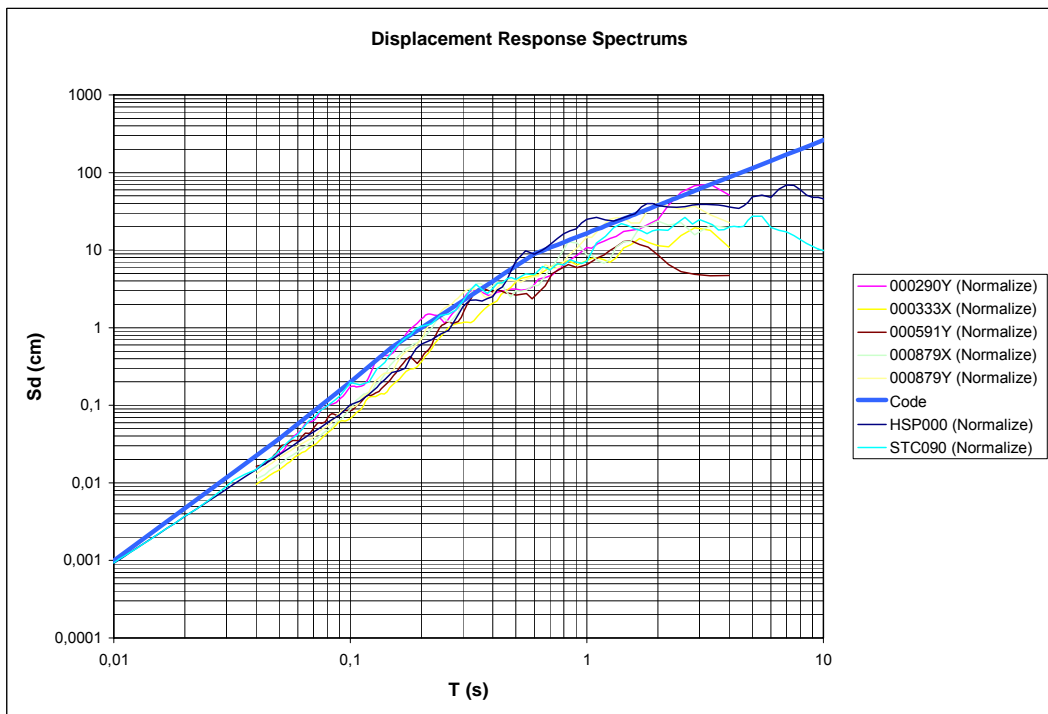


Figure A.3.1 Normalized Acceleration Response Spectrums



**Figure A.3.2** Not Normalized Acceleration Response Spectrums



**Figure A.3.3** Displacement Response Spectrums

## A.4 MAXIMUM AXIAL FORCES ON ISOLATORS

**Table A.4.1** Maximum Axial Forces on the Isolators for Each Analysis Case

Analyze Case	Isolator	Tme-History	StepType	P
Text	Text	Text	Text	Ton
Two Sided EB+VD	EB	HSP000_Y	Max	104,9682
	VD	HSP000_X	Min	-55,6957
One Sided EB+VD	EB	HSP000_Y	Max	113,2771
	VD	HSP000_Y	Max	55,9142
Two Sided EB	EB	HSP000_Y	Min	-83,1755
One Sided EB	EB	HSP000_X	Max	100,9146
Two Sided VD	VD	333XA_Y	Max	22,9194
One Sided VD	VD	333XA_Y	Max	22,9343
Two Sided LRB	LRB	HSP000_Y	Min	-239,822
One Sided LRB	LRB	HSP000_Y	Max	178,3798
Two Sided FPS	FPS	333XA_Y	Min	-358,239
One Sided FPS	FPS	HSP000_X	Min	-453,814

## A.5 MODE SHAPES OF ISOLATION CASES FOR FIRST FOURTH MODES

(Figures were exaggerated to understand behavior of the system)

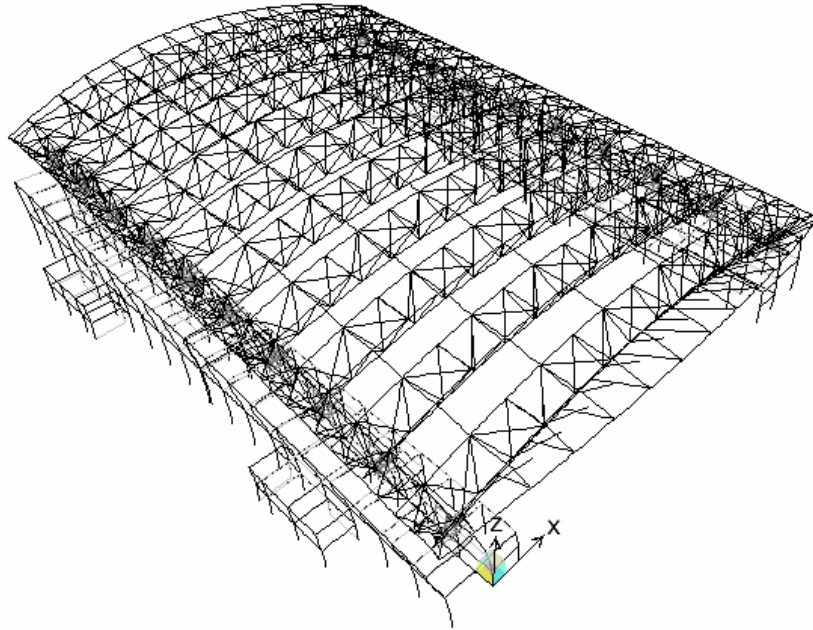


**Figure A.5.1** Two Sided EB+VD Isolation Shape of First Mode (0.94sec).

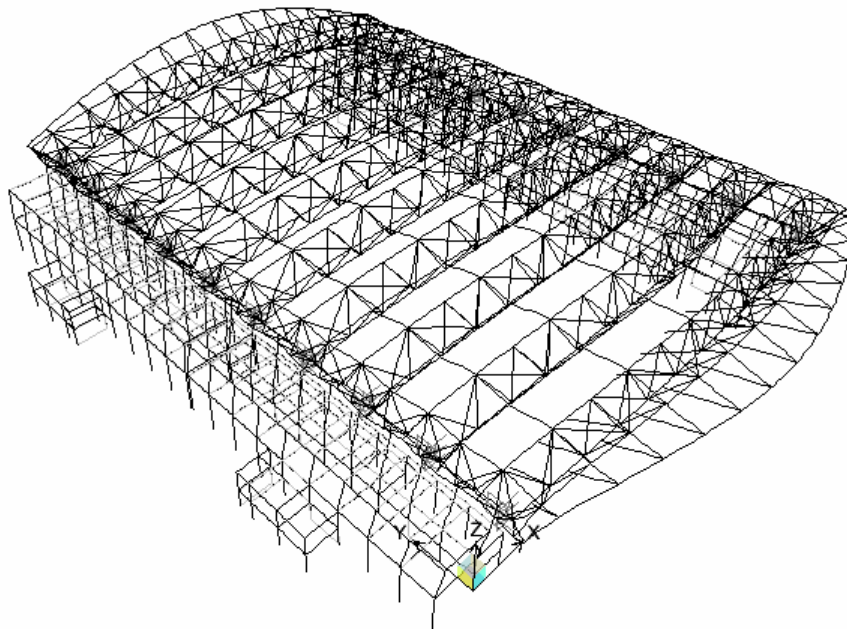


**Figure A.5.2** Two Sided EB + VD Isolation Shape of Second Mode (0.87sec.).

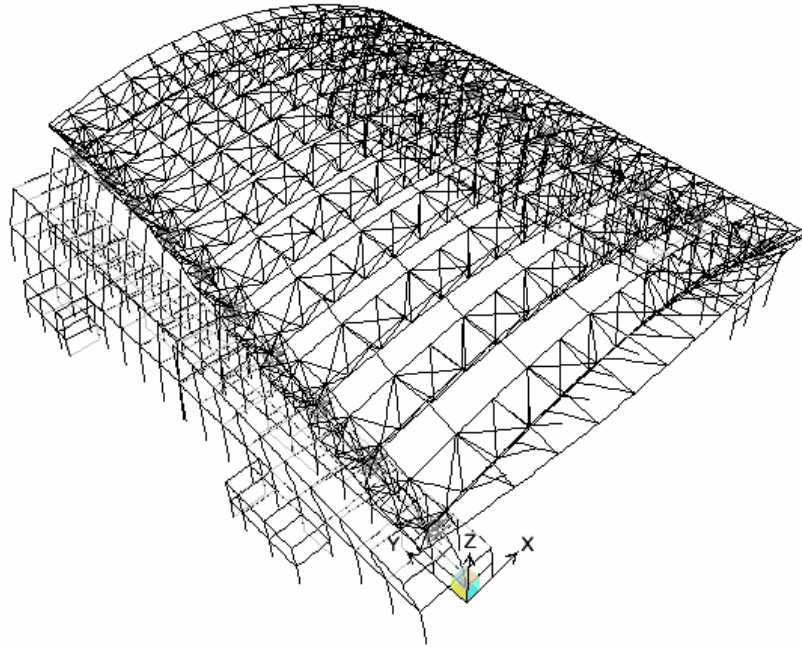


**Figure A.5.3** Two Sided EB + VD Isolation Shape of Third Mode (0.84sec.).

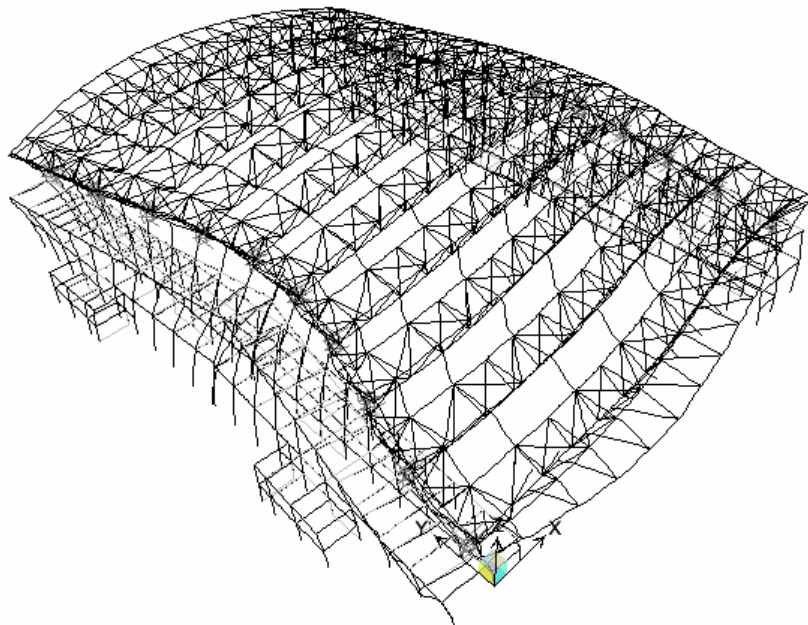


**Figure A.5.4** Two Sided EB + VD Isolation Shape of Fourth Mode (0.59).

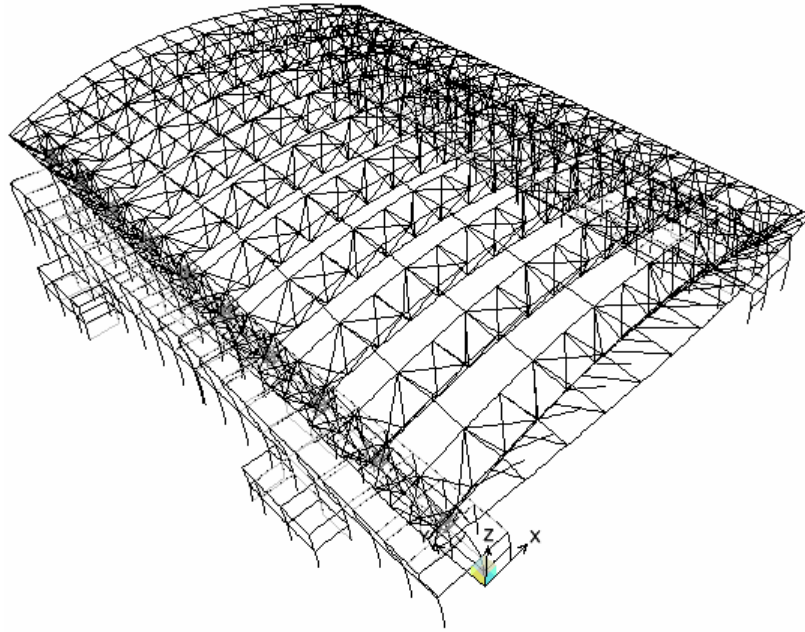


**Figure A.5.5** One Sided EB + VD Isolation Mode Shape of First Mode (0.89sec.).

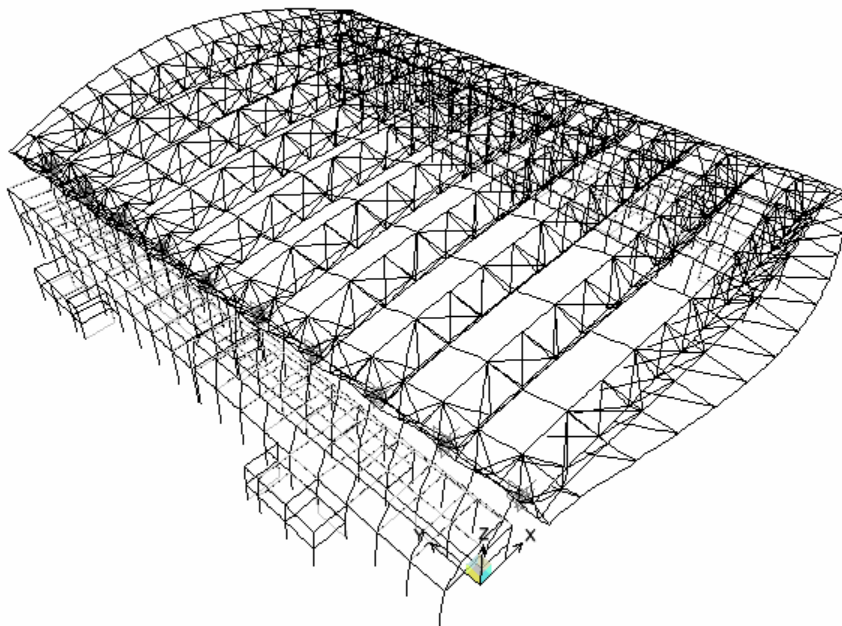


**Figure A.5.6** One Sided EB+VD Isolation Shape of Second Mode (0.82sec.).

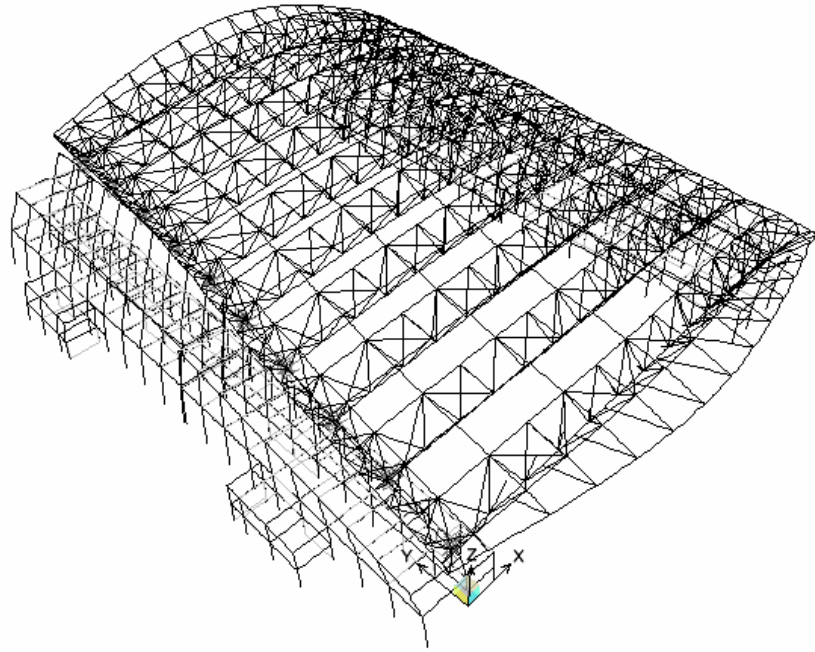


**Figure A.5.7** One Sided EB+VD Isolation Mode Shape of Third Mode (0.79sec.).

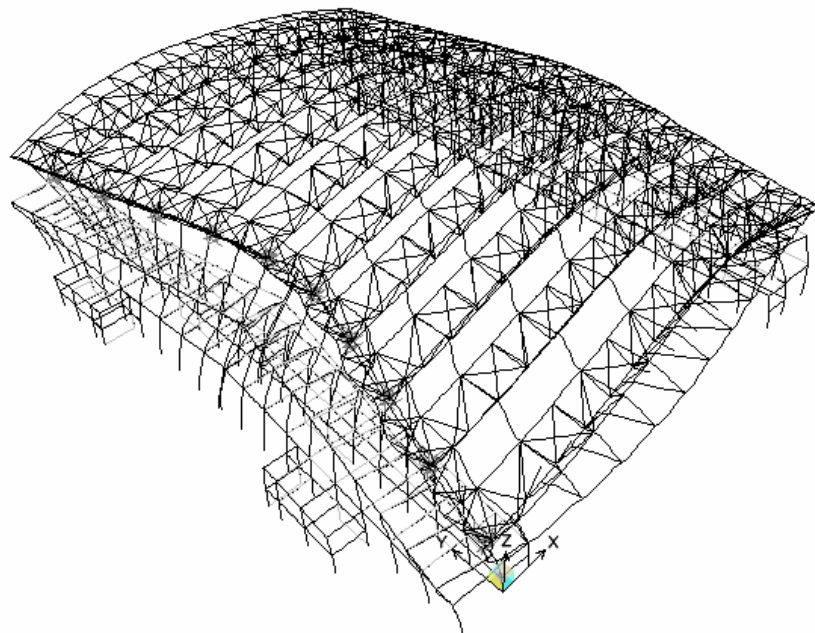


**Figure A.5.8** One Sided EB + VD Isolation Shape of Fourth Mode (0.60sec.).

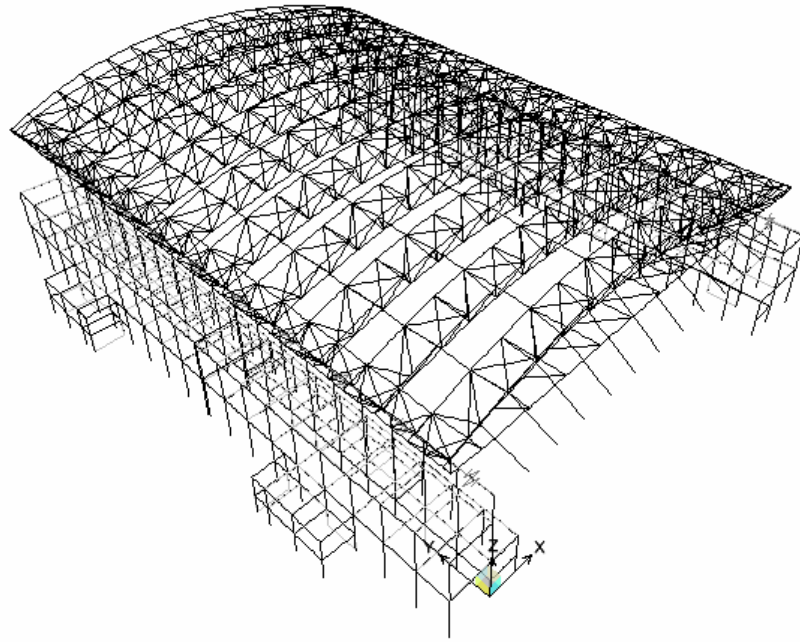


**Figure A.5.9** Two Sided EB Isolation Mode Shape of First Mode (1.62sec.).

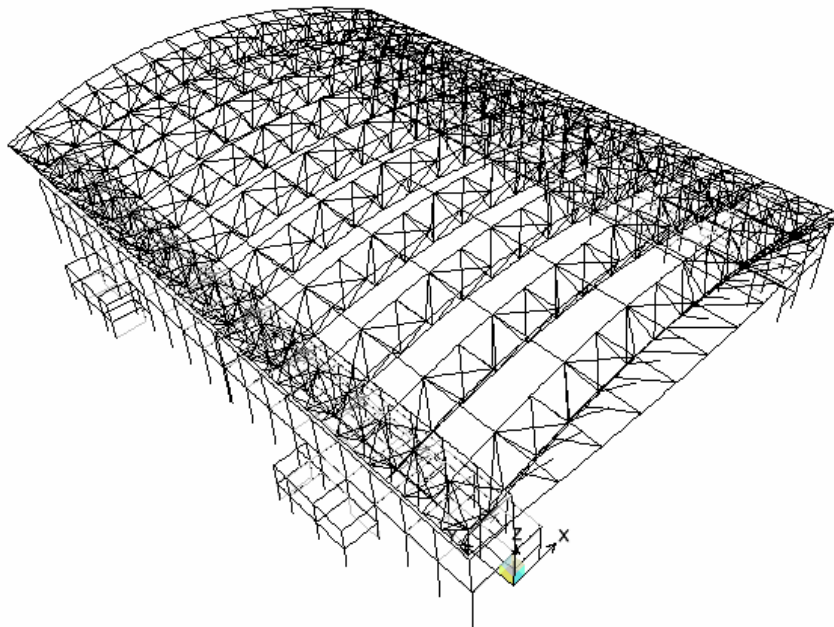


**Figure A.5.10** Two Sided EB Isolation Mode Shape of Second Mode (1.62sec.).

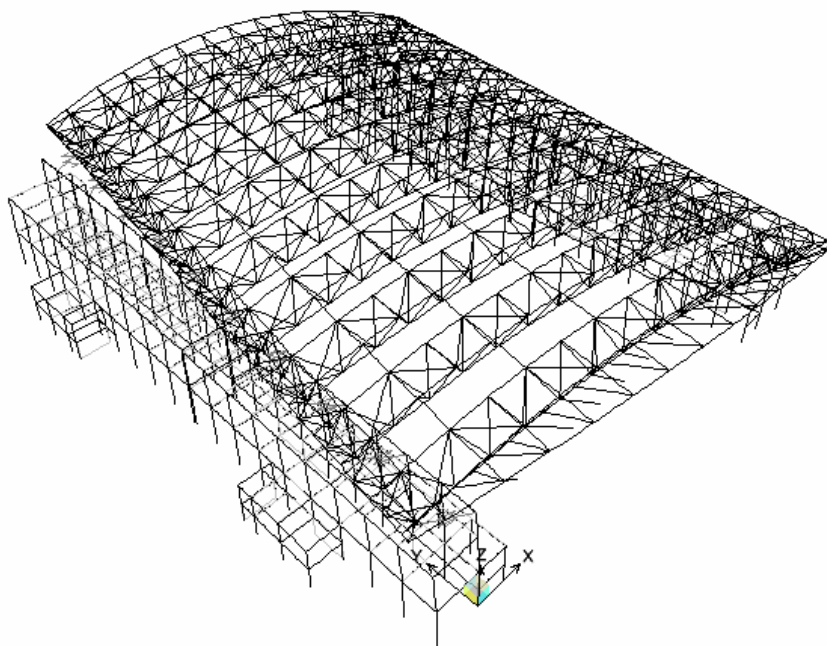


**Figure A.5.11** Two Sided EB Isolation Mode Shape of Third Mode (1.38sec.).

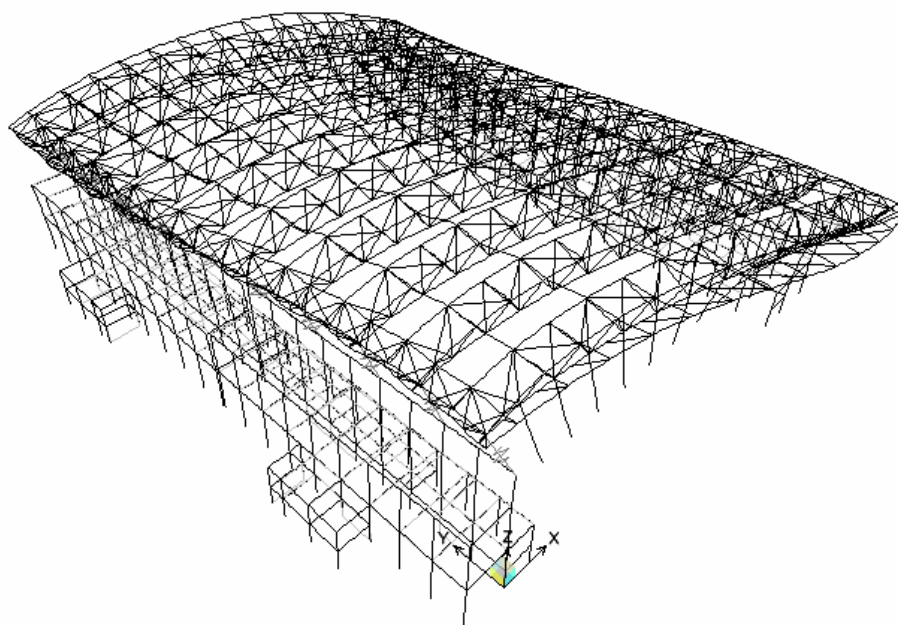


**Figure A.5.12** Two Sided EB Isolation Mode Shape of Fourth Mode (0.74sec.).

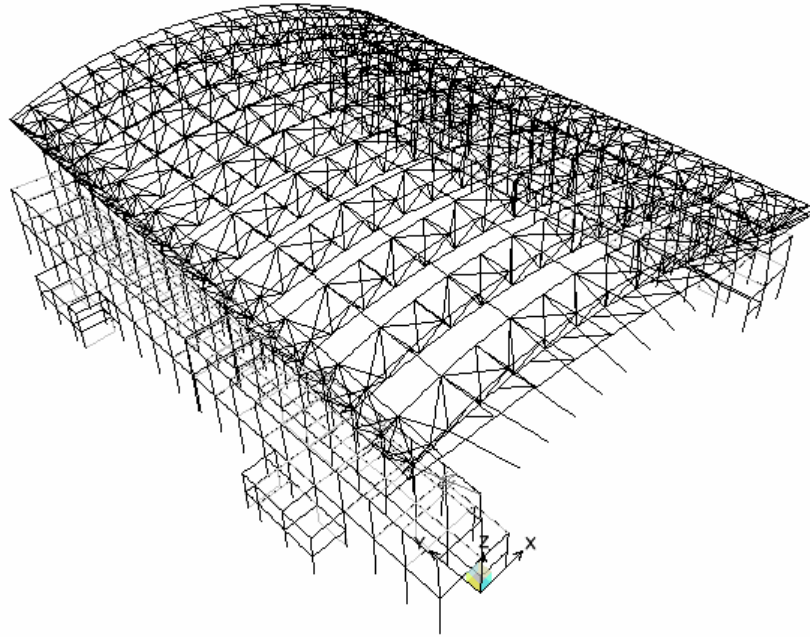


**Figure A.5.13** One Sided EB Isolation Mode Shape of First Mode (1.28sec.).

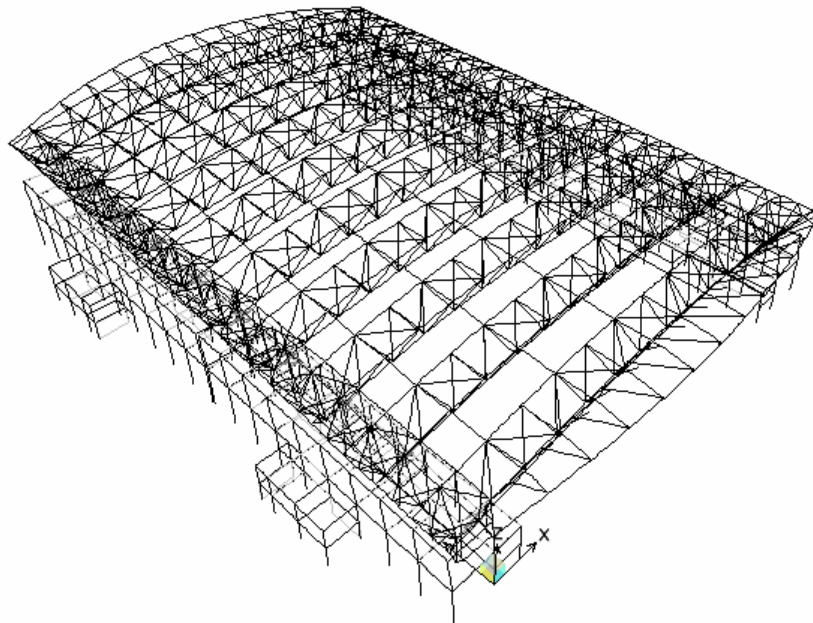


**Figure A.5.14** One Sided EB Isolation Mode Shape of Second Mode (0.98sec.).

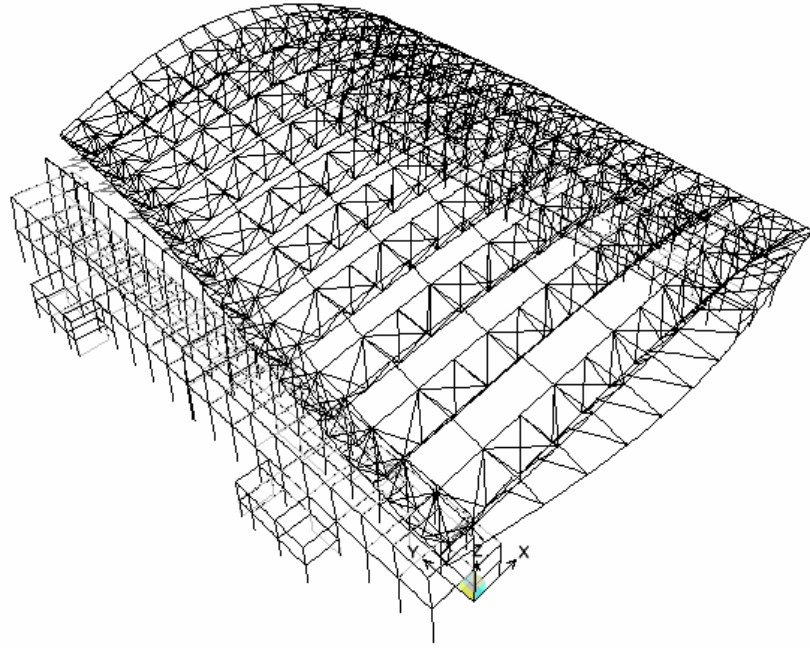


**Figure A.5.15** One Sided EB Isolation Mode Shape of Third Mode (0.84sec.).

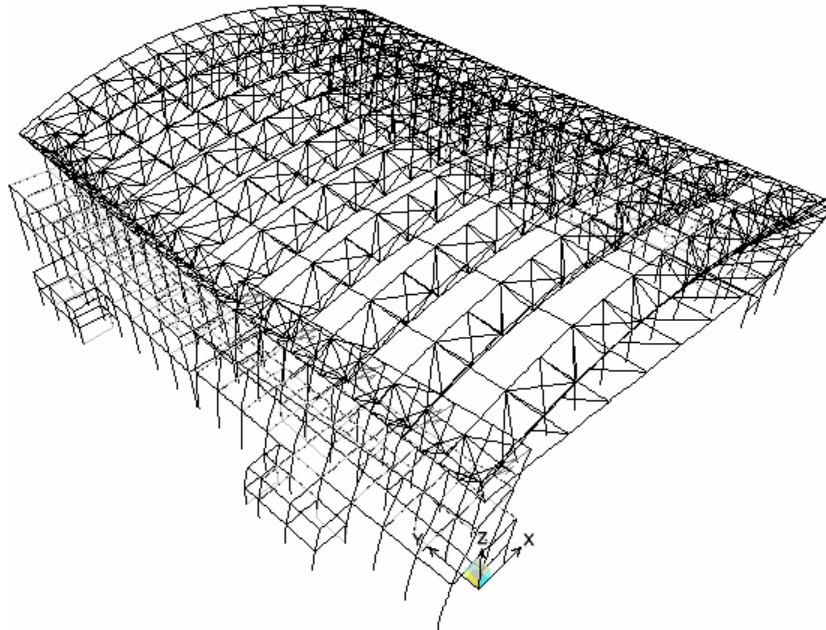


**Figure A.5.16** One Sided EB Isolation Mode Shape of Fourth Mode (0.62sec.).

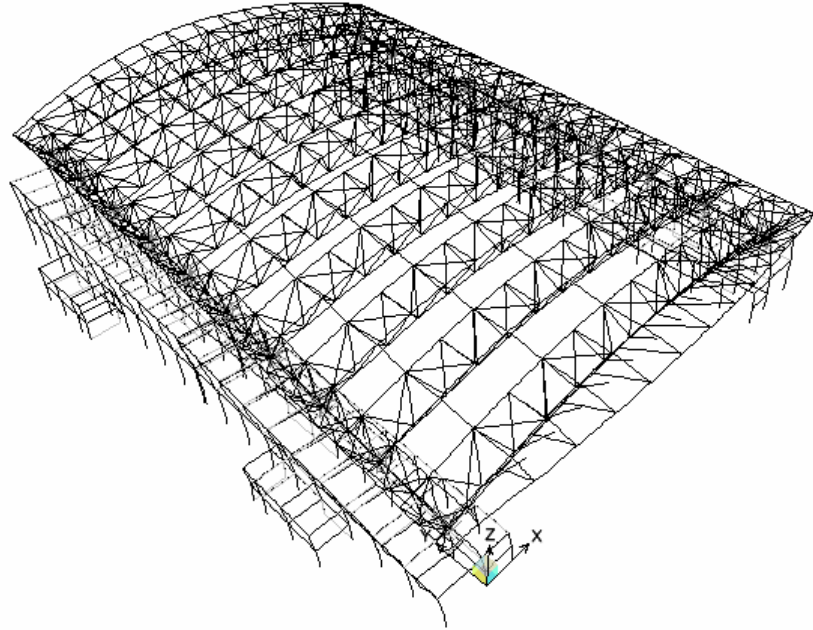


**Figure A.5.17** Two Sided VD Isolation Mode Shape of First Mode (0.85sec.).

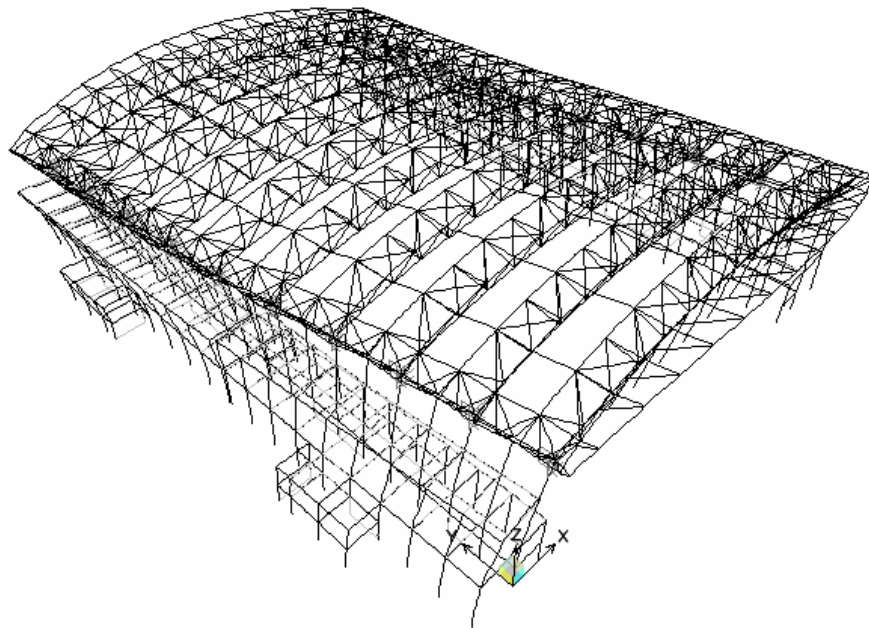


**Figure A.5.18** Two Sided VD Isolation Mode Shape of Second Mode (0.77sec.).

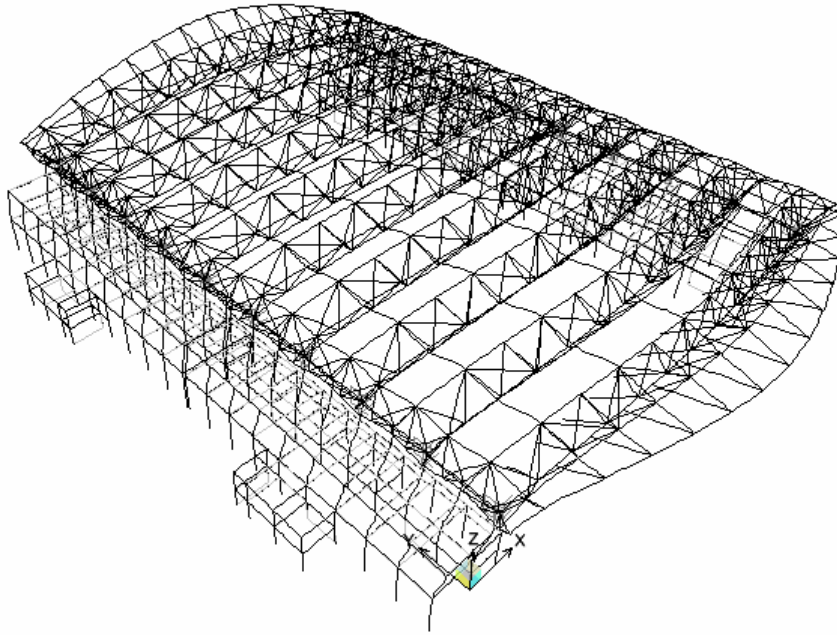


**Figure A.5.19** Two Sided VD Isolation Mode Shape of Third Mode (0.75sec.).

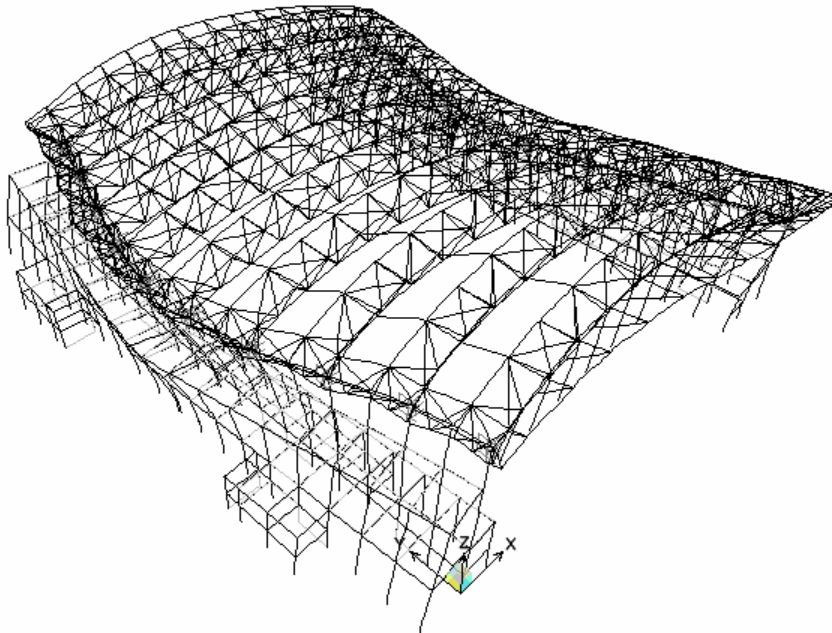


**Figure A.5.20** Two Sided VD Isolation Mode Shape of Fourth Mode (0.58sec.).

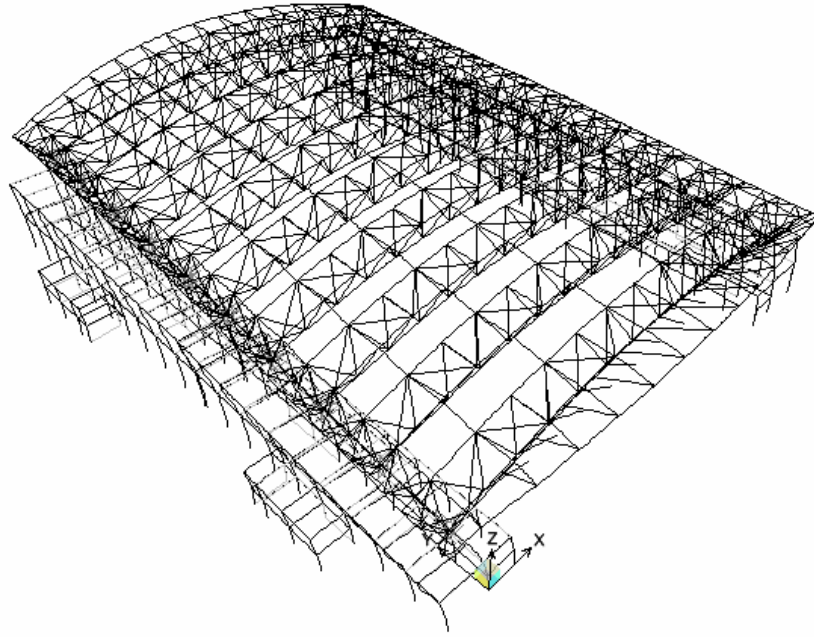


**Figure A.5.21** One Sided VD Isolation Mode Shape of First Mode (0.85sec.).

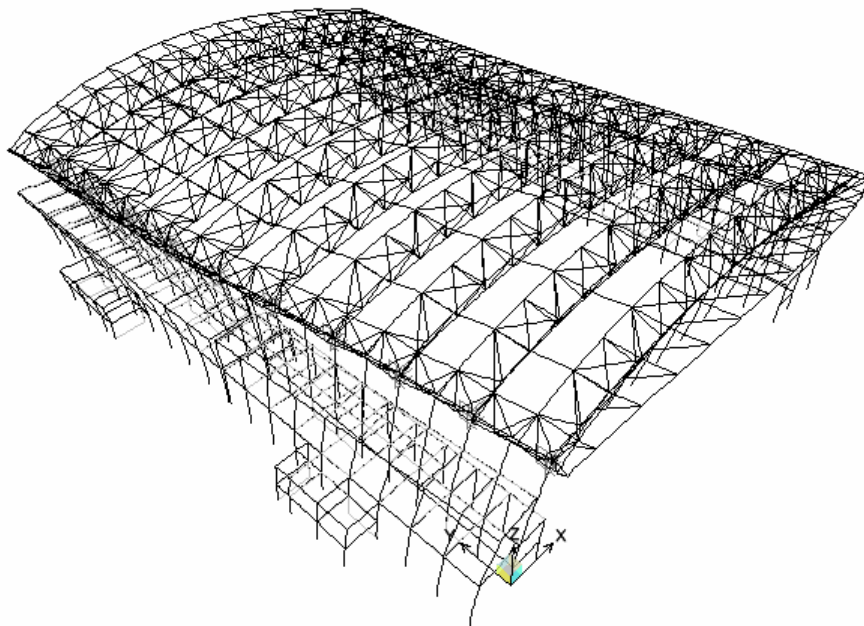


**Figure A.5.22** One Sided VD Isolation Mode Shape of Second Mode (0.77sec.).

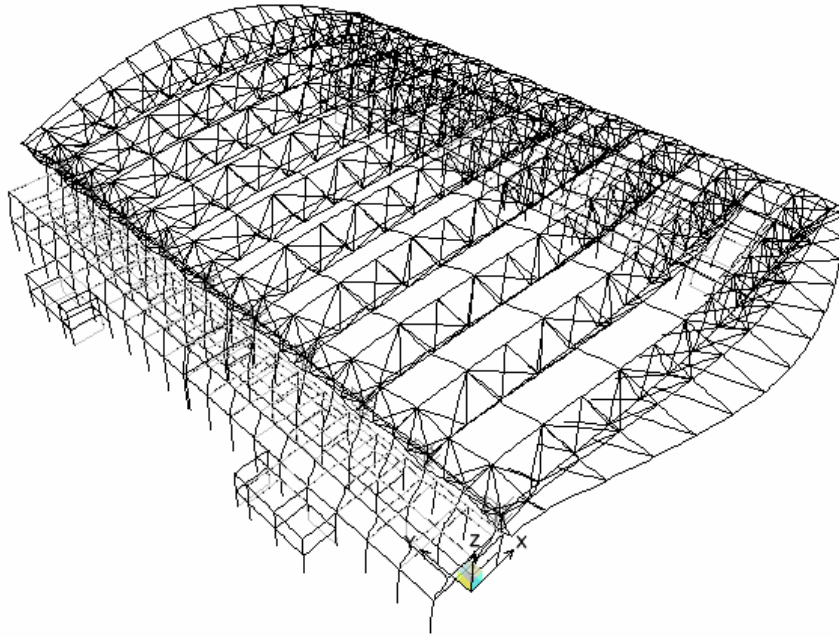


**Figure A.5.23** One Sided VD Isolation Mode Shape of Third Mode (0.75sec.).

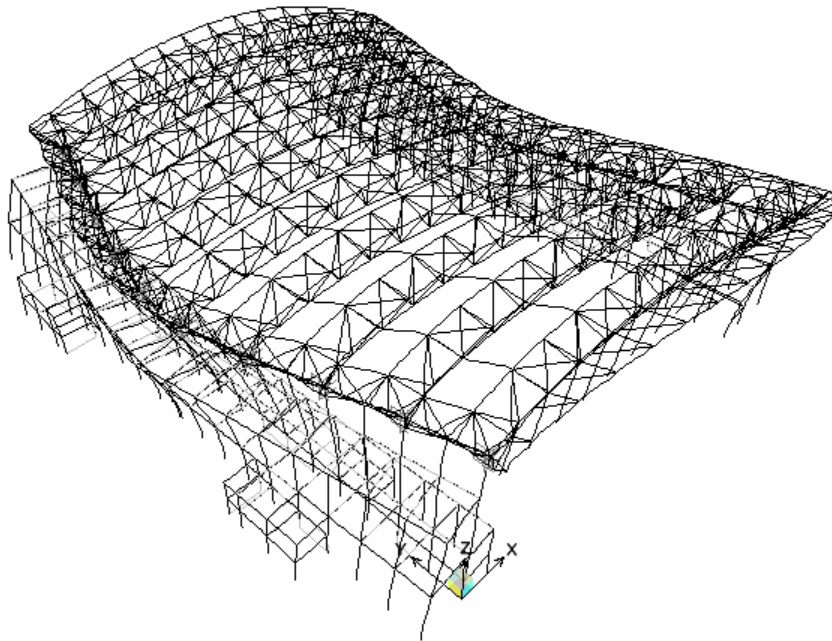


**Figure A.5.24** One Sided VD Isolation Mode Shape of Fourth Mode (0.59sec.).

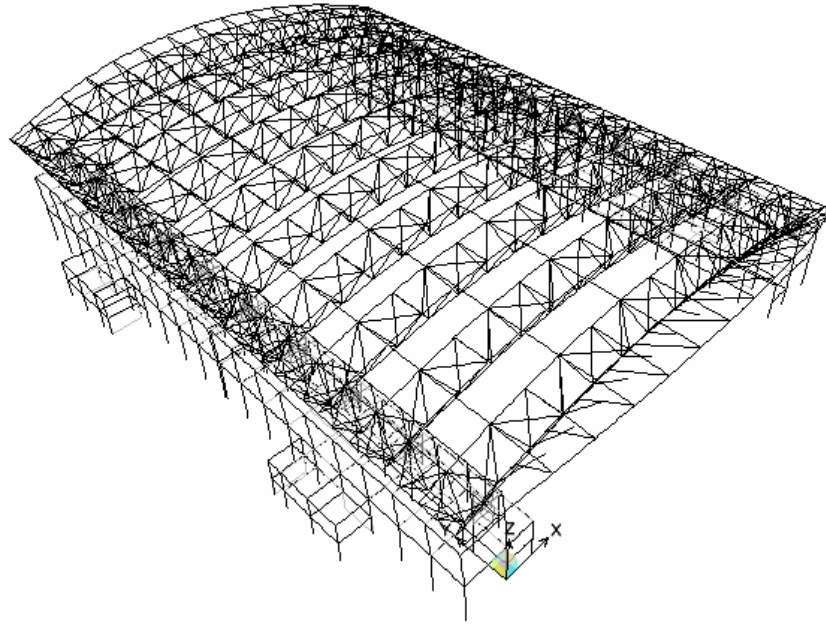


**Figure A.5.25** Two Sided LRB Isolation Shape of First Mode (1.53sec.).

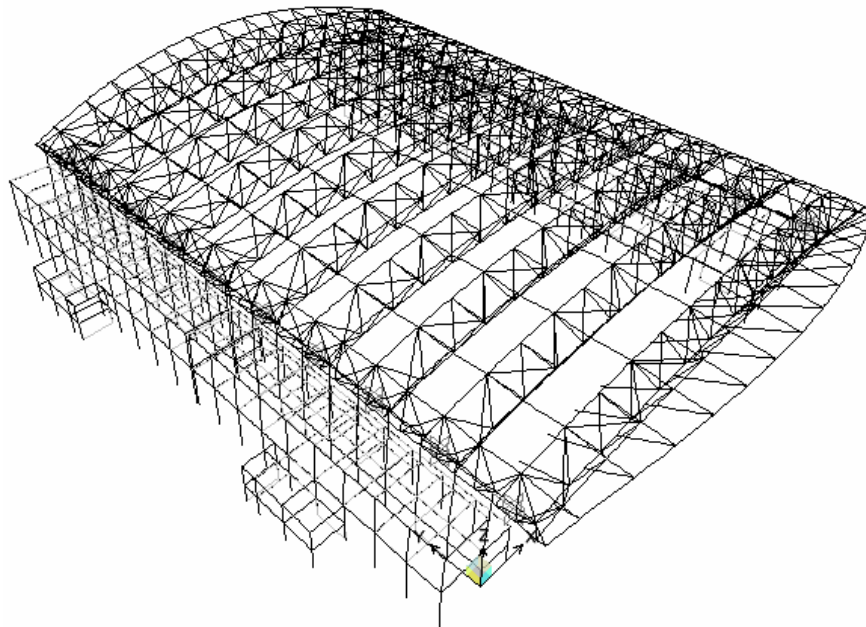


**Figure A.5.26** Two Sided LRB Isolation Shape of Second Mode (1.51sec.).

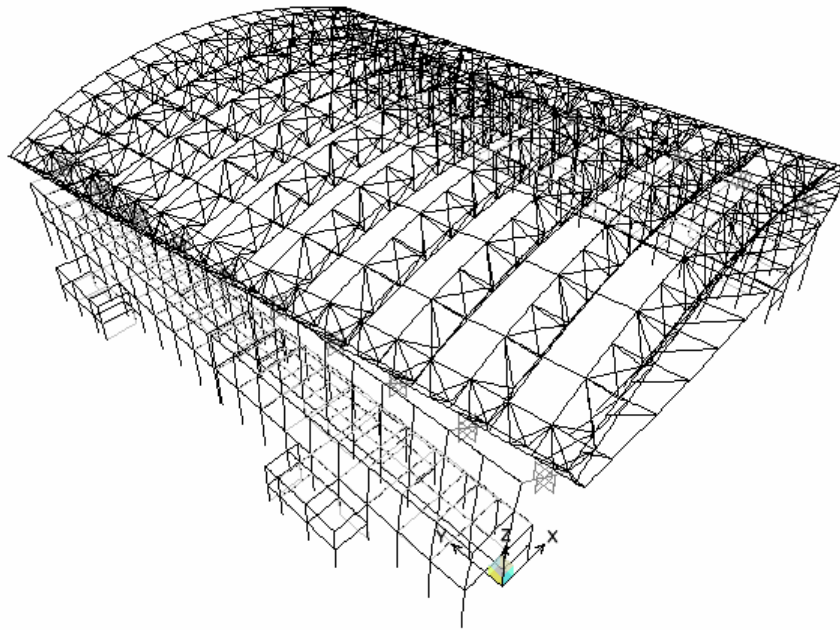


**Figure A.5.27** Two Sided LRB Isolation Shape of Third Mode (1.34sec.).

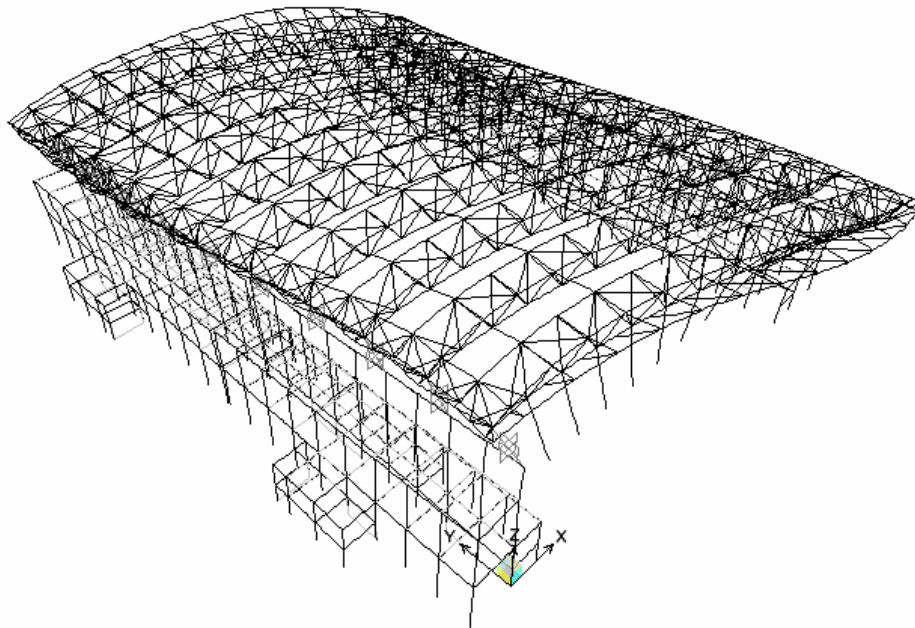


**Figure A.5.28** Two Sided LRB Isolation Shape of Fourth Mode (0.80sec.).

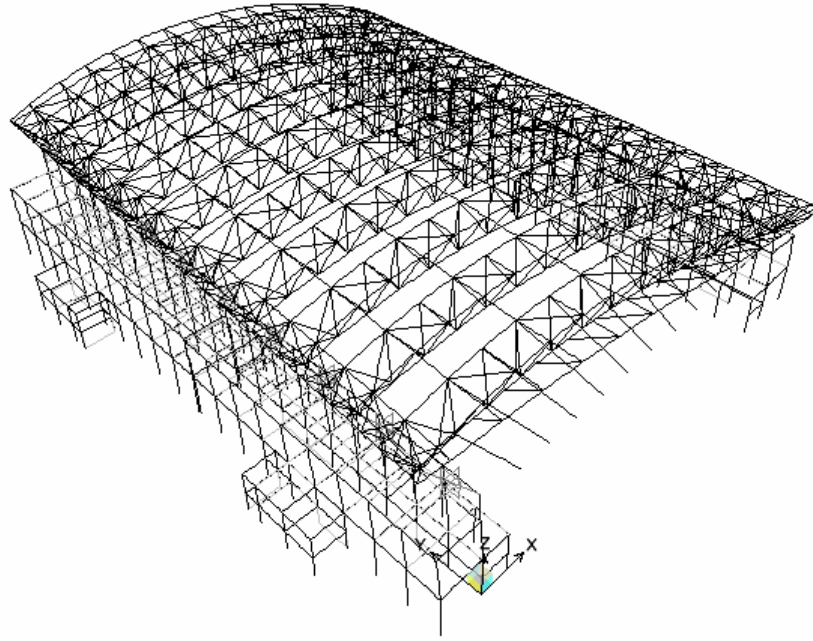


**Figure A.5.29** One Sided LRB Isolation Shape of First Mode (1.25sec.).

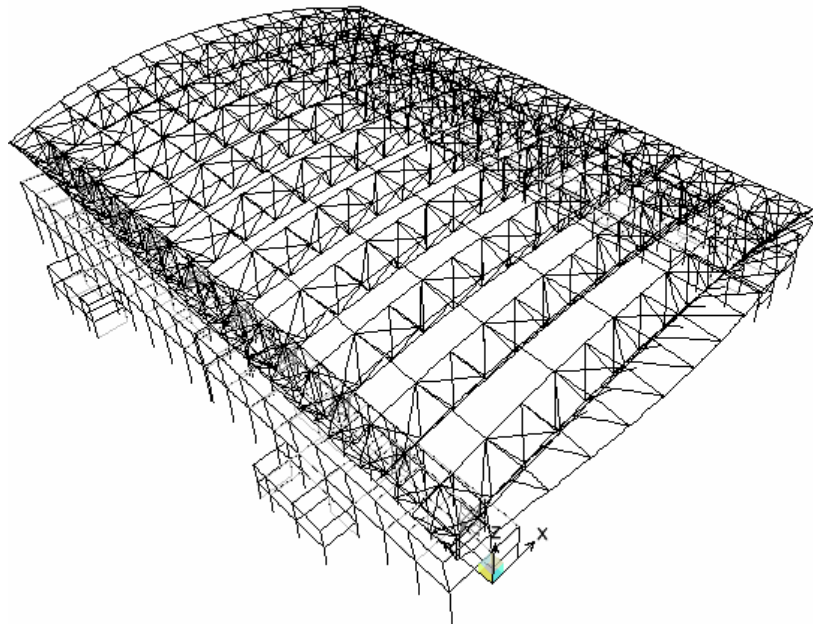


**Figure A.5.30** One Sided LRB Isolation Shape of Second Mode (0.99sec.).

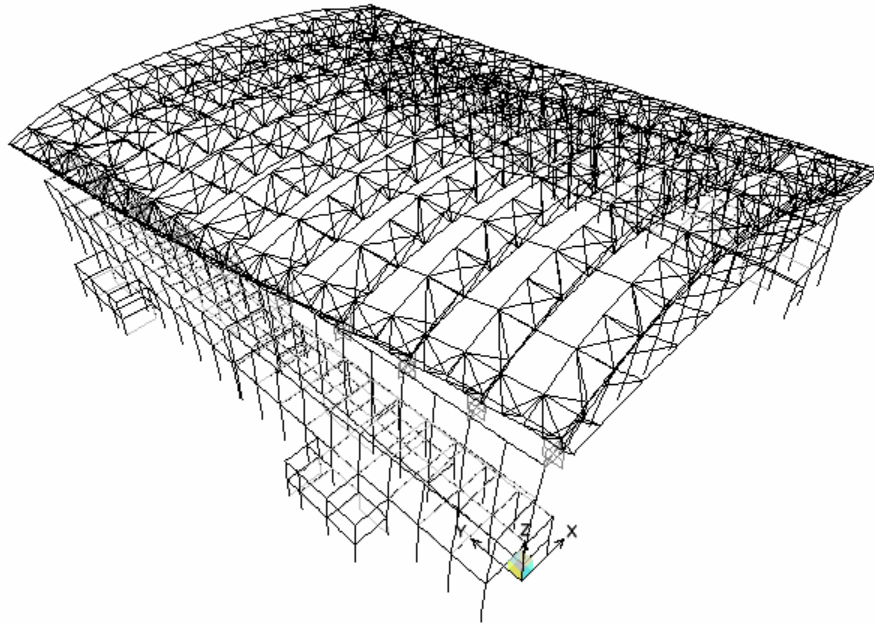


**Figure A.5.31** One Sided LRB Isolation Shape of Third Mode (0.86sec.).

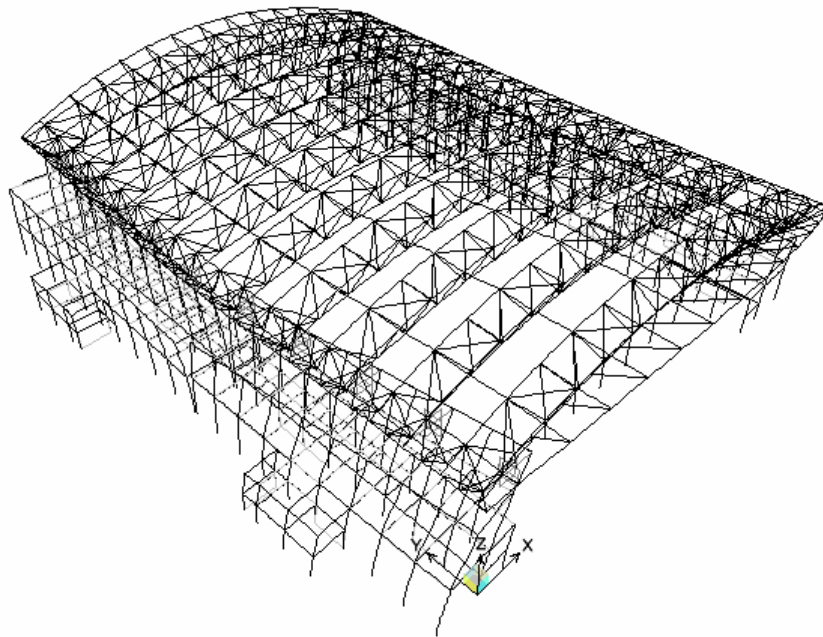


**Figure A.5.32** One Sided LRB Isolation Shape of Fourth Mode (0.64sec.).

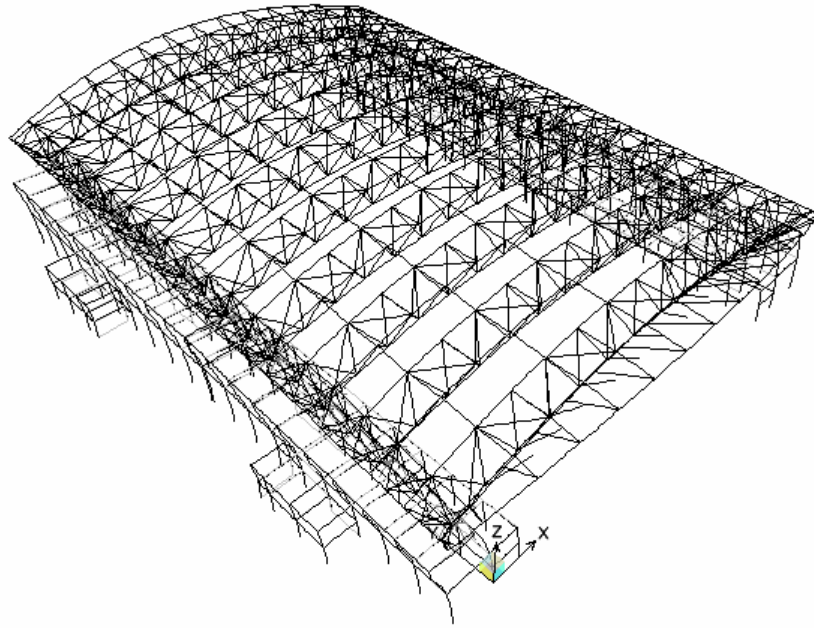


**Figure A.5.33** Two Sided FPS Isolation Shape of First Mode (0.90sec.).

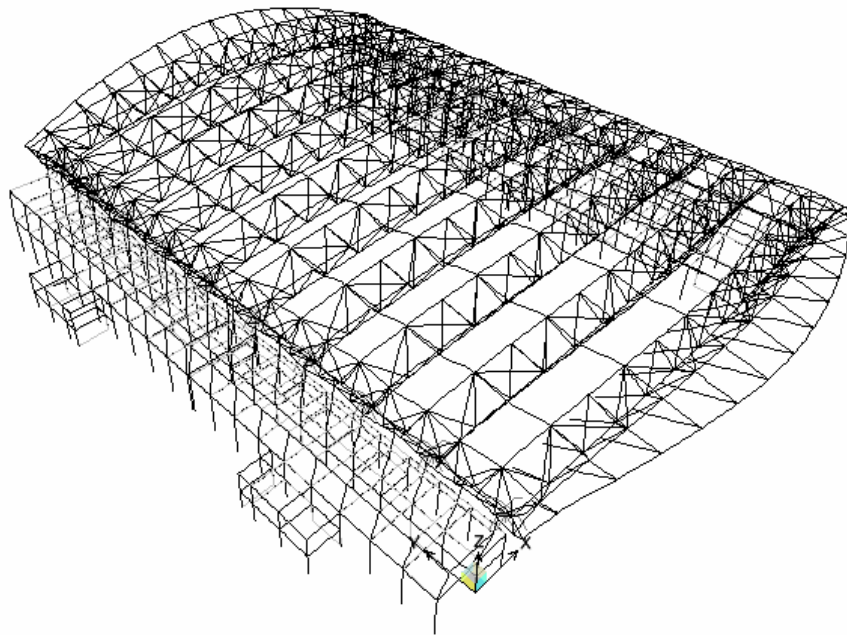


**Figure A.5.34** Two Sided FPS Isolation Shape of Second Mode (0.83sec.).

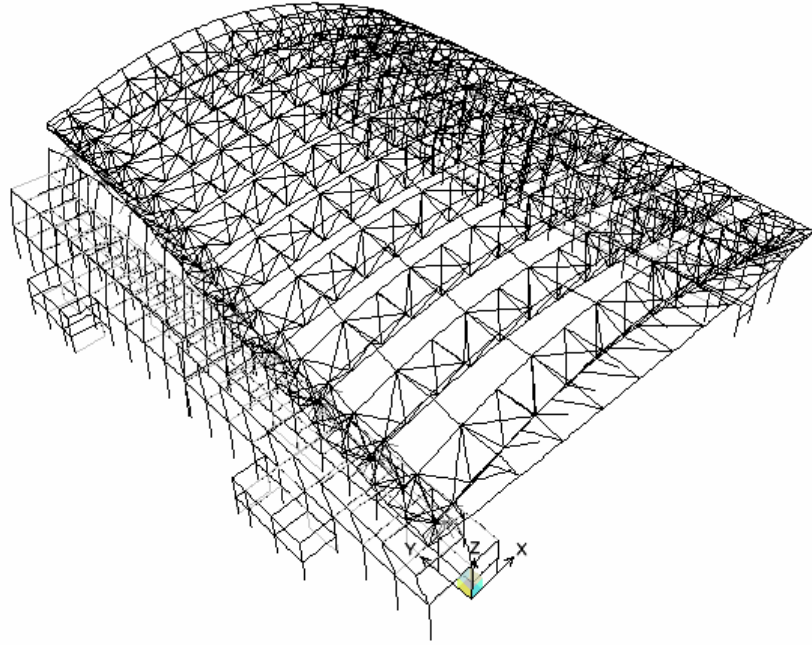


**Figure A.5.35** Two Sided FPS Isolation Shape of Third Mode (0.76sec.).

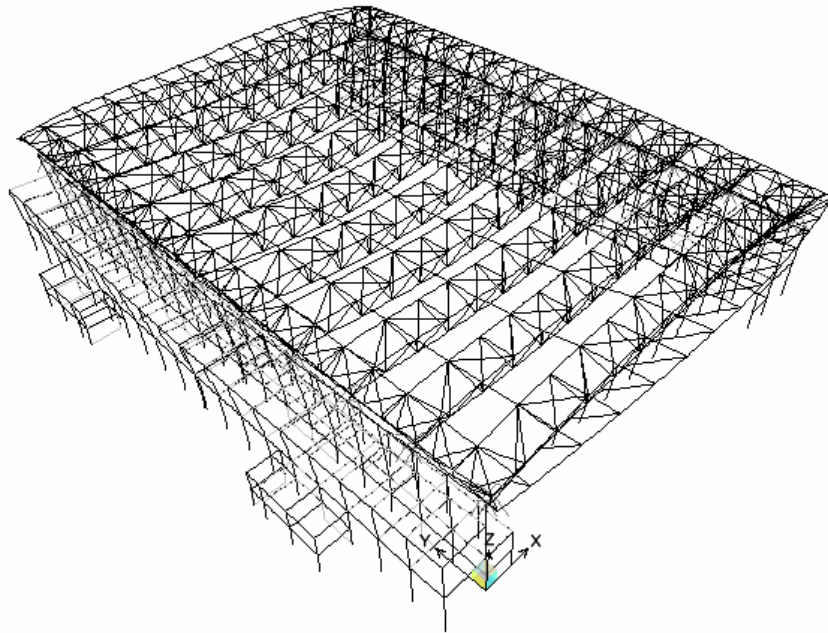


**Figure A.5.36** Two Sided FPS Isolation Shape of Fourth Mode (0.55sec.).

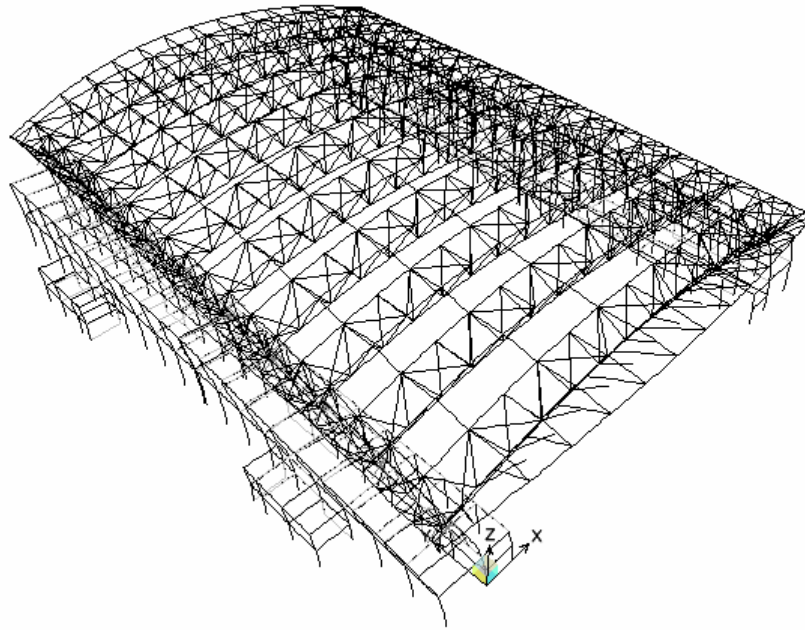


**Figure A.5.37** One Sided FPS Isolation Shape of First Mode (0.87sec.).

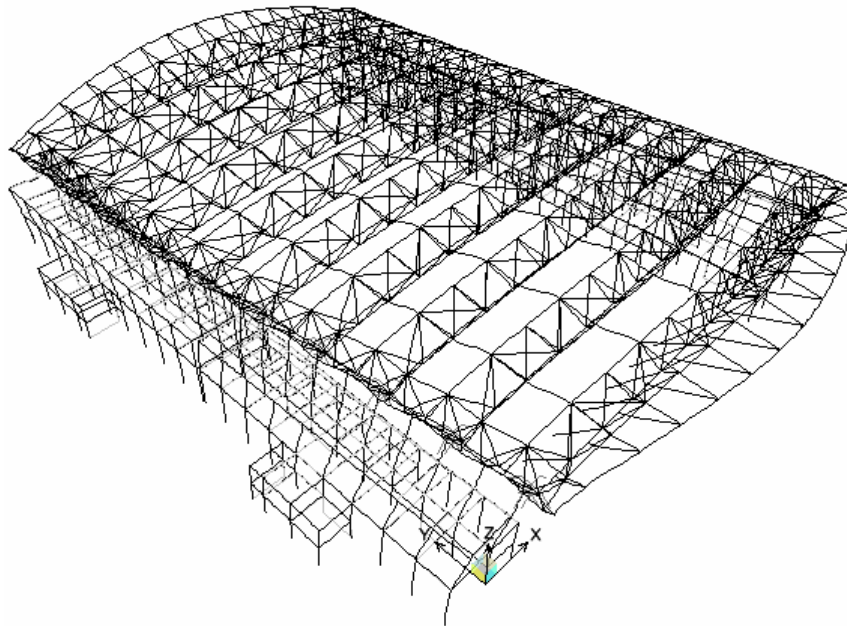


**Figure A.5.38** One Sided FPS Isolation Shape of Second Mode (0.80sec.).

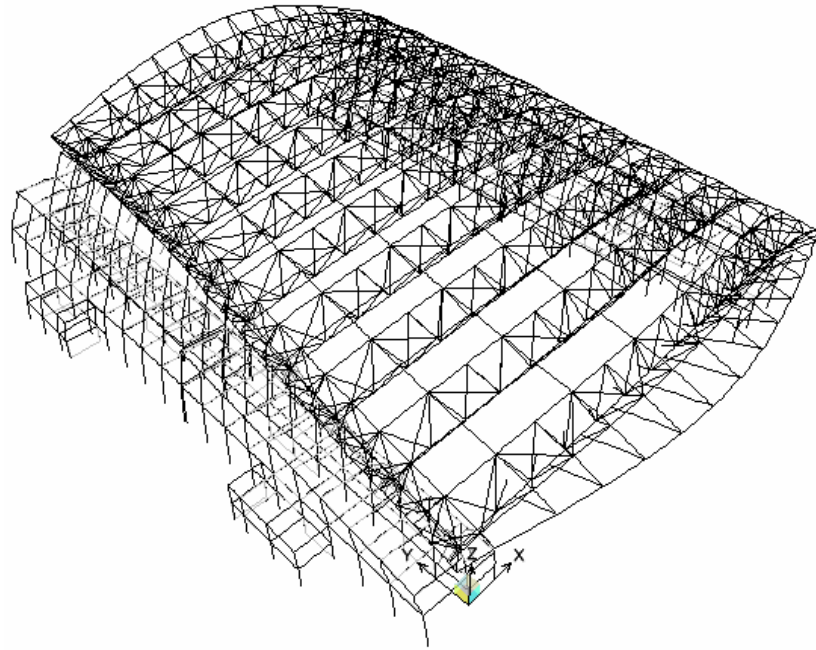


**Figure A.5.39** One Sided FPS Isolation Shape of Third Mode (0.78sec.).

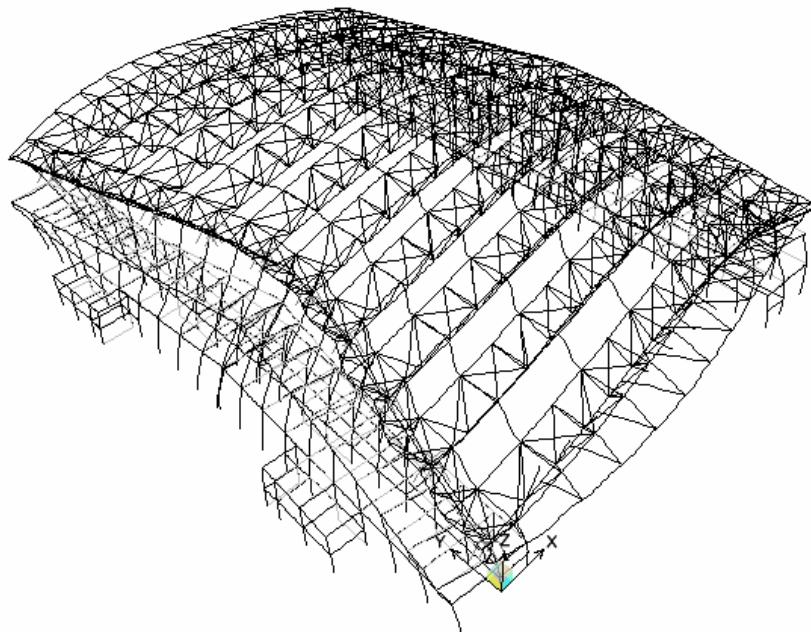


**Figure A.5.40** One Sided FPS Isolation Shape of Fourth Mode (0.59sec.).

## A.6 DEFORMED ENVELOPE SHAPES OF TWO SIDED EB+VD ISOLATION CASE FOR TIME-HISTORY ANALYSES

(Figures were exaggerated to understand behavior of the system)

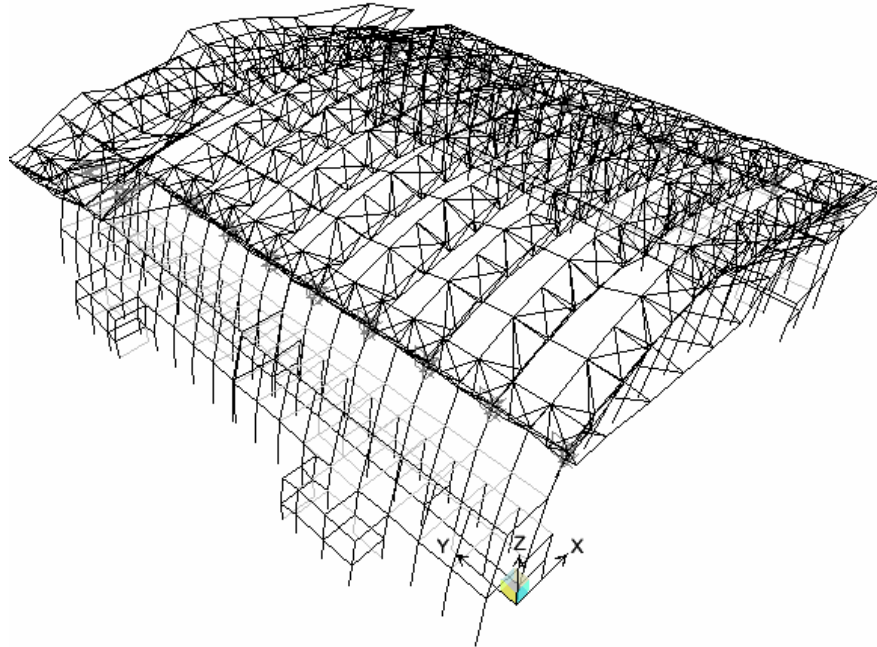


**Figure A.6.1** 290YA\_X Analyze Case Deformed Shape

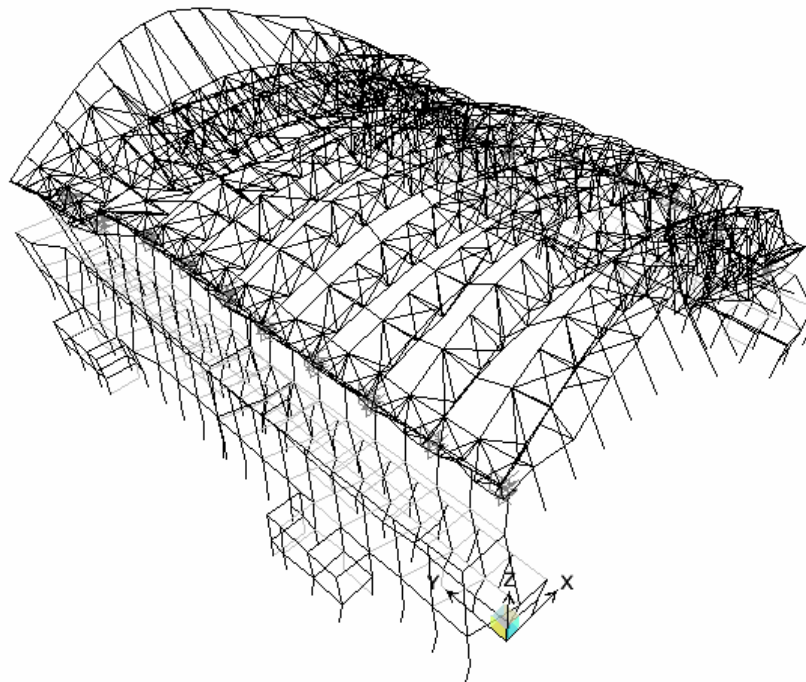


**Figure A.6.2** 290YA\_Y Analyze Case Deformed Shape

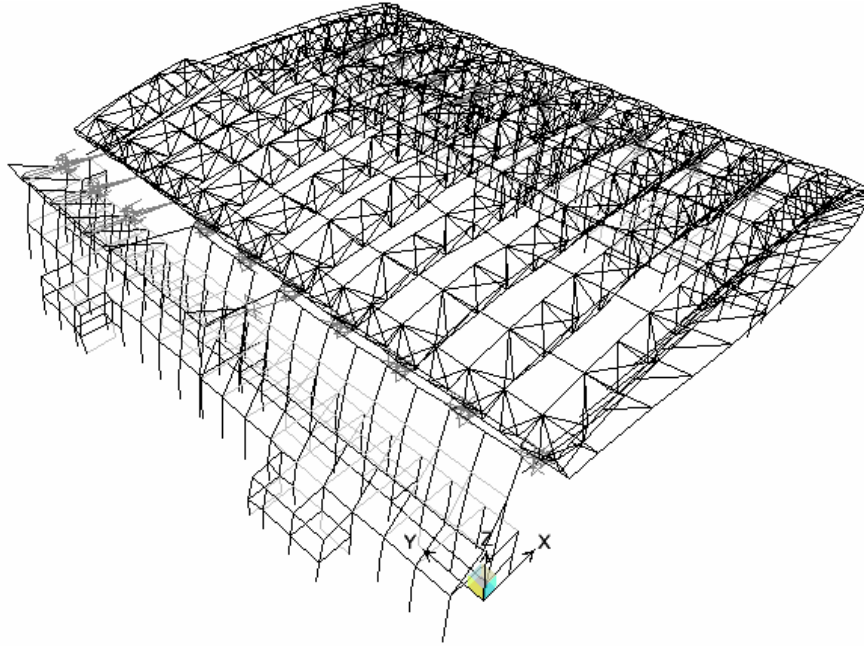


**Figure A.6.3** 333XA\_X Analyze Case Deformed Shape

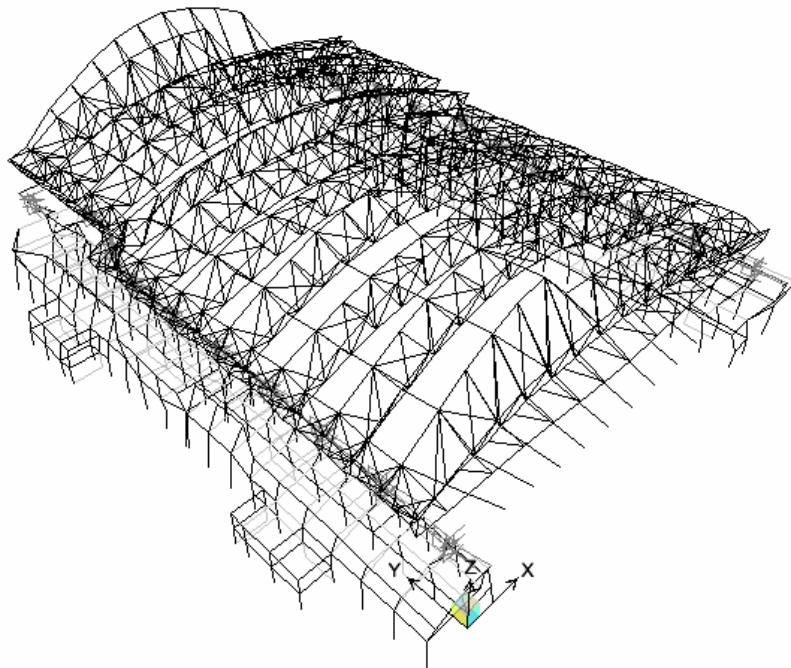


**Figure A.6.4** 333XA\_Y Analyze Case Deformed Shape

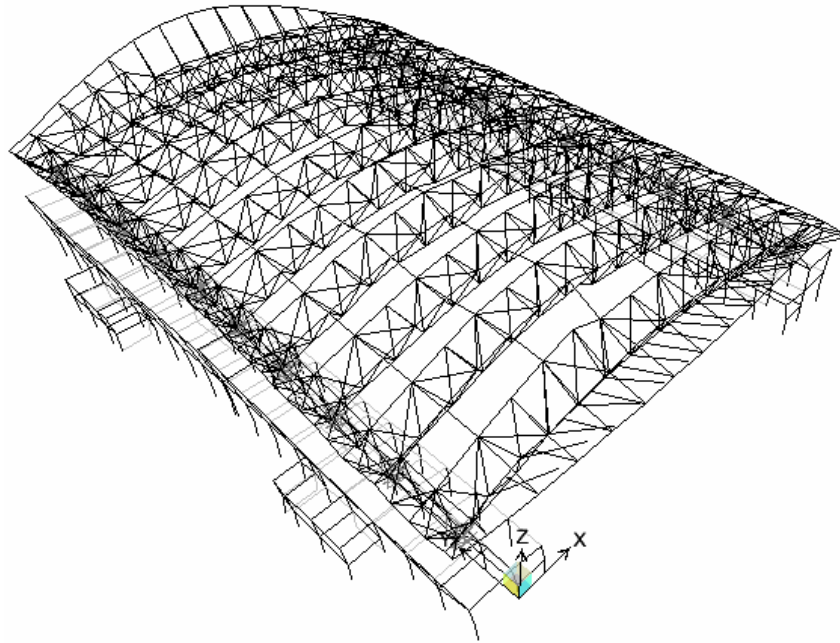


**Figure A.6.5** 591YA\_X Analyze Case Deformed Shape

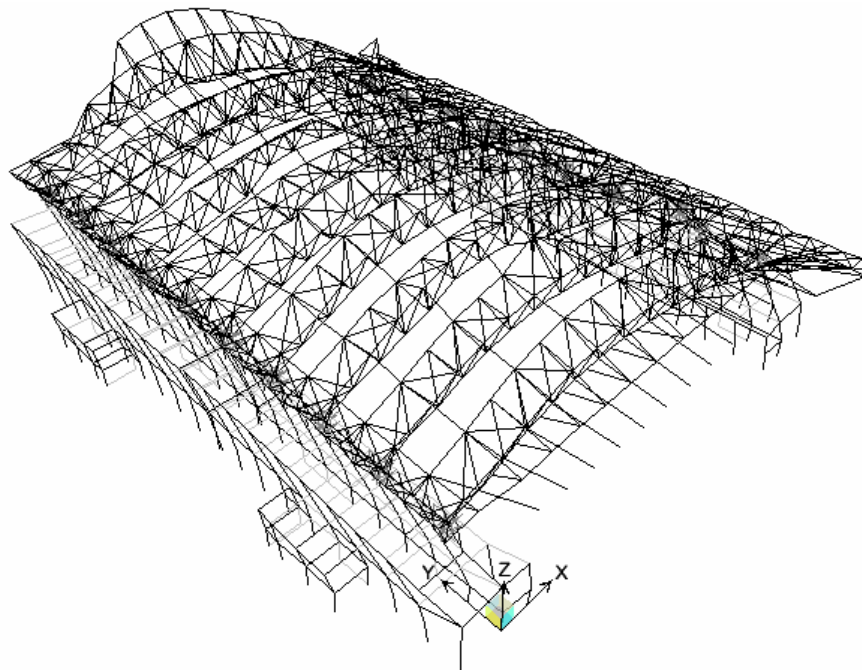


**Figure A.6.6** 591YA\_Y Analyze Case Deformed Shape

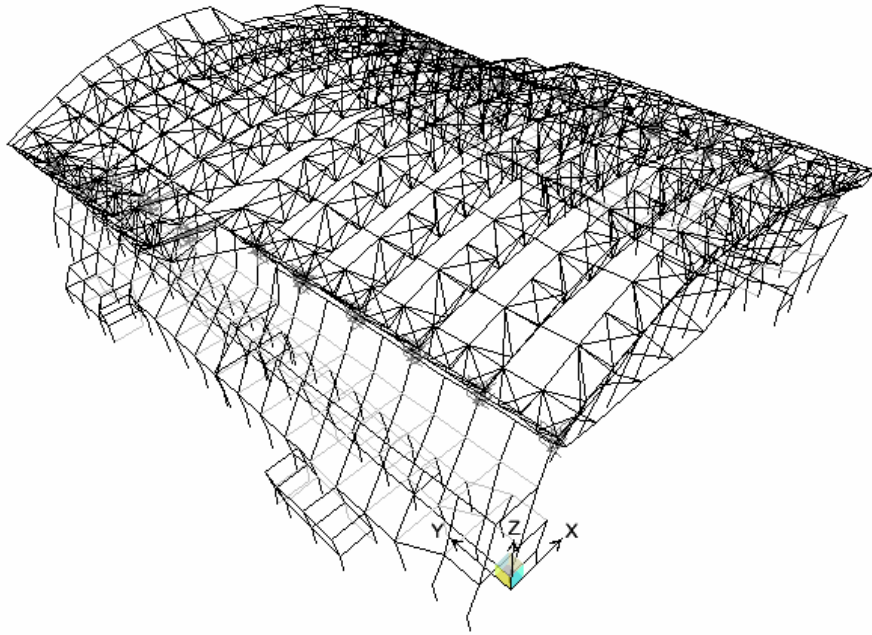


**Figure A.6.7** 879XA\_X Analyze Case Deformed Shape

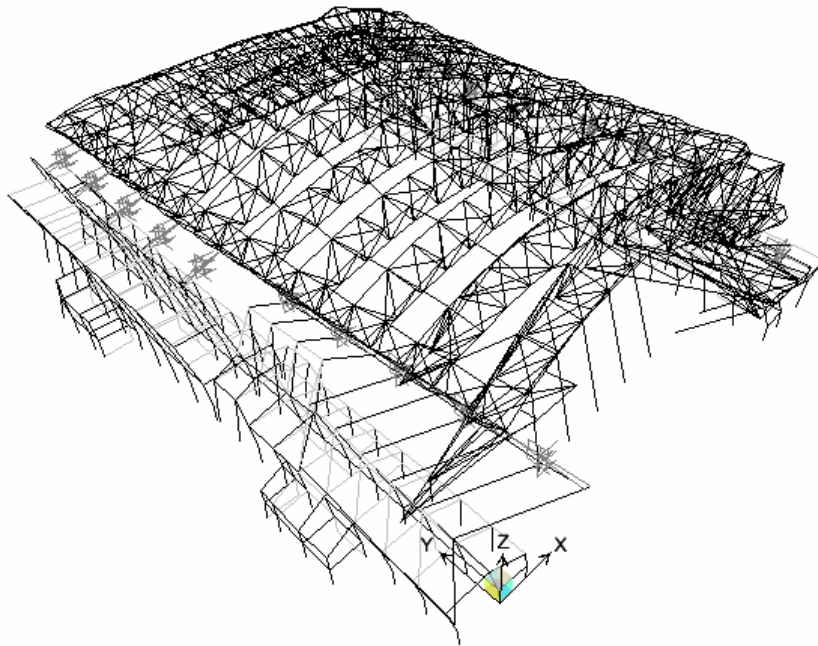


**Figure A.6.8** 879XA\_Y Analyze Case Deformed Shape

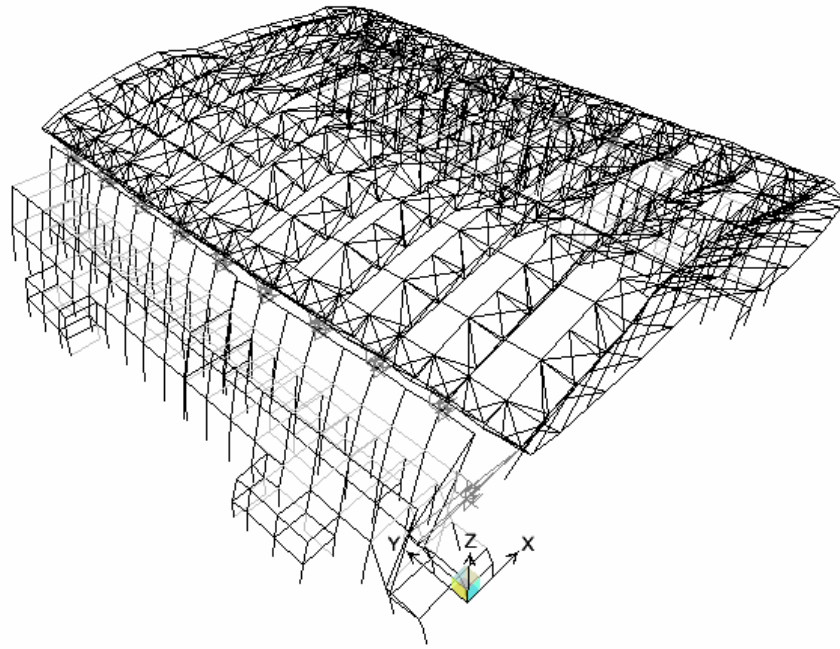


**Figure A.6.9** 879YA\_X Analyze Case Deformed Shape

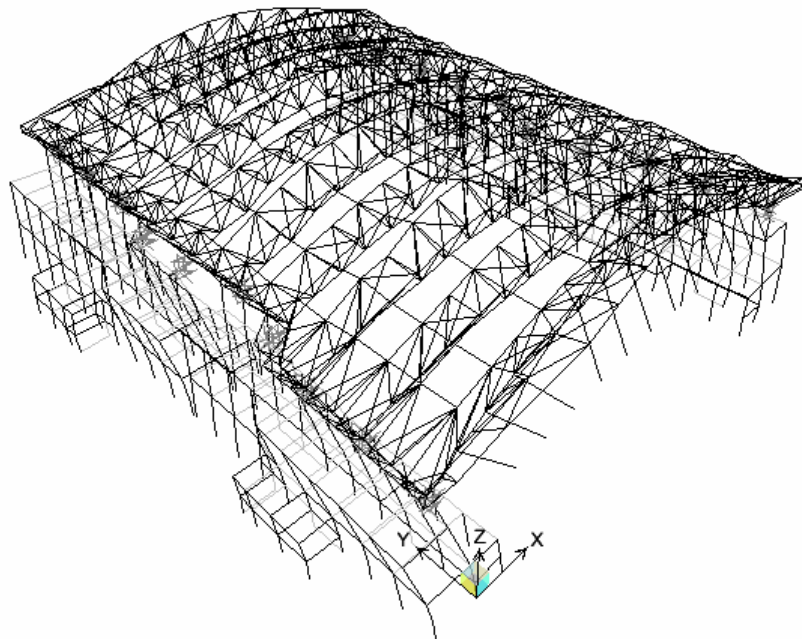


**Figure A.6.10** 879YA\_Y Analyze Case Deformed Shape

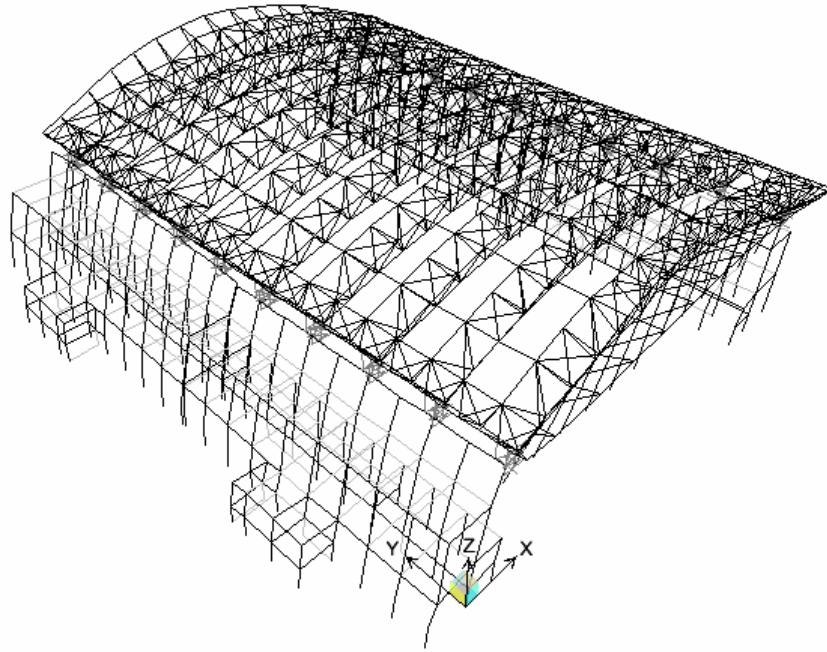


**Figure A.6.11** HSP000\_X Analyze Case Deformed Shape

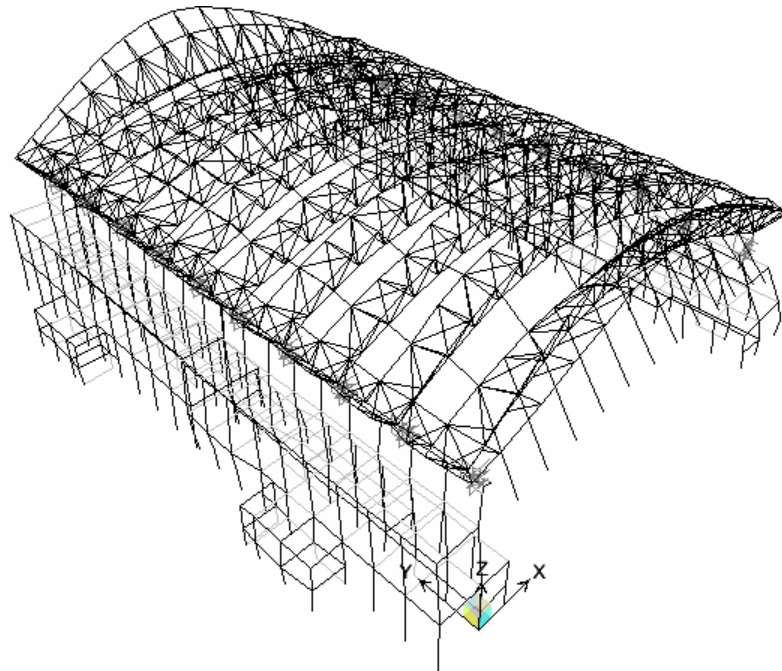


**Figure A.6.12** HSP000\_Y Analyze Case Deformed Shape

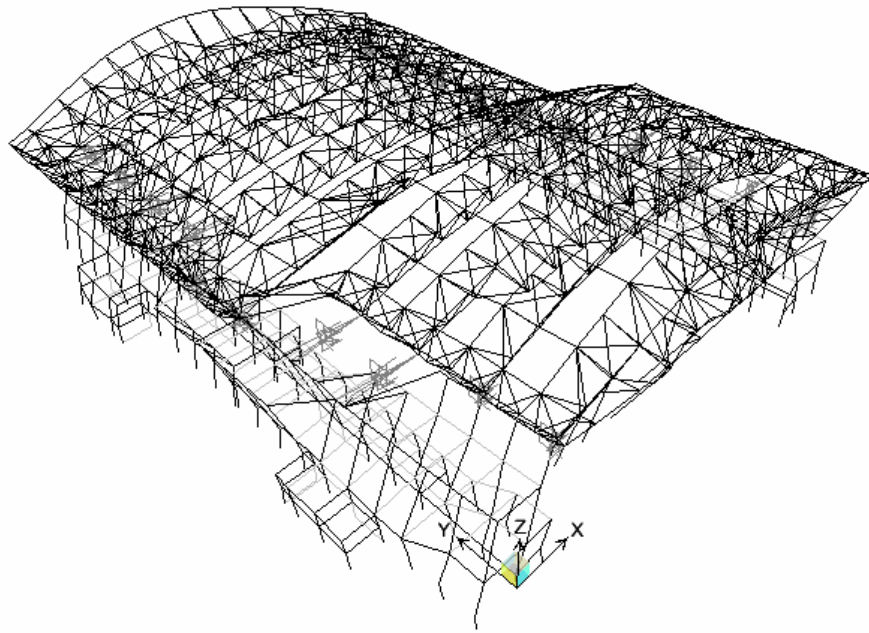


**Figure A.6.13** STC090\_X Analyze Case Deformed Shape

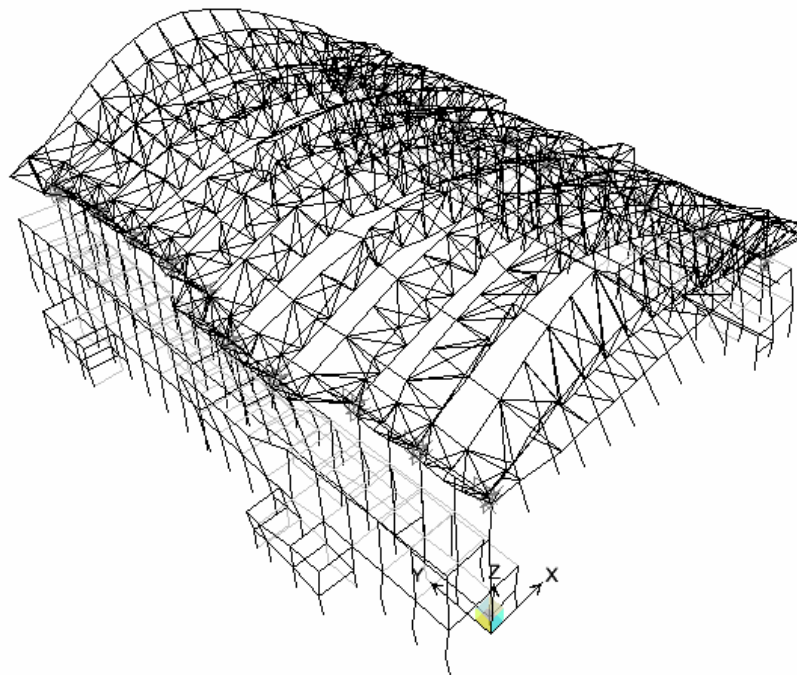


**Figure A.6.14** STC090\_Y Analyze Case Deformed Shape